Title
Applications of single molecule fluorescence detection

Author
Glass, Jennifer L.

Publication Date
2000-10-01

LBNL-46997

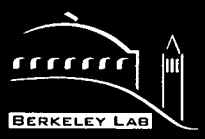

ERNEST ORLANDO LAWRENCE
BERKELEY NATIONAL LABORATORY

Applications of Single Molecule Fluorescence Detection

Jennifer L. Glass

Materials Sciences Division

October 2000

Ph.D. Thesis

DISCLAIMER

LBNL-46997

Applications of Single Molecule Fluorescence Detection

Jennifer Lynn Glass
Ph.D. Thesis

Department of Physics
University of California, Berkeley

and

Materials Sciences Division
Ernest Orlando Lawrence Berkeley National Laboratory
University of California
Berkeley, CA 94720

October 2000

This work was supported by the Director, Office of Science, Office of Basic Energy Sciences, Materials Sciences Division, of the U.S. Department of Energy under Contract No. DE-AC03-76SF00098.

Applications of Single Molecule Fluorescence Detection

by

Jennifer Lynn Glass

B.A. (Wellesley College) 1993
M.A. (University of California, Berkeley) 1996

A dissertation submitted in partial satisfaction of the

requirements for the degree of

Doctor of Philosophy

in

Physics

in the

GRADUATE DIVISION

of the

UNIVERSITY OF CALIFORNIA, BERKELEY

Committee in charge:

Professor Daniel S. Chemla, Chair
Professor Dan Rokhsar
Professor Carolyn Bertozzi

Fall 2000

Abstract

Applications of Single Molecule Fluorescence Detection

by

Jennifer Lynn Glass

Doctor of Philosophy in Physics

University of California, Berkeley

Professor Daniel S. Chemla, Chair

Abstract

Single pair fluorescent resonance energy transfer (spFRET) was used to monitor the conformational dynamics of individual DNA hairpins both free in diffusion and attached to a glass surface. Exponential distributions were found for the native and denatured state lifetimes, which are expected in the simple two-state model of a DNA hairpin. For hairpins with a loop size of forty adenines and a stem size of either seven or nine bases the respective closed-state lifetimes are 45 (± 2.4) ms and 103 (± 6.0) ms while the respective open-state lifetimes are 133 (± 5.5) ms and 142 (± 22) ms. As predicted, the closed-state lifetime is dependent on the stem length and is independent of the loop characteristics. The measured native and denatured state lifetimes are larger than the numbers expected by extrapolation from a previous study. The bio-specific and chemoselective ligation methods used to immobilize DNA hairpins and other biological macromolecules to glass surfaces, along with both gel and polyacrylamide immobilization methods, are described in detail.

Ratiometric detection of seminaphthorhodafluor (SNARF) fluorophores was used to examine local environmental effects and changes in pH on the single molecule level. SNARF also served as a simple two-state system to examine the distribution of properties of a population on a single molecule level. The protonation-deprotonation process for this fluorophore is shown to be diffusion-limited and evidence for observations of individual protonation events is presented.

Oxygen scavenging systems were examined for their utilities in the prevention of photobleaching of the fluorescent molecules rhodamine 6G (R6G) and fluorescein as well as the tetramethylrhodamine (TMR) and cyanine-5 (Cy5) dyes used in DNA hairpin spFRET measurements. Fluorescence correlation spectroscopy (FCS) was employed to examine the effects of four oxygen scavengers, glucose oxidase (GOD), Trolox™, propyl gallate (PG), and mercaptoethylamine (MEA) on the triplet states and photobleaching of R6G and fluorescein. A figure of merit was employed to determine the overall effectiveness of the oxygen scavengers in producing the maximum emission from fluorescent molecules.

Acknowledgements

I owe an enormous debt of gratitude to many people for supporting me through the (many) years of my doctoral degree. There is no way I could have made it through these grueling years without love and encouragement from my friends and family. To everyone who listened to even five minutes of my grumbling and tirades on the state of my graduate career, I thank you. To my Mom, Dad, Step-Mom, Marilyn, Nancy, and Teresa - you've been with me through it all, and I couldn't have finished this without you. I also owe thanks to my thesis advisor Daniel Chemla and to Shimon Weiss for providing me with plenty of funding, a great lab in which to do my research, and quite a lot of patience. I also thank the National Physical Sciences Consortium and Lawrence Livermore National Laboratory for supporting me with a terrific fellowship.

To all my friends at LBL and my classmates in the physics department, I'm going to miss you terribly. I doubt I will ever manage to find such high quality slacker vortices anywhere else. To Gino Segre, Andreas Schumacher, John Corson, Neil Fromer, Dave Klein, Peter Kner, and Jocelyn Grunwell, thanks for making life at LBL fun. To my dear friends Jeff Moehlis, Rich Mallozzi, and Kristine Lang, I promise that one of these days you'll get over the shock of finding out I've actually finished.

Table of Contents

Chapter 1

Introduction to single molecule detection and fluorescence

A brief history of single molecule detection

The ability to perform experiments on single molecules has opened up new areas of physics, chemistry, and biology. Measurements of single molecule quantum jumps [1], spectral diffusion [2,3], photon antibunching [4] and other quantum phenomena has offered new insights into photophysical properties of fluorescent molecules and local environmental effects on quantum systems. Single chemical reactions can be measured, and previously low-yield reactions can now be monitored within confined geometries [5]. Diffusion in two dimensional lipid bilayers has been recorded [6], and the interaction of diffusing molecules with surface charge double-layers has been studied [7]. There has been a revolution in biological experimentation brought about by the ability to fluorescently tag and monitor single molecules via optical techniques such as confocal microscopy, evanescent field imaging, and wide field imaging. Single ATP turnover events [8], DNA folding, and peptide folding [9] have been observed. Motor protein studies have perhaps benefited the most to date from the application of single molecule techniques, allowing the motions of single kinesins along microtubules [10] and conformations, rotations, and step-wise mechanical motions of myosin along actin filaments to be recorded [11-13]. Most dramatically, the "rotational catalysis" model of the F1-F0 ATPase (a.k.a. H^+-ATP synthase) complex was

finally proven beyond doubt by the group of Kinosita by imaging individual molecular rotor complexes in motion [14].

The field of single molecule detection (SMD) and spectroscopy (SMS) has seen enormous growth in the past ten years since single molecules were first isolated at liquid helium temperatures in solid matrices by W.E. Moerner [15] and Michel Orrit [16]. Talks and seminars on the subject of single molecules have graduated in the past decade from audiences of 15 to 20 people to full conference ballrooms. The appeal of single molecule measurements becomes clear when they are compared to traditional ensemble techniques. In ensemble measurements, the behaviors of an enormous number of individual molecules are averaged together to result in the measurement of one particular bulk behavior. When this is done, the distribution of properties within the ensemble is lost, and rare events are impossible to detect. For systems with a large degree of inhomogeneity, which is often the case in complex living systems, knowledge of the distribution of properties is invaluable. When measurements are done on the single molecule level, it is possible to recover property distributions, to detect rare events, to observe the trajectory of a molecule's behavior, and to evaluate how a molecule's interaction with its local environment changes in the course of time. It is also possible to view molecular kinetics on the single molecule level without the need to synchronize events. Examples of this include photophysical processes, protein or nucleic acid folding, and enzymatic reactions. In some cases ensemble measurements on a system are simply not possible, due to small amounts of the sample being studied.

Techniques for single molecule detection are varied, each with its own particular strengths and weaknesses. Mature scanning probe microscopies such as atomic force microscopy (AFM) and scanning tunneling microscopy (STM) are powerful methods of

imaging and performing spectroscopy on single atoms and molecules. STM sample requirements are very restrictive and the best STM work is done in vacuum, which precludes active biological samples. STM and AFM are also limited to samples that are immobilized or bound to surfaces, and while AFM has been applied with good results to biological systems in solution [17,18], it is difficult to use AFM to study rapid processes such as enzymatic catalysis and chemical reactions.

If the focus of a measurement is on a macromolecule of biological interest, a probe microscopy is often considered overly invasive. While optical techniques have the disadvantage that their spatial resolutions are typically diffraction-limited to on the order of half the wavelength of light used, they are often preferable for use with biological systems. Optical methods can be applied non-invasively not only to molecules bound to surfaces but also to molecules embedded in matrices, freely diffusing, or in living cells. Fluorescence methods are particularly valuable, since they usually result in high signal-to-background ratios. With the wide range of fluorescent probes and indicators currently available, it is now possible to measure local pH, Mg^{2+}, Ca^{2+}, Na^{+}, and K^{+} concentrations, as well as electrical potentials, solvent exposure, aggregation, and rotational properties of molecules. In order to obtain single molecule resolution via optical methods, it is necessary to spatially separate the molecules of interest by either immobilizing them far apart on a surface or in a gel, or by working with such low concentrations in diffusion that the probability of finding more than one molecule in the excitation volume is negligible. In addition, fluorescence measurements applied to single molecules have the requirements of specific labeling and low false positive detection. It should be remembered that in all types of single molecule measurements, the observation of a behavior on a single molecule is

insufficient and that statistics on many molecules are required to determine the precise distribution of properties present within a given population of molecules.

Single molecule optical detection was first achieved at cryogenic temperatures by the group of W. E. Moerner. Their technique, which utilized the selective absorption of locally-perturbed single dopant molecules within an inhomogeneously broadened population in a p-terphenyl crystal, allowed the photophysical properties of single molecules to be resolved for the first time. The frequency selection technique allows the investigation of a broad range of quantum phenomena at low temperatures but is not generally applicable. The room temperature isolation of a single molecule was first achieved by Keller and others in a focused hydrodynamic flow [19]. In their case, the molecule detected was the multichromophoric phycoerythrin B which has the effective brightness of ~ 25 fluorophores. The first observation of a single fluorophore at room temperature was achieved by Shera et al [20] by measuring bursts of fluorescence emission from molecules moving through a flow cell.

It was the measurement of the photophysical properties of a single immobilized fluorophore by the hybrid technique of near-field scanning optical microscopy (NSOM) that energized the field. NSOM was developed by Eric Betzig in order to overcome the diffraction limit of conventional far field optics [21-23]. NSOM beats the diffraction limit by localizing excitation in the near field, passing light through a tapered, metal-coated fiber tip and placing the tip close enough to a fluorescent molecule (through AFM-like shear force feedback) to excite the molecule with the emitted evanescent field. The fluorescence from the molecule is collected by conventional high numerical aperture far field optics. The spatial resolution of the technique is limited by the tip size itself (usually on the order of

50-100nm). NSOM allows such optical measurements as single molecule spectroscopy [24], energy transfer [25], and dipole orientation [23]. NSOM, however, suffers from the drawbacks of tip irreproducibility, low throughput powers, and sample perturbation by the tip itself. NSOM is currently not applicable to biological samples in solution.

In some cases it is possible to trap single molecules [26, 27] and apply optical or physical techniques such as stretching or twisting to gain knowledge of the material or mechanical properties of biological molecules. Examples of this include measurements of double-stranded and single stranded DNA persistence lengths [28], observation of domains within titin muscle proteins [29], and studies of the elasticity of supercoiled DNA [30]. These types of trapping require either a large molecule such as lambda-DNA or attachment of the molecule of interest to a larger particle such as a bead, which is not feasible in most cases of smaller molecules such as single proteins or enzymes.

Far field optical detection of immobilized single molecules at room temperature got its start with work by the group of Rigler and by Trautman and Macklin. Dapprich et al [31] immobilized dye molecules in gel and utilized confocal scanning microscopy to image single molecules. Trautman and Macklin obtained information on the spectral fluctuations and lifetimes of dye molecules immobilized in a polymer matrix and compared the information obtained with far field to the same type of molecules examined via NSOM [32,33]. They found that in exchanging NSOM measurements for far field ones, information such as detailed dipole orientation information and spatial resolution are lost while non-invasiveness and higher data acquisition rates are gained. The increase in the data acquisition rate with far field measurements allowed the obtainment of single molecule lifetimes for the first

time. Far field excitation results in signal to noise that is superior to NSOM since it is possible to use higher excitation powers without the concerns of heating a metal tip.

Others soon followed the lead of Trautman, Macklin, and Rigler in switching to the much easier far field experiments, and the technique of NSOM was quickly left in the dust. In addition to far field confocal microscopy, wide field techniques to detect single molecules were also developed. With the improvement in detectors and filters for blocking Rayleigh-scattered excitation light and other background fluorescence, it became possible to capture wide-field CCD images containing several individual molecules [8, 34]. Evanescent field imaging via total internal reflection geometries got around background problems by confining excitation volumes to the ~ 180nm evanescent field, using either a prism or the objective itself to form the evanescent field. Two-photon microscopy has also found a place in the single molecule field [35, 36], since it offers superior background reduction over one-photon techniques. The excitation volume defined by two-photon absorption depends on the square of the excitation intensity rather than linearly on the intensity, resulting in a smaller overall excitation volume for Gaussian input beams. This is especially useful in optical sectioning, since any bleaching of the sample will occur in the reduced region of absorption, allowing better imaging of consecutive sections. Since the two-photon absorption involves two long wavelength photons, the fluorescent emission will typically be at a shorter wavelength than the excitation. The contribution of autofluorescence to the background in fluorescence measurements dies off the farther into the red one excites, so the overall background for two-photon measurements can be reduced over that of one-photon. The current difficulty with two-photon techniques lies in finding fluorophores with sufficient absorption and photostability properties.

Once single molecule far field detection became routine, photophysical issues such as dark states and quantum jumps [1], spectral fluctuations [3], and rotational jumps [37] of surface-immobilized molecules were pursued. Once researchers began to obtain a better understanding of the photophysics involved in single molecule fluorescence measurements, they began to turn their attention towards applying these ultrasensitive methods to problems in biology and chemistry. An important example of this is the application of single-pair fluorescence resonance energy transfer (spFRET) to biological systems. spFRET was first demonstrated by Ha, et al, on double stranded DNA under non-physiological conditions [25]. The details of spFRET and its application to a DNA hairpin system will be discussed in Chapter 6. The application of single molecule detection and spectroscopy to the study of biological systems is currently one of the hottest areas of research in biophysics. Work by the groups of Yanagida and Kinosita on motor proteins and Lu, Xie, and Yeung on enzymatic catalysis [38,39] are leading the way in this rapidly expanding field. It has taken not even a decade for the first single molecule experiments to blossom into an entire fast-moving field of research.

Fluorescence: A Description

A Jablonksi diagram for the absorption and emission processes of a typical fluorescent molecule are shown in Figure 1. At room temperature, since the difference in energy between vibrational levels is on the order of 150meV, there is not enough energy to populate a significant number of the excited vibrational states of the singlet S_0 electronic level. Upon absorption of a photon, an electron is typically promoted to one of the higher

vibrational levels of the first excited electronic state S_1. Absorption is a very fast process, occurring on a femtosecond time scale. From one of the higher S_1 vibrational states, a fluorophore in condensed phase rapidly undergoes internal conversion to the lowest vibrational S_1 state, and this typically occurs on a picosecond time scale. The lifetime of the excited state varies from fluorophore to fluorophore and is very sensitive to the local environment, with most fluorophores having a lifetime around 10 nanoseconds in standard solvents. From the lowest vibrational level of S_1, the fluorophore has several possible relaxation pathways, and fluorescence occurs when a photon is emitted as the molecule relaxes from the S_1 to the S_0 level. The molecule can relax to any of the S_0 vibrational levels, and internal conversion rapidly converts the molecule to the lowest S_0 vibrational state. The second relaxation pathway is by nonradiative decay from S_1 to S_0. This can occur via several mechanisms, including collisional quenching and fluorescence resonance energy transfer (FRET). The molecule can also undergo intersystem crossing from the S_1 to the first excited triplet state, T_1, but since this is a spin-forbidden transition, the rate is slow for most fluorescent molecules (100-1000 times slower than the S_1 to S_0 transition rate). Once in the triplet state, the molecule may find its way to the singlet ground state by either nonradiative processes or by emitting a phosphorescence photon. Because this final relaxation is also a spin-forbidden transition, the lifetimes of triplet states can be quite long, lasting from microseconds to seconds. Factors from the environment can affect the triplet state lifetime as we will see in Ch. 4.

Since absorption occurs from the lowest S_0 vibrational level and emission occurs from the lowest S_1 vibrational level, the absorption spectrum of a fluorescent molecule reflects the S_1 vibrational levels while emission reflects the S_0 vibrational levels. Usually

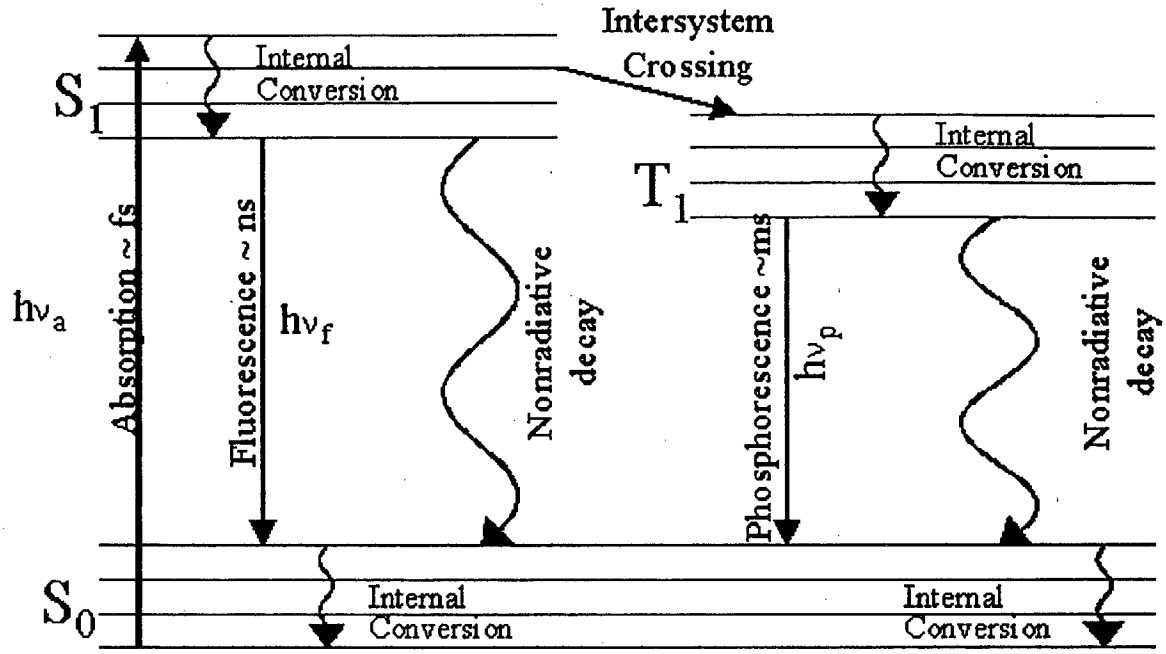

Figure 0: Jablonski diagram for a typical fluorescent molecule.

these two spectra are mirror images of each other, and this behavior is expressed in the Franck-Condon principle, which says that all electronic transitions are vertical. The emission spectrum of a fluorescent molecule is independent of the excitation wavelength, since any excitation higher than the lowest vibrational level of S_0 rapidly decays via internal conversion to the lowest S_0 level (Kasha's rule). A Stoke's shift is observed between the excitation wavelength and the emission wavelength, because excitation into the S_1 levels is rapidly followed by energy loss due to internal conversion in condensed phases. In addition, the fluorescence relaxation is usually to one of the higher vibrational levels of S_0. Since the wavelength separation of the emission from the excitation allows the efficient filtering of excitation light from the fluorescence measurement, this Stoke's shift makes background-free single molecule fluorescence detection possible.

The absorption and emission spectra of a fluorescent molecule are not fixed; they can be greatly affected by the local environment of the fluorescent molecule, and this sensitivity has been utilized for many years to study the immediate environments of fluorophores, most notably using the amino acid tryptophan. The spontaneous diffusion of single molecule spectra have been studied by several groups (Moerner; Orrit, Wild, Basche, Xie, Ha). This type of diffusion can occur either on slow (~ tens of seconds) timescales [3] or quite rapidly (< 1ms) [25]. The changes in spectrum are related to the local environment and sudden chemical changes of the fluorophores (Figure 2). Fluctuations in absorption can lead to fluctuations in overall emission intensity, since diffusion of the absorption peak away from the excitation line used will result in a lower fluorescence output.

In some cases the change of spectrum is due to a simple chemical reaction such as a protonation or deprotonation event. This will be seen in the discussion of the fluorescent molecule seminapthorhodafluor (SNARF) in Ch 5. For molecules such as green fluorescent protein (GFP) it is believed that an internal protonation event can lead not only to a change in spectrum but to a complete cessation of emission, known as a dark state [40]. When this occurs on the appropriate observation time scale, a "blinking" behavior is observed in which the molecule goes repeatedly from a fluorescent to a non-fluorescent state. For GFP, this reaction is understood, but for many other fluorophores that show similar dark states and blinking behaviors, the cause remains a mystery.

Another notable feature of fluorescent molecules is their propensity to undergo an irreversible photochemical reaction upon excitation. This process is known as photobleaching, and it often makes fluorescence experiments difficult. This difficulty

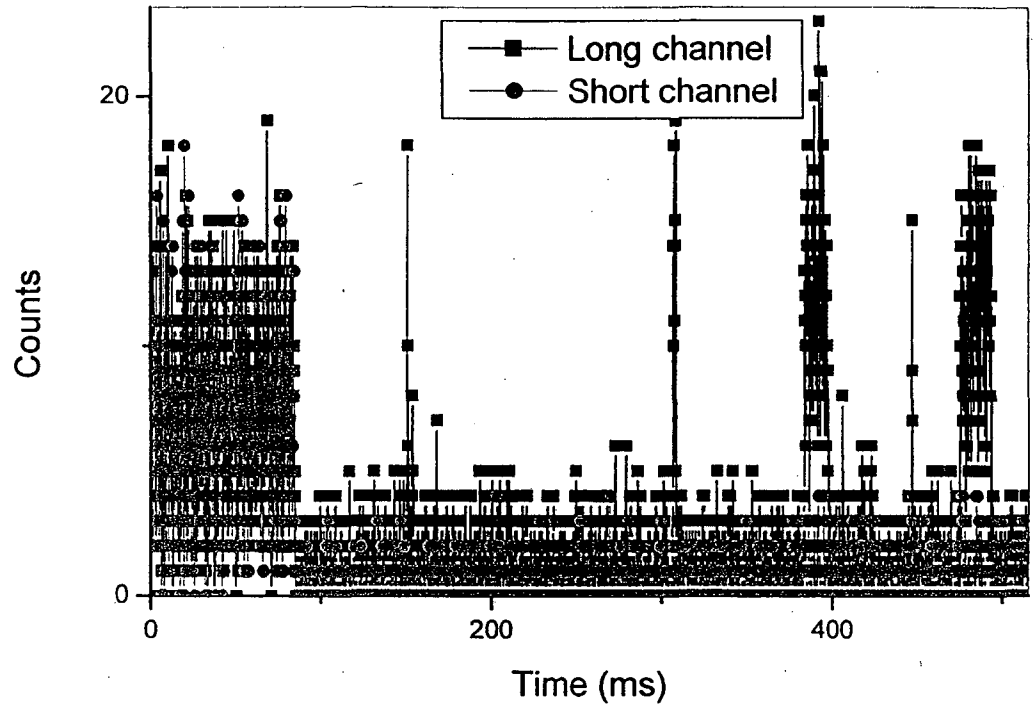

Figure 2: Example of spectral jump. Fluorescence emission from a SNARF molecule immobilized on a surface. The long wavelength channel (>610nm) is shown in black while emission from shorter wavelengths are shown in gray.

arises not just on the single molecule level but in any application involving fluorophores, whether confocal microscopy sectioning of cells, FCS measurements, or FRET measurements. Radicals such as singlet oxygen are believed to be behind the photodestruction phenomena, and researchers have gone to great lengths to rid their systems of such radicals. Our efforts on this front will be presented in Chapter 6.

Chapter 2 describes the details of the experimental apparatus used for the measurements presented in this thesis. Chapter 3 contains descriptions of some of the various sample preparation techniques used and a discussion of some of the important aspects of immobilization strategies for single molecule experiments. The study of DNA hairpin fluctuations is presented in Chapter 4. Chapter 5 deals with the model system of

the pH indicator SNARF, specifically, using SNARF to measure subpopulations and examine local environments. The technique of fluorescence correlation spectroscopy (FCS) is introduced in detail in Chapter 6 and aspects of photobleaching and our work on oxygen scavenging systems are presented.

Chapter 2

Description of Experimental Techniques

Far field fluorescence detection (Figure 1)

The primary component of the single molecule detection and spectroscopy experimental apparatus is a Zeiss Axiovert 100 inverted optical microscope, used in the epifluorescent geometry. The optical path has been modified to allow excitation from the side of the microscope. Depending on the absorption spectrum of the fluorescent molecules involved, an air-cooled argon laser (488, 514nm), a helium-neon laser (632nm), or an argon-pumped dye laser (tunable from 570 to 640nm) is used for excitation. The optical path to the microscope includes line filters to remove unwanted spontaneous emission from the laser, an electro-optic modulator to control polarization or power, and wave plates to further correct the polarization properties of the excitation light. The laser light is passed through a single mode optical fiber prior to entering the microscope. The fiber serves as a spatial filter, with the output end of the fiber acting as a point source and produces a clean Gaussian excitation beam profile. In order to improve signal to noise, the excitation and collection volumes are minimized by the use of a high numerical aperture objective lens

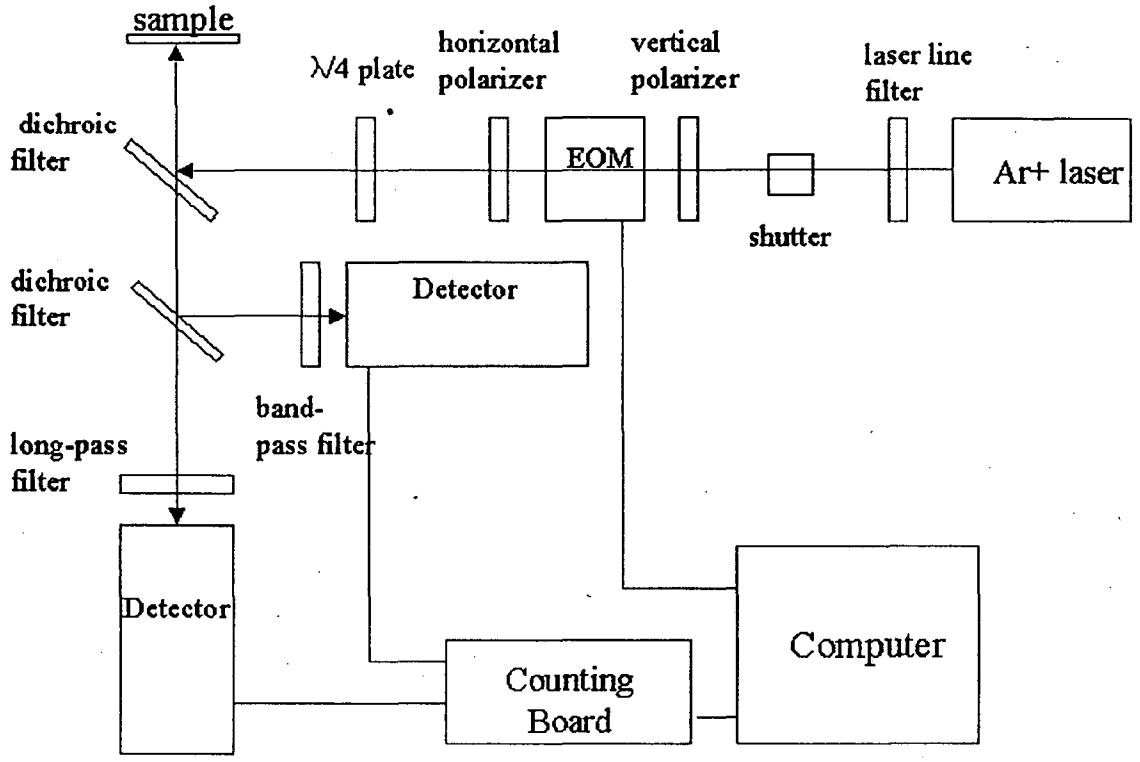

Figure 1: Schematic of the experimental apparatus.

(typically 100X, 1.4 NA Zeiss Infinity-Corrected) which forms a diffraction-limited focal region. The same objective lens is used for excitation and collection. A confocal geometry is also employed, in which a pinhole is placed after the objective in the fluorescence emission path to further constrain the effective sample volume by filtering out unwanted background light from out-of focus regions. Pinhole selection is often crucial to an experiment, since selection of too large a pinhole results in excess contribution to background while too small a pinhole rejects too much of the desired signal. The emission light is sent either to avalanche photodiode detectors (APDs) or to a Spex imaging spectrometer. In the case of the APDs, one-to-one imaging of the confocal pinhole onto the APD detection area (~150μm diameter) is performed. The avalanche photodiode detectors

are AQ 141 photon counting modules from EG&G-Canada with high quantum efficiencies (>50%) over the visible range and dark counts of less than 100. Since there is a non-negligible detector dead time, the detectors saturate at a level of approximately 2 MHz. Photon counts received by the detectors are converted to TTL pulses that are amplified and stretched before being sent to a National Instruments PC TIO-10 counting board. The overall collection efficiency of the system is estimated to be 2 to 5%, depending on the type of measurement being performed. In the case where two detectors are used, the emission is split by either a dichroic mirror (for spectral measurements) or a polarizing beam splitter cube (for polarization anisotropy measurements). Notch filters and long pass or band pass filters are employed to reduce cross talk and laser leakage into the detectors.

Sample Positioning

Coarse x-y-z positioning of the sample is done via the microscope stage micrometers. For raster-scanning the sample in imaging applications and to collect time traces on immobilized samples, a piezoelectric scanner is used. A photo of the scanner is shown in Figure 2. The scanner consists of three piezoelectric tubes sectioned into four outer quadrants and wired such that when a motion in the x direction is desired, the tubes bend along two oppositely positioned quadrants in either the plus or minus direction, depending on the polarity of the applied voltage. Friction between the bottom of the aluminum sample holder and the sapphire balls that top each of the piezo tubes moves the sample with the tubes. The same is true for the y direction, and so by ramping the voltage in the x direction, slowly incrementing the y voltage, and simultaneously monitoring the fluorescence signal, an image is formed of the sample's fluorescence. For obtaining time

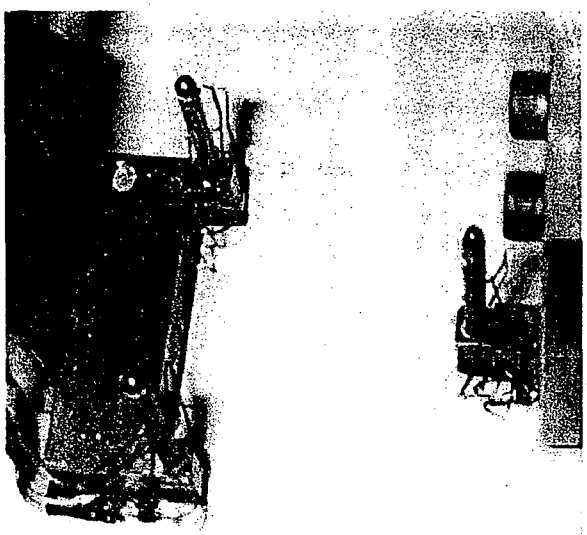

Figure 2: Picture of piezo scanner.

traces, the voltage can again be modulated to scan the sample and when a fluorescent molecule is found the stage is frozen until all data is collected from that molecule [41] . In this manner, data on hundreds of molecules can be collected from a single sample. The linear range of the piezos used in our experiments was 10μm x 10μm in the x-y plane. By changing the voltage between the insides and outsides of the three piezos simultaneously, the sample can be moved in the z-direction. The range of z motion of our piezos was limited to 1.5μm. The sample cells used vary depending on the type of measurement being performed. With flow cells it is possible to exchange fluids using a single sample, and heater units allow the measurement of changes due to temperature.

Polarization Modulation

For polarization modulation measurements, the electro-optic modulator was used to vary the direction of the linear polarization of the excitation, with the emitted fluorescence being split onto the two detectors with a polarizing beam splitter cube. By analyzing the polarization state of the emission compared to the excitation polarization state, it is possible to extract information about the rotation freedom of the fluorophore [37]. For example, if the absorption moment of the fluorophore is fixed (and hence the emission dipole moment is also fixed) then there will be a modulation in the total intensity

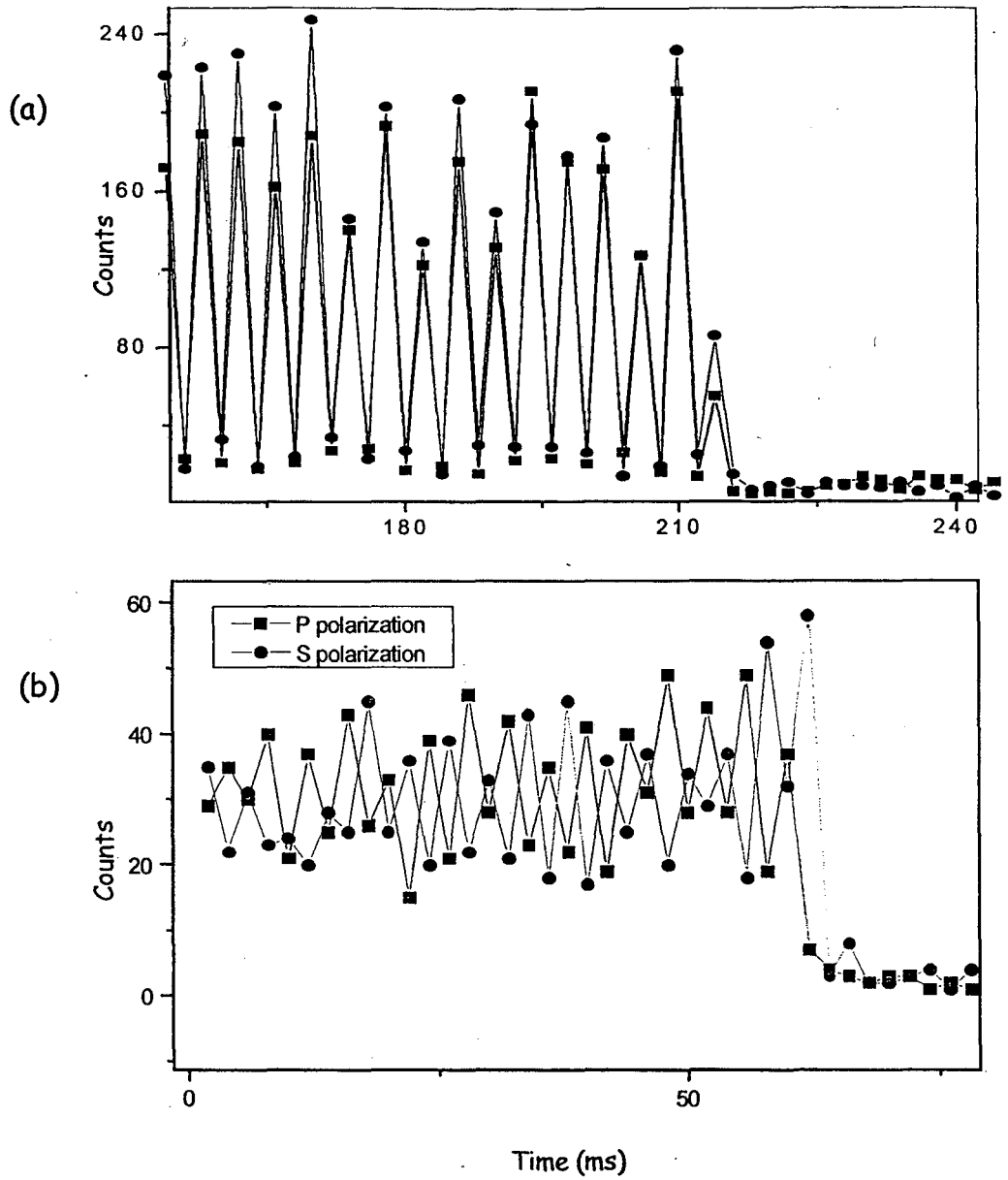

Figure 3: Polarization modulation time traces. A fixed fluorophore is shown in (a) and a freely rotating fluorophore is shown in (b).

of the fluorescence emission as the plane of the linear excitation polarization is rotated. If the fluorescence emission is broken up into its s and p components, then information about the orientation of the emission dipole may be obtained. For an emission dipole there will be modulation in the s and p channels as the plane of the excitation polarization is rotated. If

the emission dipole is fixed, the signals measured on the s and p channels will be correlated with one another (Figure 3(a)). If, however, the emission dipole is rotating faster than the experimental integration time but slower than the fluorescence lifetime, the signals on the s and p channels will be anticorrelated (Figure 3(b)). If there is restriction in the fluorophores freedom of rotation, the phase shift between the signals will not be 180 degrees but will have a phase dependent on the amount of restriction and the speed of rotation. If the fluorophore is rotating faster than the fluorescence lifetime, the polarization of its emission will be randomized and there will be no correlation between the two polarization channels. The rotational freedom of the fluorophore covalently bound to a biological macromolecule can give information on the motion of the macromolecule itself in some instances, since a fixed fluorophore implies a likewise fixed macromolecule. A rotationally free fluorophore does not, however, imply a free macromolecule.

Spectral Fluctuations

Spectral fluctuations can also be resolved by performing two channel measurements with the emission split onto the two channels by a dichroic with a spectral cutoff centered at the peak of the emission of the fluorescent molecule. Fluctuations around the spectral mean result in correlated intensity fluctuations on the two channels. For fluctuations in the absorption properties of the dye, there is an overall increase or decrease in the fluorescence intensity as the peak of absorption moves closer to or farther away from the wavelength of the laser excitation. Fluctuations in the emission spectrum result in anticorrelated emission on the longer and shorter wavelength channels with no change in the overall emission intensity. Changes in the absorption and emission spectra of

the dyes are typically due to changes in the local environment (eg the local hydration of the dye changes) or changes in the dye structure (eg protonation and deprotonation events).

Methods of data collection

Data is collected in several different fashions. For fluorophores freely diffusing in solution, either Fluorescence Correlation Spectroscopy (FCS) is performed or fluorescent bursts are collected. For immobilized molecules, imaging can be done and if a single molecule is isolated in the focal spot, traces of the fluorescence intensity versus time can be recorded or a single molecule spectrum can be obtained for particularly long-lived molecules. Each method of data collection used depends on the type of biophysical measurement being performed, and the experimental parameters for the different types vary significantly. Individual experiments utilizing these techniques are described in more detail in the following chapters.

Fluorescence Correlation Spectroscopy (FCS)

Fluorescence correlation spectroscopy, or FCS, was introduced in 1972 by Magde, Elson, and Webb [42]. FCS is not typically a single molecule technique but rather is applied to small ensembles of molecules. A small ensemble of molecules is created through the combined use of low concentrations of molecules, high numerical aperture objectives, and confocal pinholes (Figure 4). The idea behind FCS is that any behaviors of fluorescent molecules that produce fluctuations in the overall observed fluorescence show up in the

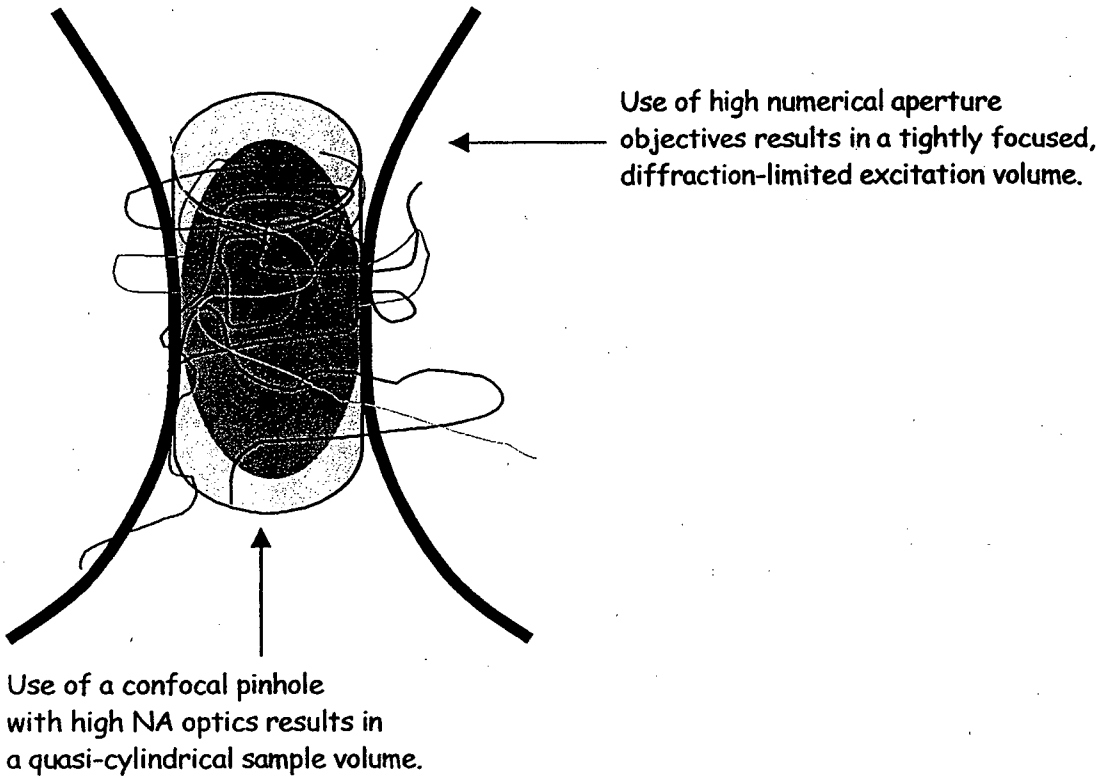

Figure 4: Cartoon of FCS sample volume.

autocorrelation function of the intensity. With the appropriate model of the system under observation, the timescales of the various behaviors can be extracted. Examples of behaviors of fluorophores that can produce fluorescence fluctuations include diffusion into and out of the sample volume, intersystem crossing to the triplet state, extended dark states, and protonation-deprotonation events. Cross-correlations between two distinct spectral channels can also be performed, for example in the determination of co-localization properties of molecules and in Fluorescence Resonance Energy Transfer (FRET) measurements. Autocorrelations can be performed on the fly by special hardware or by software after data collection. The FCS measurements presented in this thesis all utilized software correlations.

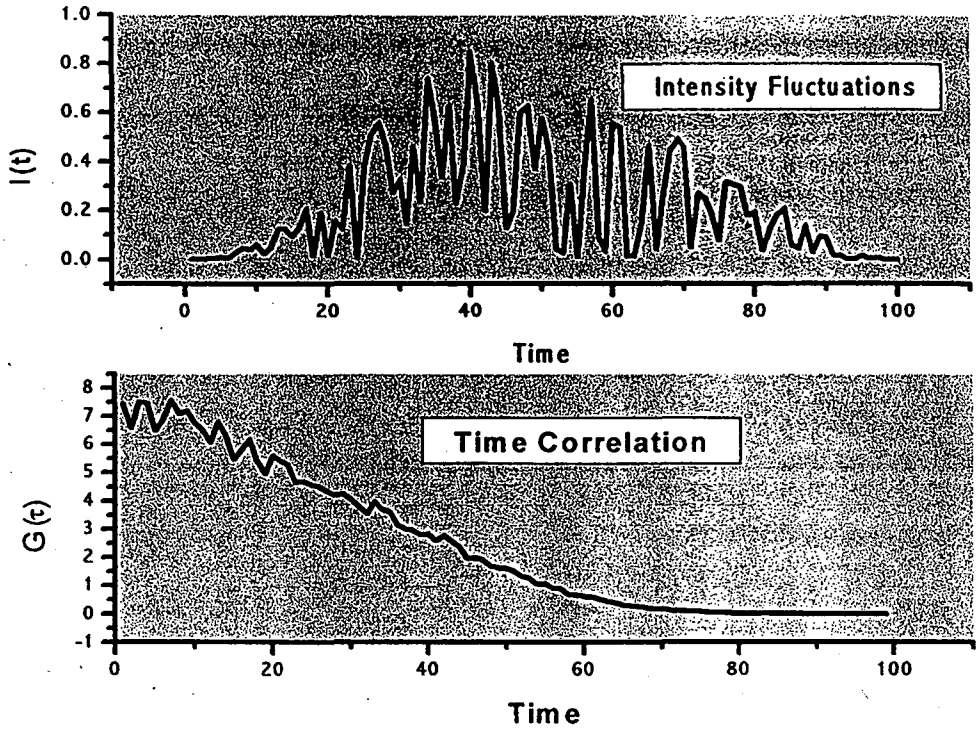

Figure 5: Simulated fluorescence intensity fluctuations and calculated autocorrelation.

FCS is beneficial in cases in which information is desired on processes that occur on a time scale faster than the typical diffusion time of a molecule through the excitation volume. Due to shot noise contributions at low signal level, it is difficult to obtain an adequate signal to noise ratio for single molecule fluorescence intensity measurements on short timescales. Because most often FCS measurements employ higher concentrations of molecules (typically 1 - 10nM), signal to noise does not present a difficulty, and data acquisition can be extended to reduce the noise in the autocorrelation function itself. The difficulty in FCS comes from the model used to fit the data. Often several models must be applied before acceptable fits to the data are obtained, and in some cases the model is very dependent on optical properties. Models for simple processes such as diffusion through the

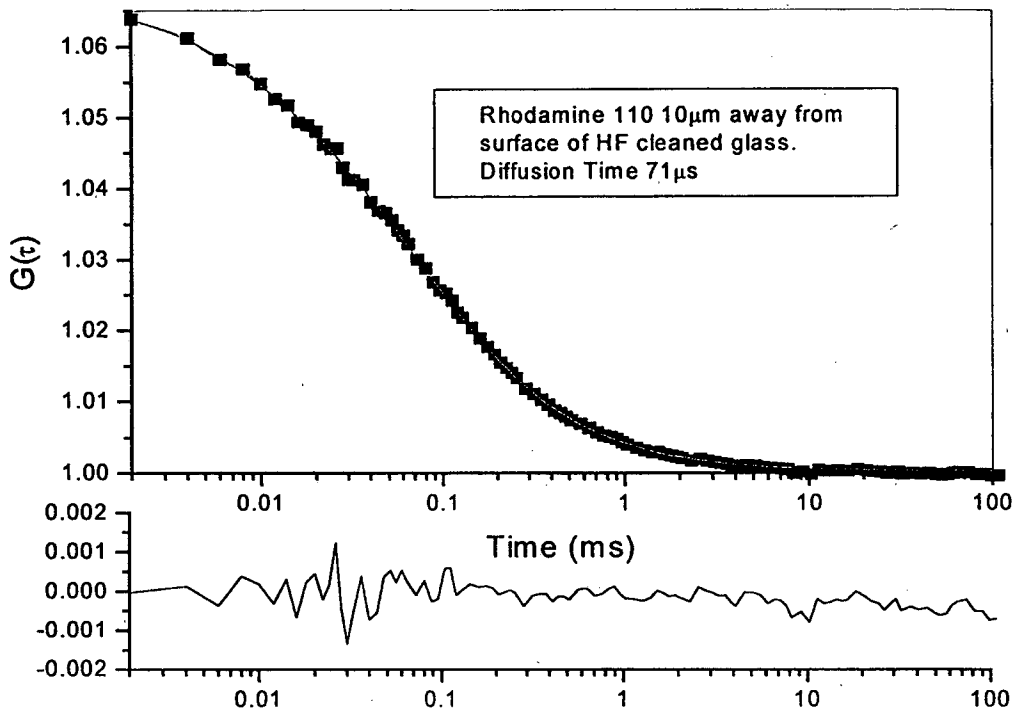

Figure 6: FCS trace of freely diffusing Rhodamine 110 dye with fit using equation (1). The lower trace shows the residual.

excitation beam and intersystem crossing were developed primarily by Rigler et al and are robust and widely-used [40, 43, 44]. A typical fluorophore diffusing in a solvent will display an autocorrelation trace similar to that shown in Figure 6 and can be fit with an expression of the following form:

$$G(\tau) = \frac{\langle I(t)I(t+\tau)\rangle}{\langle I(t)^2\rangle} = \frac{1}{N(1-F_{triplet})}\frac{1}{1+\frac{\tau}{\tau_{diff}}}\left[F_{Triplet}e^{-\tau/\tau_{Triplet}} + (1-F_{Triplet})\right] + DC \qquad (1)$$

Here the effective sample volume with N molecules is assumed to be cylindrical with a diffusion time across the volume of τ_{diff} and a fraction, $F_{triplet}$, of the molecules in the triplet state with a lifetime of $\tau_{triplet}$. Any other timescales must be integrated into the basic formula that includes the diffusion and triplet states.

Single Molecule Diffusion

In cases where equilibrium population distributions are desired, fluorescence bursts of single molecules diffusing through the excitation beam can be collected. An example of this is shown in Figure 7. These bursts can be analyzed for statistics such as duration and burst height or for two channel measurements such as FRET or polarization anisotropy. Thresholds are set on data from the channels in order to adequately remove erroneous bursts from background but not cut out too much of the actual single molecule signal. Because of computer overhead, the time resolution for fluorescent burst collection and time trace collection presented in this thesis was limited to 0.2ms, and data from fluorescent bursts is analyzed per point, rather than per burst.

Diffusion measurements have the advantages that a large amount of statistics can be gathered in a relatively short amount of time, populations are easily distinguished, and there are no perturbations from environmental factors such as proximity to surfaces. In many cases, however, it is desirable to examine a single molecule for an extended period of time, for example in protein folding, catalysis, or motor protein measurements. In these cases, some way of immobilizing the molecule of interest must be found. An ideal immobilization strategy would not affect the primary functions of the molecule. Methods for immobilization are varied, ranging from electrostatic trapping and covalent bonding to

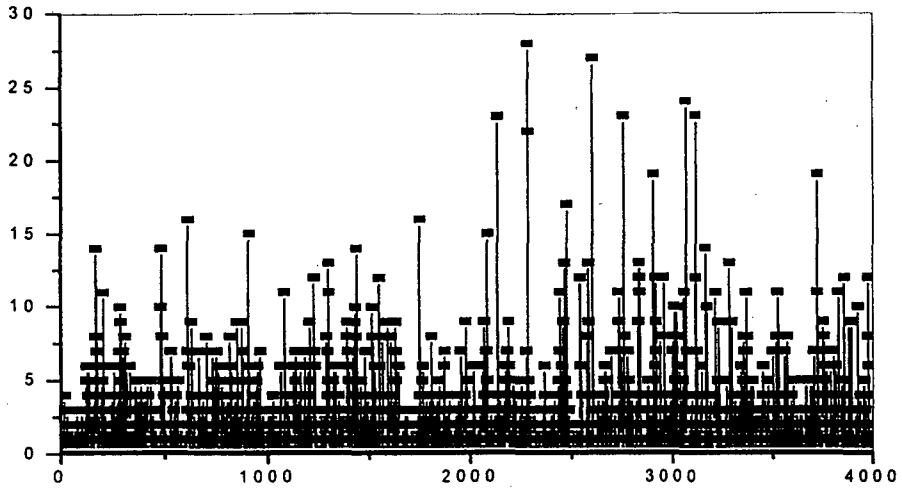

Figure 7: Example fluorescence bursts in time trace of freely diffusing single molecules.

physically trapping molecules in containers such as vesicles or the pores of gels. A large part of this thesis work dwells on the issues of immobilization techniques. The details of surface immobilization strategies will be discussed more fully in Chapter 3.

Single Molecule Imaging and Time Traces

As was mentioned briefly before, images of single molecule samples are acquired by raster-scanning the sample over the excitation beam focus. When a fluorescent molecule passes through this focus, a burst of fluorescence emission is recorded by the APDs. The intensity of emission as a function of sample location forms the image of the sample. A fluorescent molecule is much smaller than the area of the laser focus, which is typically diffraction-limited to 0.25-0.4μm in diameter, depending on the wavelength and objective used. When a fluorescent molecule is scanned across the excitation beam, the fluorophore acts to map out the excitation area in the x-y plane, giving a spot in the image that is the

cross-section of the laser focus at the location of the molecule. And example of an image formed in this fashion is shown in Figure 8. In cases where two detectors are used to examine the fluorescence emission, the images formed by the two detectors are collected simultaneously pixel by pixel.

Sometimes it is desirable to isolate a single molecule and watch its behavior over time. In such cases the data collected using APDs takes the form of a fluorescence intensity time trace. Such a time trace is shown in Figure 9. Depending on the time resolution of the measurement, various aspects of a fluorophore's behavior can be examined, including passages to the non-emitting triplet state, dark states, and photobleaching. For both images and time traces, the clear resolution of such photophysical behaviors is used as proof that there is a single molecule under observation. Photodestruction can be clearly resolved in both the image shown in Figure 8 and the time trace shown in Figure 9. This type of abrupt end to fluorescence is indicative of the photobleaching of a single molecule. When more than one molecule is present, photobleaching typically produces decreasing steps in the measured fluorescence intensity, unless there are a large number of molecules under excitation, in which case the fluorescence is seen to decay gradually until steps appear.

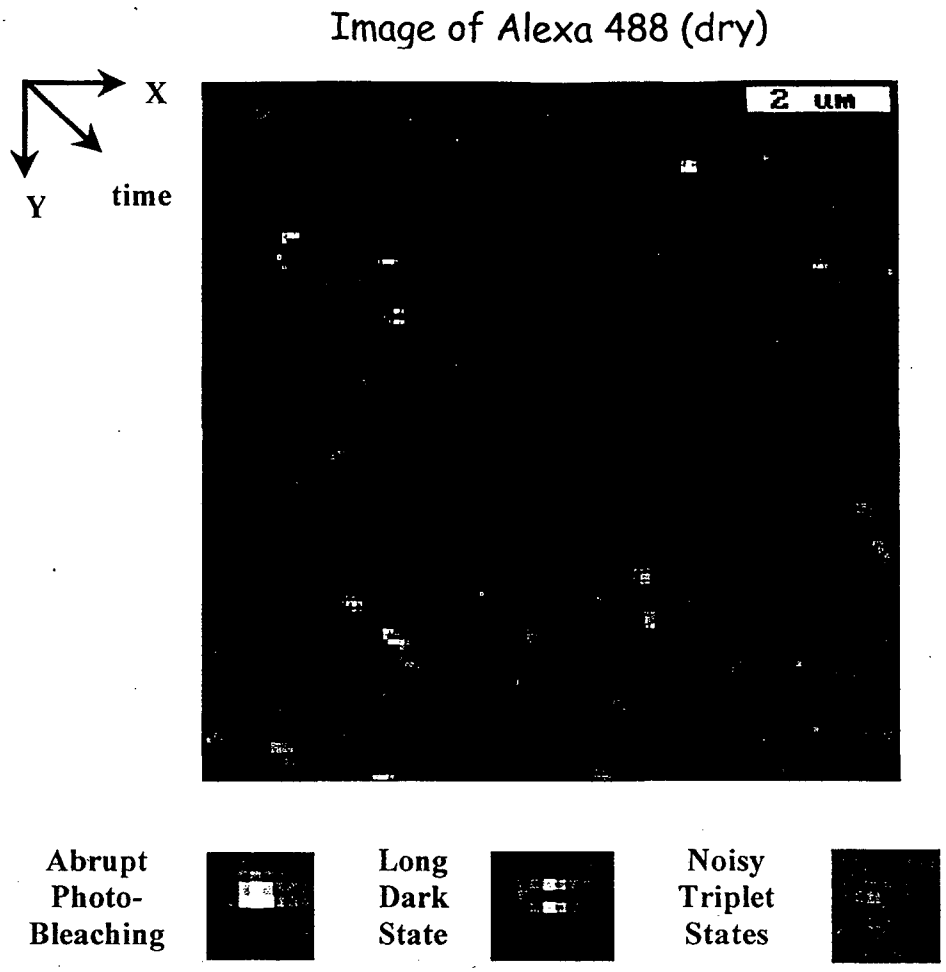

Figure 8: Image of individual Alexa 488 dye molecules.

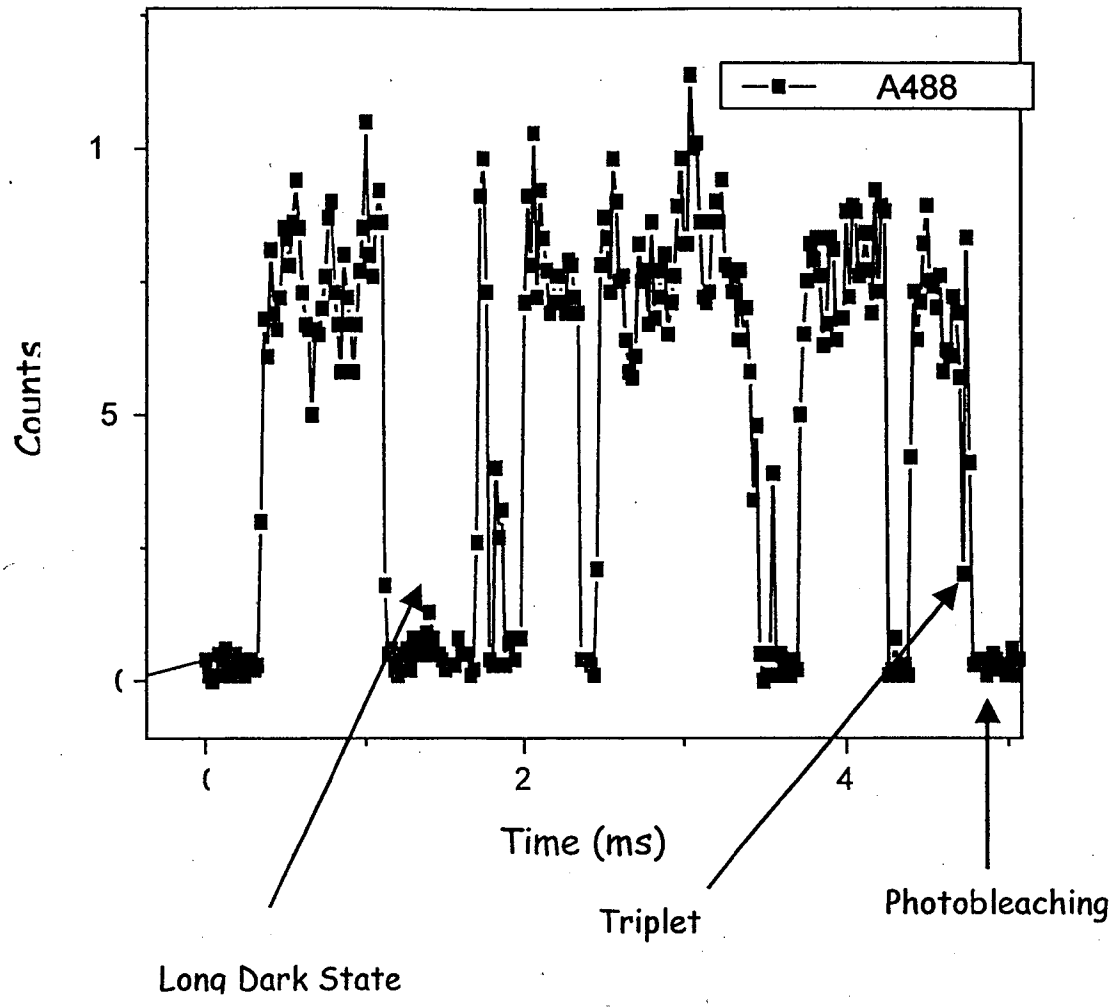

Figure 9: Example of fluorescence intensity versus time (time trace) taken on a single Alexa 488 molecule.

Chapter 3

Immobilization Strategies

Introduction

For single molecule measurements in which the time scales of the process under investigation are sufficiently long, it is often desirable to isolate one molecule and watch its behavior over time. For this to be possible, the molecule must be trapped within the excitation beam in some fashion. The simplest method of immobilization can be accomplished by charge interactions that involve trapping the molecule on a glass surface that has been treated such that its charge is the complement of the molecule to be trapped. This was the first type of surface immobilization technique applied in our laboratory, used to trap dye-labeled DNA molecules on glass. While this is an effective and often desirable way to immobilize single molecules, nonspecific binding to surfaces can cause problems in certain measurements, since interactions with the surface can change the nature of a molecule's behavior. If the exact nature of attachment to a surface is unknown, interpretation of data can be difficult. To circumvent this problem, strategies were developed to attach macromolecules to glass surfaces in a specific manner. These include chelated linkers, biotinylated BSA-streptavidin-biotin linkages, covalent binding of streptavidin to surfaces followed by biotin-streptavidin binding, dextran immobilization, and

chemoselective ligation. Each type of immobilization strategy will be summarized below, with detailed sample preparations listed in the Implementation section at the end of this chapter. Since silanization is often the secondary step in these preparations, the silanization process will also be described.

Silane chemistries: Figure 1

The use of silanes allows the functionalization of glass surfaces with an enormous variety of chemical groups. The formula for an organosilane is $R_nSiX_{(4-n)}$ with R being the chemical group having the desired functionality (eg amine or carboxyl groups) and X being a hydrolyzable group, typically methoxy or ethoxy, that is released in the silanization process in the form of an alcohol. The water for hydrolysis is found either in the environment (on the substrate surface or in the atmosphere) or is present in solution for silanes dissolved in water or buffer. It is also possible to use silanes in an emulsion, if the preparation is shaken periodically. The silanization process consists of four steps: (1) hydrolysis of the X groups, (2) condensation or cross-polymerization of the remaining functionalized SiOH groups of the silane, (3) hydrogen bonding to the SiOH groups of the glass surface, and (4) SiO bond formation between the glass surface and the functionalized silicon. Further details of this process can be found in [45]. The degree of coverage of functional groups depends on several details including the solvent used if the product is not applied neat, the concentration, and the time allowed before rinsing. Some silanes require oven curing to complete the final bonding step, while some are sufficiently bonded after a short N_2 drying

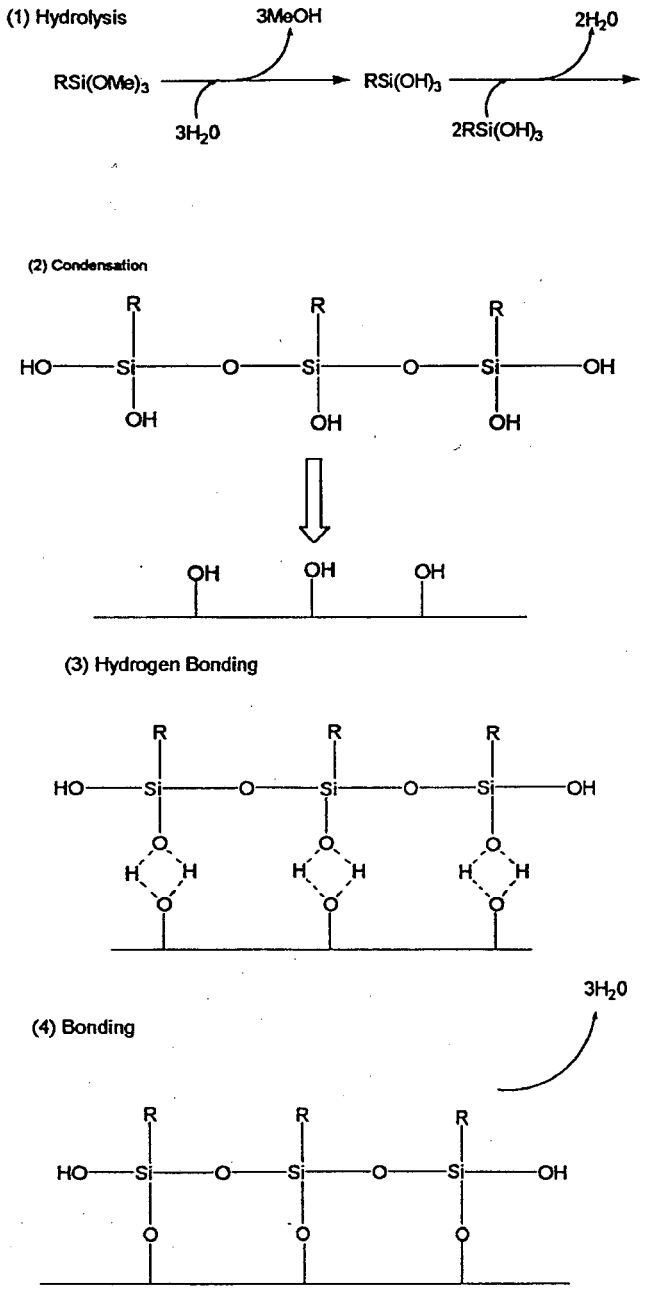

Figure 1: Schematic of the silanization process.

step. Some are soluble in water or buffer, while some are not. Sample preparation methods will vary widely depending on the type of silane used and the desired coverage.

Charge Immobilization:

Figure 2

For this immobilization, a simple charge interaction between the molecule under study and the coverslip is utilized. To determine if a glass treatment is required, it is necessary to know the pI of the molecule to be studied at the pH used in the experiment. An HF-cleaned glass coverslip is negatively charged at neutral pH due to the presence of the silanols on the surface, so if it is desired that a negatively-charged molecule be immobilized on this surface, an intervening layer of positive charge must be supplied. An example of this is the immobilization of DNA on glass via a layer of 3-

aminopropyltriethoxysilane (APS). The silanization process with APS results in a glass surface functionalized with amino groups that are positively charged at neutral pH. Since the DNA backbone is negatively charged, the DNA sticks to the surface of the amine-coated coverslip via a nonspecific charge interaction. This charge interaction holds in solution as long as the pH does not go above the pKa of the amino groups or large amounts of salt are used.

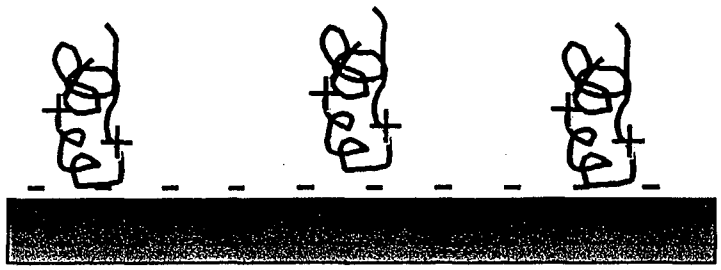

Figure 2: Cartoon of immobilization via charge interaction.

Chelation: Figure 3

Proteins can be altered to incorporate a sequence of six histidines at the N- or C-terminals. These six histidines form what is known as a 6-His tag, which has a high affinity for nickel when the nickel is bound in a chelating complex with N-(5-amino-1-carboxypentyl)iminodiacetic acid (Ni-NTA). Ni-NTA can be purchased conjugated to alkaline phosphatase or horseradish peroxidase proteins (Qiagen) for non-specific binding to glass surfaces. A silane functionalized with the NTA group can also be purchased (UCT) and then charged with nickel in an additional step. We found that using the Ni-NTA-HRP

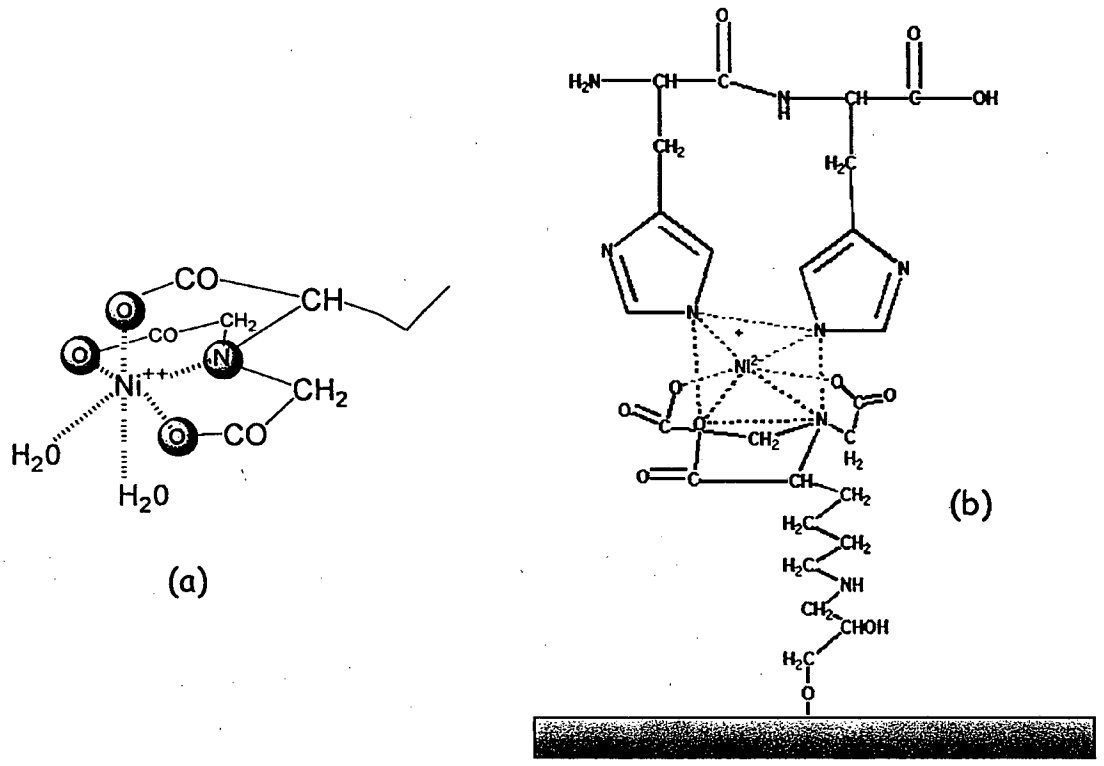

Figure 3: (a) Ni-NTA and (b) Ni-NTA-His tag immobilization scheme.

preparation was unreliable and switched to the silane preparation.

Biospecific linkages (non-specific to glass): Figure 4

Even if there is a charge interaction expected between a macromolecule and the negatively charged silanol groups on the surface of HF-cleaned glass, a washing step will remove the molecules from the HF-cleaned surface unless there is further chemical treatment. Another type of coverslip cleaning method utilizes potassium hydroxide. Some molecules, such as biotinylated-bovine serum albumin (BSA) and streptavidin stick non-specifically to KOH-cleaned coverslips, and the coverage remains in water. The molecules

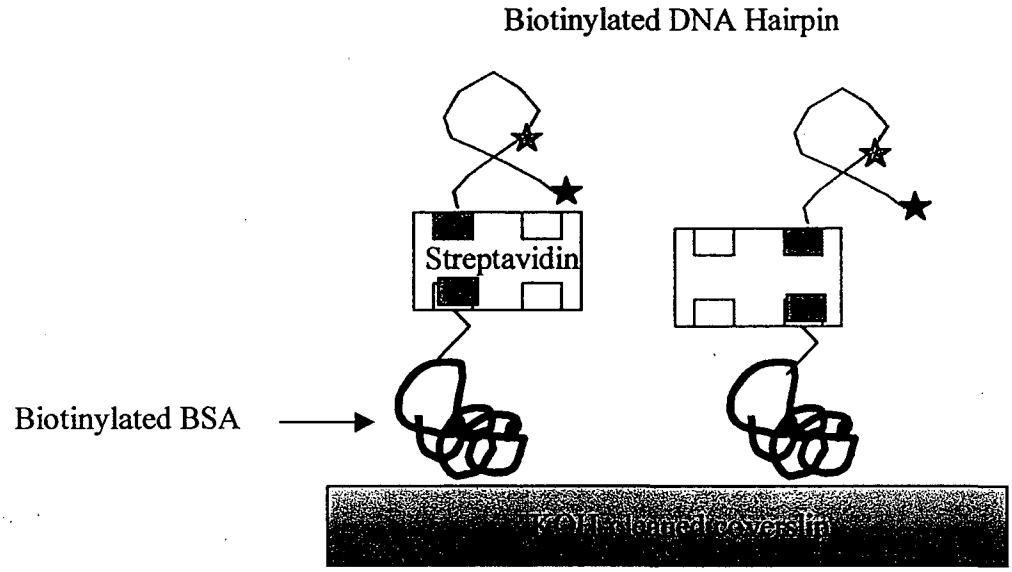

Figure 4: Biotinylated DNA – streptavidin – biotinylated BSA immobilization (non-specific to glass).

can be removed, however, in high fluid flow, a property that produces difficulties with buffer-switching measurements.

Other methods of coverslip cleaning include sonicating coverslips in Helmanex, a spectroscopic-grade detergent, for 20 minutes, followed by a DI water rinse and N_2 drying step. Streptavidin sticks non-specifically to this surface, even under buffer conditions. Biotin sticks on a dry Helmanex-cleaned surface but is removed in aqueous conditions. Flame cleaning can also be done by passing a coverslip quickly back and forth through an open flame, followed by cleaning with alcohol and DI water. Chromic acid cleaning is often used for glassware cleaning and is an alternative to HF.

The fact that proteins such as BSA will stick nonspecifically to KOH-cleaned glass can be useful in immobilization strategies, since the protein can serve both as a sample anchor to the surface and a blocking agent to minimize surface-sample interactions. If the

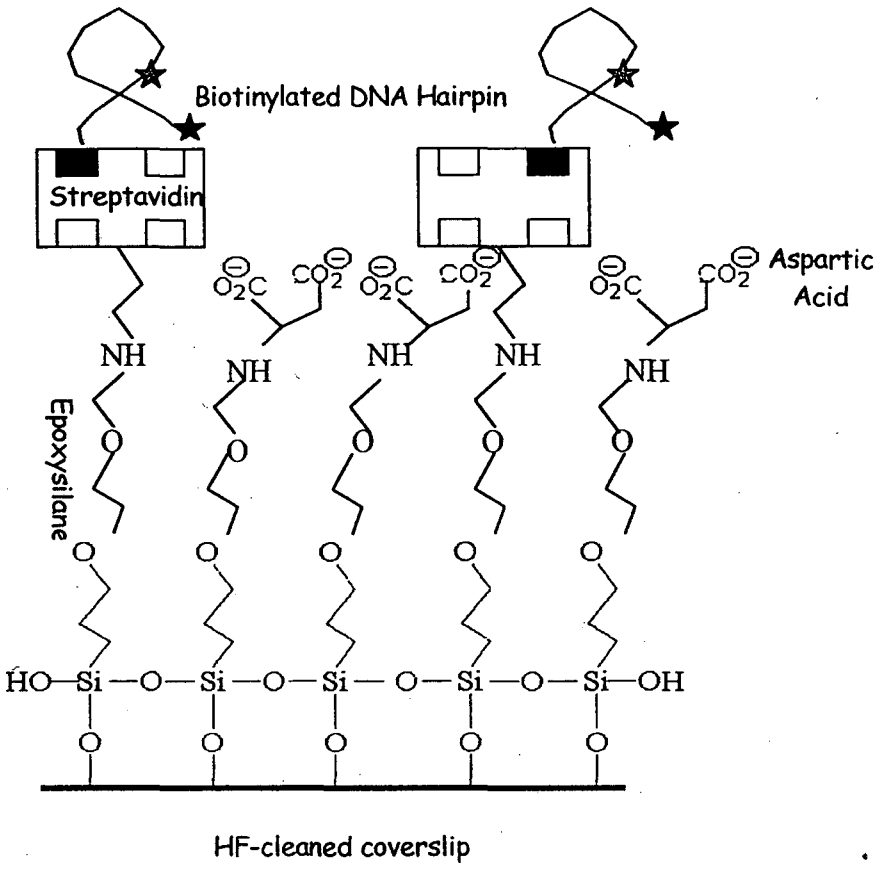

Figure 5: Biotinylated DNA – streptavidin – epoxysilane immobilization (specific to glass).

BSA is functionalized, this functionality can be used to bind other molecules to it in a specific manner.

Biospecific linkages (specific to glass): Figure 5

As was mentioned previously, the biotinylated BSA is not covalently bound to the glass, and it has a tendency to be washed from the surface, taking the sample with it. To prevent this, we developed chemistries to covalently bind the streptavidin to the glass surface, substituting a silanization step for the biotinylated-BSA. This silanization step involves coating the glass surface with an epoxysilane, which can then be used to covalently

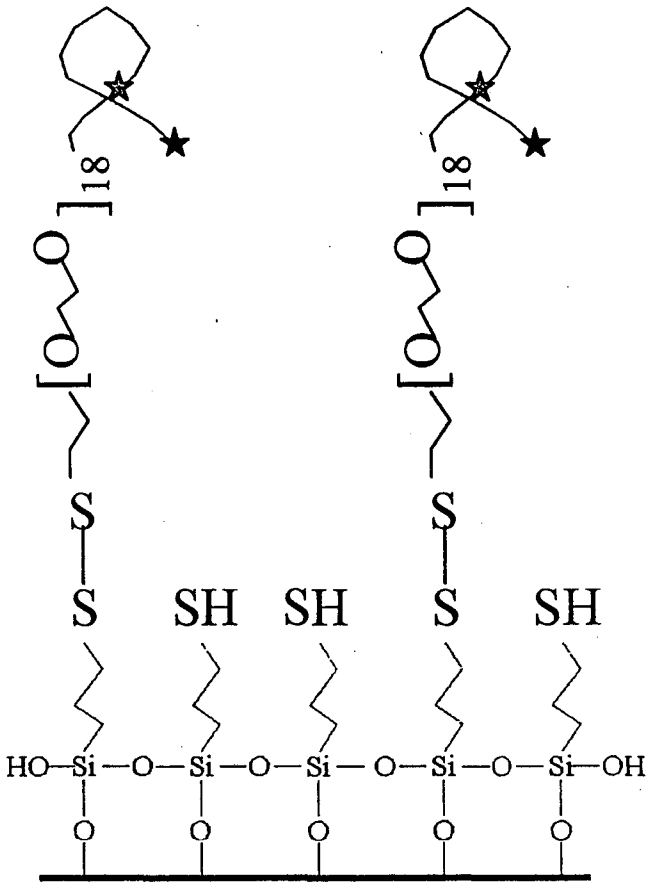

Figure 6: Thiol-terminated-DNA-mercaptosilane immobilization (specific to glass).

bind streptavidin directly to the glass via the amine groups of the protein. This type of covalent binding can of course be applied to any protein with an intact N-terminus or any molecule (such as functionalized fluorophores) with an available amine group.

Chemoselective Ligation: Figure 6

Disulfide Bond Immobilization of DNA Hairpins to Glass Coverslips.

Rather than rely on the binding of proteins to immobilize the sample, it is possible to directly bind the molecule of interest to the glass through covalent bonding. An example of

this is a DNA strand that is manufactured to have a specific chemical group on one end, in our case a sulfhydryl group at the end of a long tetra-ethylene glycol linker. By funtionalizing the glass surface with a silane that contains sulfydryl groups as well, the end of the DNA linker can be bonded to the surface by a disulfide bond under the appropriate conditions.

In all immobilization schemes, it is important to check that there are no problems with contamination in the form of fluorescence from molecules other than the sample. To prevent contamination problems, the highest purity silanes (99.9%) and proteins should be used. Proteins and chemicals should be replaced periodically, especially the silanes, which tend to polymerize over time. To prevent water contamination and subsequent polymerization of the silanes, aliquots can be distributed from the primary source under nitrogen, with these aliquots being used for daily sample preparations. Coverslips more than a day old should be discarded, and blank coverslips should be examined in all cases to insure that there are no false fluorescent signals from surface contaminants.

Gels: Figure 7

Another immobilization strategy is to dissolve the molecule of interest at single molecule concentration in a gel of either polyacrylamide or agarose, depending on the size of the molecule to be monitored. Polyacrylamide gels are formed by the polymerization of acrylamide in the presence of bisacrylamide, a crosslinking agent. The polymerization produces a 3D network of pores that can trap molecules, depending on the relative size of the molecule and the pore. A 7.5% polyacrylamide gel will produce pores ~ 50Å in diameter,

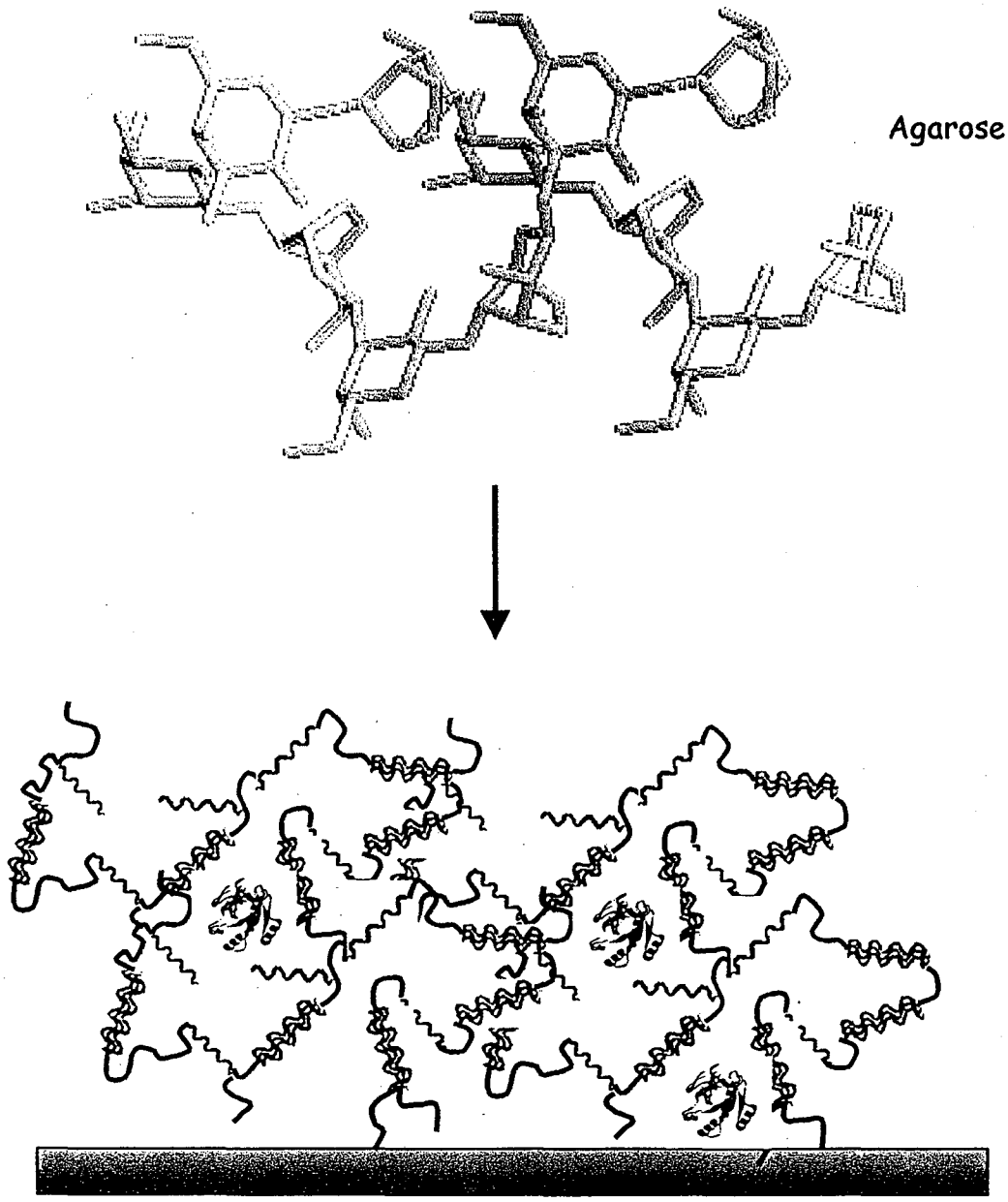

Figure 7: Gel immobilization scheme.

while a 30% gel will reduce the pore size to ~ 20Å [46]. Conventionally a 19:1 ratio of acrylamide to bis-acrylamide is used for DNA gels and a 29:1 ratio for proteins.

Agarose is a polysaccharide that forms long chains of 1,3-linked β-D-galactopyranose and 1,4-linked 3,6-anhydro-a-L-galactopyranose. These chains can network via bundles of double-helices into a 3-D structure, forming pores with average sizes from

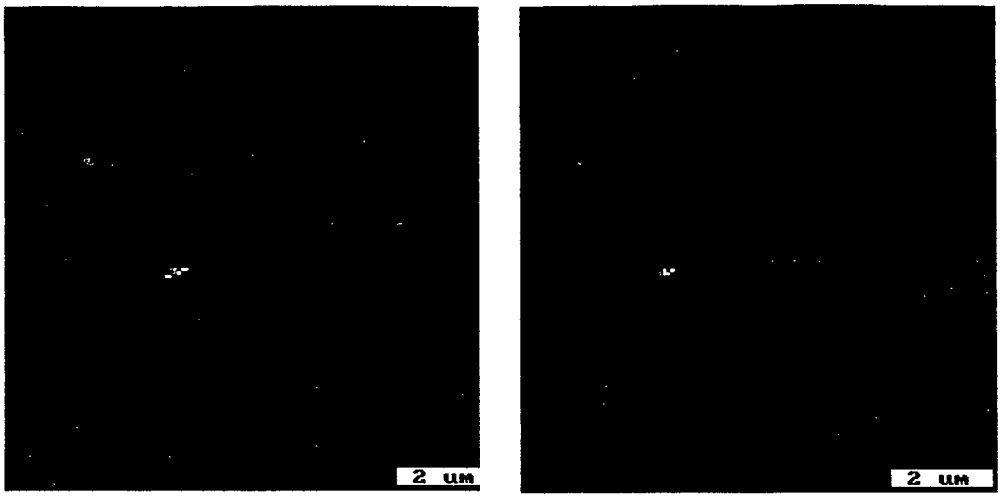

Long Wavelength Short Wavelength

Figure 8: SNARF-labeled streptavidin in 1% agarose gel.

100 to 300nm in diameter [47]. A typical protein such as albumin has a molecular weight of 69kD, a length of 150Å, and a diameter of 38Å, and it can be trapped in either agarose or polyacrylamide gels.

Agarose is much simpler and safer to work with than polyacrylamide, but the large pore sizes produced with agarose preclude its use with smaller molecules. Polyacrylamide is known to act as a quencher for many fluorophores. Gel immobilization was tried in our group without success for single SNARF molecules in polyacrylamide (the SNARF was quenched) and for DNA hairpins in agarose (the pore sizes were too large even at very high agarose concentrations). It was possible to immobilize SNARF-labeled streptavidin in agarose gel, however, and an example of an image taken within the gel is shown in Figure 8. Streptavidin is a 60kD protein that is large enough to be trapped within the agarose pores. It was found that for pH's lower than the pI of the protein, the streptavidin stuck to the surface of the glass coverslip rather than remaining within the gel. This non-specific trapping of the

protein on the surface was believed to be due to a charge interaction and could not be negated even with surface coatings of silanes of various functionalities.

Dextran Immobilization:

Dextran is a polysaccharide that can also be functionalized or labeled with fluorescent dye. For local environment measurements, SNARF-labeled dextran with amines was purchased from Molecular probes and bound directly to the surface via the same chemistry used to bind streptavidin to the epoxysilane-treated glass. This immobilization worked well, however, the presence of the charge-double layer at the glass surface altered the spectrum of the SNARF to such an extent that this method was eventually abandoned. Immobilization of 10,000 MW SNARF-labeled dextrans was attempted in agarose gels up to 10% but diffusion still dominated the images acquired. Polyacrylamide gels were also tried, with percentages varying from 4 to 30%. The fluorescence was quenched within the polyacrylamide, so no sample was observed.

Since TMR-labeled streptavidin purchased from Molecular Probes was easily immobilized in 1% agarose gel, we labeled streptavidin with SNARF in order to reproduce this. The protein labeling and purification is very simple. Carboxylated SNARF was purchased from Molecular Probes and was covalently attached to the amino groups present on the streptavidin. There are three lysines and the N-terminus on streptavidin, and the labeling reaction yields and average of 3.3 dye molecules per protein molecule if the dye is used in saturating concentration.

The surface immobilization chemistries presented in this chapter are recipes that have been proven to work, however, they are by no means the only immobilization methods, nor is it necessary to follow these recipes in a strict manner. Variations in sample concentration, silane aging, buffer conditions, etc, will require the adjustment of the recipes to meet the needs of a particular experiment. The applications of these immobilization chemistries in various single molecule measurements will be described in the following chapters.

Implementation of Immobilization Chemistries (Recipes)

Charge Immobilization:

A coverslip is first cleaned for 2 minutes in a 5% solution of hydrofluoric acid, then rinsed with DI water. Typically free fluorophores, DNA, and proteins do not stick to HF-cleaned coverslips. The HF'd coverslips are dried with N_2 and then immersed in a 1% solution of 3-aminopropyltrimethoxysilane for 2 minutes. After this, the coverslips are rinsed with DI water and dried with N_2. The surface at this point should be very hydrophobic if the silanization is successful. To prepare single molecule DNA samples, single molecule concentrations of the labeled DNA are incubated in a drop on the glass surface for the appropriate amount of time (this depends on the exact concentration of sample used). The sample is then rinsed with DI water and dried with N_2.

Characterization: Washing samples thoroughly with a high salt solution (1M NaCl) will remove molecules attached to the surface via charge interactions.

Chelation:

The sample preparation for a 6-His tagged protein is as follows:

1) Clean glass coverslip in 5% HF acid for 2-5 minutes and follow with a thorough DI water rinse

2) Soak coverslip 10 minutes in a 2% solution of N-[(3-trimethoxysilyl)propyl]ethylene-diamine triacetic acid in water, followed by a DI water rinse.

3) Soak coverslip for 10 minutes in a 50mM solution of $NiSO_4$ in water followed by a DI water rinse and N_2 dry.

4) Incubate the appropriate concentration of 6-His protein on the coverslip, with incubation time varied depending on concentration used and coverage desired.

5) Buffer rinse. The protein should not be allowed to dry out and denature.

Characterization: To determine specificity, an agent that competes with the histidines for nickel can be applied to remove the bound proteins from the surface. For example, the histidine tag may be removed from the nickel complex with a high concentration of imidizole. Alternatively the protein can be removed by protonating the histidines at a pH below 6. The 6-His-tagged protein should also be applied to a surface that lacks the Ni-charging step to determine the degree of non-specific binding to the glass surface.

Biospecific linkages (non-specific to glass):

The following is a recipe used for immobilizing biotinylated DNA samples using the nonspecific binding of biotinylated BSA to glass and streptavidin as the intermediate between the BSA and DNA:

1) Clean coverslips by a 20 minute sonication followed by soaking in 1M KOH in a

staining dish for a minimum of three hours to overnight. Rinse coverslips in DI water and dry with N_2.

2) Place 50μL of a 29μM solution of biotinylated BSA (Pierce) was on the coverslip and incubate for ten minutes. Wash the coverslip with DI water and dry with N_2.

3) Incubate 10μL of a 0.1mg/mL solution of streptavidin (Pierce) on the surface for ten minutes. After incubation, wash and dry the coverslip.

4) A sample of 50nM biotinylated DNA should be incubated in a 10μL drop on the surface for 30 minutes. Wash the sample with DI water and dry with N_2.

Characterization: DNA samples lacking the biotin group should not stick to this surface. Additionally, if a sufficiently soluble form of biotin is available, a blocking step with a high concentration of biotin (no DNA) can be applied after the streptavidin step. Subsequent application of biotinylated DNA should show negligible binding of the DNA due to the lack of available binding sites.

Biospecific linkages (specific to glass):

1) Soak coverslips in 5% HF acid for 2-5 min. The coverslips should then be washed with DI water and dried with N_2.

2) To the center of each coverslip add 10μL of distilled 3-glycidoxypropyltrimethoxysilane (Aldrich), and incubate for 5 min. The coverslip is then washed with DI water and dried with N_2.

3) To the silanized coverslip add 10μL of a 0.1mg/mL solution of streptavidin in 10mM Na_2CO_3 buffer, pH 9, and incubate for 5 min. The cover slip is then washed with DI water and dried with N_2.

4) The remaining epoxides can be quenched with 10μL of 2mM aspartic acid in a 0.5 M carbonate buffer, pH 9. Wash the coverslip with DI water and dry with N_2.

5) Add to the coverslip 10μL of a 200nM biotinylated-DNA hairpin in a 50mM PBS buffer, pH 7.0. The coverslip should be incubated for 5 min to 15 min, washed with DI water, and dried with N_2.

Characterization: DNA hairpins that did not have biotin groups do not stick to this surface. Additionally, if a sufficiently soluble form of biotin is available, a blocking step with a high concentration of biotin (no DNA) can be applied after the streptavidin step. Subsequent application of biotinylated DNA should show negligible binding of the DNA due to the lack of available binding sites.

Chemoselective Ligation:

1) Clean glass coverslips by soaking them in a 1M KOH solution in a staining dish for a minimum of 3 hours to overnight.

2) Rinse coverslips in bulk three times with a staining dish volume-full of DI water.

3) Incubate the slips in a 1% 3-mercaptopropyltri-ethoxysilane (MPTS) (Fluka) solution in a 0.1*M* NaH_2PO_4 solution at pH 6 for 45 min to 1 h. Shake the MPTS solution periodically to disperse the silane, which forms an emulsion in the phosphate buffer.

4) Rinse the coverslips in bulk once with 0.1*M* NaH_2PO_4, pH 6, followed by a single bulk rinse with DI water.

5) Rinse the coverslips individually with DI water and dry with a stream of N_2.

6) Place slips in a covered staining dish and cure for 30 min in a glassware oven at 175°C.

7) Store the slips in a N_2 glove box until used.

Characterization: DNA hairpins without sulfhydryl groups do not bind to this surface. In addition, hairpins bound to the surface via the disulfide bond can be competed off the surface by sulfur-containing compounds such as mercaptoethanol.

Agarose Gel Preparation:

1) Dissolve desired concentration of agarose powder in buffer (use low melting point agarose for concentrations higher than 5%).
2) Heat agarose either using a hot water bath or in a microwave oven until the agarose solution forms a liquid gel.
3) Allow gel to cool but not solidify. When gel is cool enough not to denature the sample, add molecules to be immobilized in the appropriate single molecule concentration.
4) The gel can be pipetted onto a clean coverslip or on a coverslip previously spin-coated with gel. Since HF-cleaned coverslips tend to be slide around on the gel, spin-coating is preferable.

Polyacrylamide Gel Preparation:

For a ~ 1mL final volume of a 20% gel:

1) For a protein gel, pre-mix a 29:1 ratio of acrylamide to bis-acrylamide
2) Mix 0.5mL of the polyacrylamide with 0.5mL of the desired buffer
3) Add 10μL of ammonium persulfate
4) Add 1μL of TEMED. TEMED will start the gelling process, so add it only when ready for the final gel to form. Any sample should be added before or immediately after this step.

Protein labeling reaction and purification:

1) In a tube, mix 25μM streptavidin (Pierce), 220μM carboxy-SNARF, 5.22mM EDAC, 4.6mM NHSS, and sodium phosphate buffer (pH 7). In our labeling the final volume used was 100μL.

2) React at room temperature for two hours.

3) To purify, a 5000MW desalting column (Pierce) was used. The labeled protein typically came out in the second fraction.

4) Absorption spectra were taken on each fraction to determine the quantities of protein and dye present (streptavidin absorbs at 280nm with an extinction coefficient of 32,000).

Chapter 4

Monitoring the Conformational Fluctuations of DNA Hairpins Using Single-Pair Fluorescence Resonance Energy Transfer

Introduction

The technique of single pair Fluorescence Resonance Energy Transfer (spFRET) was introduced to the single molecule community by Ha et al, in 1996, where it was applied to double stranded DNA under non-physiological conditions [25]. Fluorescence resonance energy transfer is a powerful spectroscopic technique that allows biologically relevant distances between 20 Å and 80 Å to be quantified with near-angstrom resolution due to the strong distance dependence of the transfer process. FRET is the non-radiative transfer of energy from a donor molecule to an acceptor molecule that occurs through a dipole-dipole interaction [48]. When two fluorescent molecules are used, FRET results in a decrease in donor fluorophore emission intensity with a simultaneous increase in acceptor fluorophore emission intensity. FRET depends on the inverse sixth power of the distance between the two fluorophores (R^{-6}) which allows spFRET to act as a sensitive molecular ruler in biological systems [49,50]. Distance and orientation information of biomolecules are obtained when changes in energy transfer and fluorescence anisotropy of the dyes are quantified.

There are several expressions for the efficiency, E, of energy transfer [51,52]. Because our experiments involve the measurements of the intensities of the donor and acceptor fluorescence, we employ an expression of the form

$$E = \frac{R_o^6}{R_o^6 + R^6} = \frac{I_A}{I_A + \gamma I_D},$$

in which I_A and I_D are the measured intensities of the acceptor and donor fluorophores respectively, R is the distance between the two fluorophores, R_o is the Förster radius, or distance of 50% energy transfer (see Appendix), and γ is an experimental factor that includes the ratios of the donor and acceptor fluorophore quantum efficiencies as well as the efficiencies of detection for the two fluorophores. γ is estimated to be 0.8 for our measurements [53].

In order to demonstrate the measurement of spFRET on a biologically relevant system under physiological conditions, we chose to study the test system of a DNA hairpin and applied the spFRET technique to this system. DNA hairpins are inverse repeats of single-stranded DNA connected by a non-complimentary loop sequence, and they are one of the simplest structures that a nucleic acid polymer can form. Hairpins are often found at replication origins, promoters, operator sequences, and other sites of regulation in genomic DNA and are thus thought to play a critical role in the regulation of gene transcription, DNA recombination, and DNA replication [54-57]. For example, multiple alternative forms of hairpin structures can result in a variety of genetic disorders [58,59], and hairpin structures mediate the interacting hairpin loops, or "kissing complexes," of HIV dimerization [60,61]. DNA hairpins are proposed anti-sense drugs due to their high resistance to nuclease degradation, and DNA hairpin molecular beacons, in conjunction with

gene chip technology, are useful tools in disease diagnostics and drug development [62-67]. Because DNA hairpins are known to show two-state folding kinetics, they can serve as a model system for the study of single molecule kinetics on surfaces.

DNA hairpins fluctuate in solution between a folded (closed) state and a denatured (open) state. This two state transition is an equilibrium process that can be described as the ratio of (k_{closed} * [open hairpin]) / (k_{open} * [closed hairpin]) (Figure 1). The closed state is characterized by lower enthalpy than the open state due to base pairing and stacking. The open state is characterized by high entropy as a large number of configurations are possible from a single-strand of DNA. Many thermodynamic and structural studies have been performed on DNA hairpins to understand the energetics of nucleic acid folding and to derive accurate parameters for predicting the stability of various sequences involved in forming DNA secondary structure [68,69].

There are very few studies on the kinetics of hairpin folding [70,71]. The opening rate depends on the unzipping energy of the hairpin, while the closing rate relies on the collision of the two stalks of the stem, followed by nucleation and the propagation of base-pairing. Recent work used fluorescence correlation spectroscopy (FCS) and fluorescence quenching, with an average of five hairpins in the excitation beam, to show that the rate of opening of the hairpin stem was essentially independent of the loop characteristics regardless of loop size, sequence, and NaCl concentration [72]. The rate of hairpin closing scaled with the loop length and rigidity; an adenosine loop led to smaller closing rates and higher activation energies than a thymidine loop.

For single molecule experiments, we designed hairpins to open and close on a time scale of 0.2 ms or greater. For the purpose of immobilizing the hairpins to directly measure

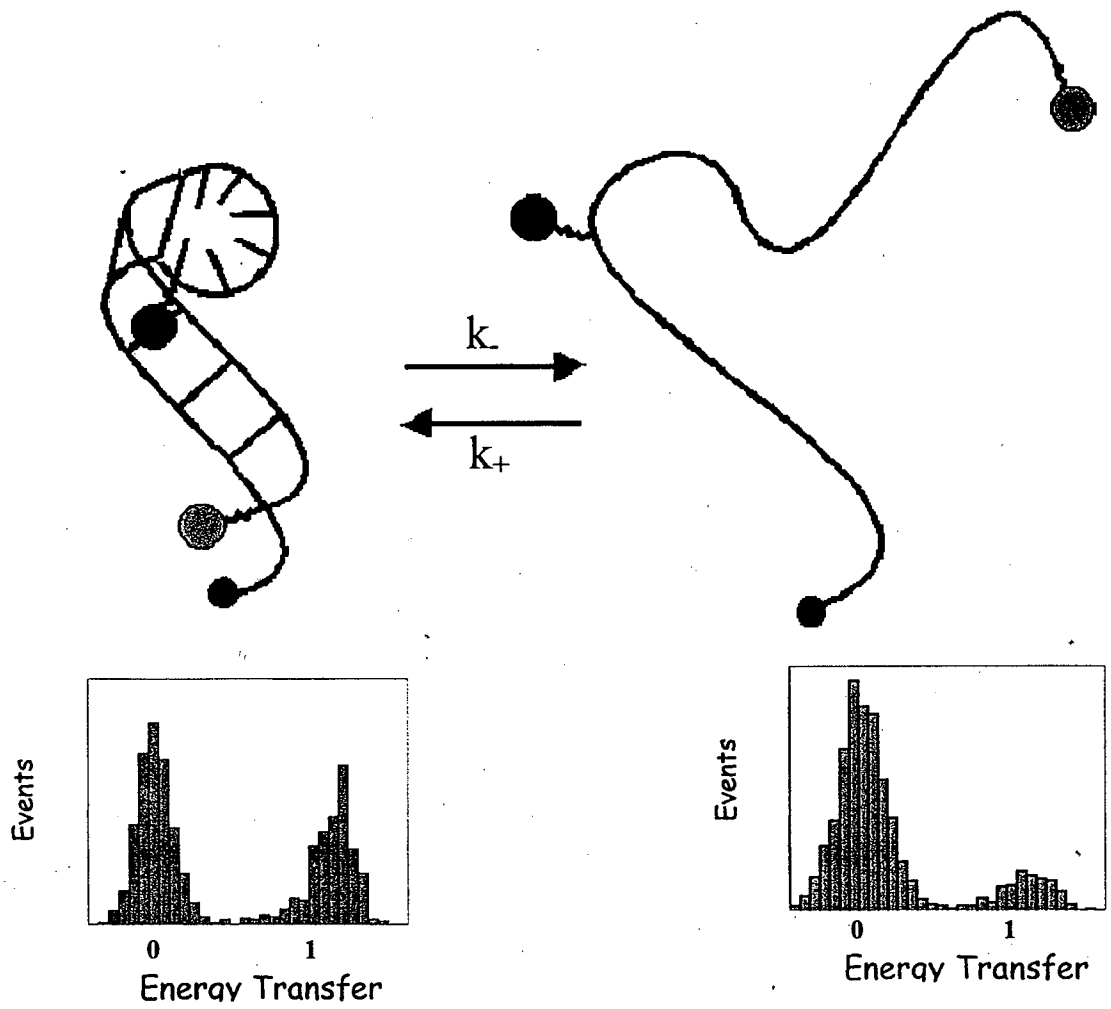

Figure 1. Schematic of the closed-to-open transition of a DNA hairpin with the approximate position of the donor and acceptor flourophores indicated. The expected energy transfer efficiency for the folded state is indicated by the simulated spectrum below the native hairpin. A denatured hairpin is a single-strand of DNA that acts as a random coil. Very little energy transfer will occur as shown by the increase in the peak at zero.

fluctuation events, we employed three different surface immobilization strategies. In the first two immobilization techniques, streptavidin was either reacted with an epoxide-derivatized glass surface or immobilized through a non-specifically adsorbed biotinylated-

BSA coated glass surface in order to exploit streptavidin's strong interaction with biotin. For the third technique, a method for single molecule studies that cross-links hairpins to glass through a disulfide-bond was developed. The diffusing hairpin folding as a function of temperature was measured, and exponential kinetics for the opening and closing of hairpins immobilized on a surface was observed.

Materials and Methods

All DNA synthesis reagents including amino modifier C6 dT (dTC_6NH_2), 5'-thiol-modifier C6, and 1μM biotin triethyleneglycol control pore glass resin (Btn TEG CPG) phosphoramidites were purchased from Glen Research. The maleimide derivative of tetramethylrhodamine (TMR-maleimide) was purchased from Molecular Probes and the N-hydroxy succinimidyl ester of Cyanine 5 (Cy5-NHS) was purchased from Amersham. Enzymes were purchased from New England Biolabs.

Sequences of the Hairpins Studied

dA40s7 HP Btn: 5' - TMR-SC_6 - CTCTTCA - $(AAA)_{13}A$ -dTC_6NH-(Cy5)-GAAGAG - TEGBtn - 3'

dA40s9 HP Btn: 5' - TMR-SC_6 - CTCTTCAGT - $(AAA)_{13}A$ -$ACdTC_6NH$-(Cy5)-GAAGAG - TEGBtn - 3'

dA40s9 HP Thiol: 5' - Cy5 - CTCTTCAGT - $(AAA)_{13}A$ - $ACdTC_6NH$-(TMR)-GAAGAG - TEG_{18} C_6S-SdT- 3'

dA30s14 HP Thiol: 5' - Cy5 - CTCTTCAGTTCACA - $(AAA)_{10}$ -TGTGAACdTC_6NH-(TMR)-GAAGAG - TEG_{18} C_6S-SdT- 3'

Sample Preparation

DNA Synthesis. dA40S7 HP Btn and dA40S9 HP Btn: Synthesis of these hairpins was accomplished using standard β-cyanoethyl phosphoramidite chemistry on a DNA synthesizer (Applied Biosystems). The hairpin was deprotected with 1mL of concentrated NH_4OH for 12 h at 55 °C and concentrated by centrifugation under vacuum. The oligonucleotide was purified on a C_{18} reversed-phase semi-preparative protein-peptide column using a gradient of 5% to 45% CH_3CN in 0.05 M tetraethyl ammonium acetate (TEAA), pH 7, over a 30 min period. All hairpin species were analyzed by electrophoresis on a 15% denaturing polyacrylamide gel and imaged visually if dye labeled and by standard ethidium bromide staining.

TMR-maleimide labeling and Cy5-NHS ester labeling. The oligonucleotides were labeled according to the procedures described in [50].

dA40S9-3'biotin modified hairpin. It was difficult to obtain significant quantities of full length hairpin by total synthesis due to the size of the hairpin and the many adenosine-adenosine couplings in the synthesis. We overcame this problem by ligating together two dye-labeled oligonucleotide fragments of the hairpins together with a complementary oligonucleotide splint and T4 DNA ligase. The oligonucleotide fragments were synthesized and purified as described above. The 5' fragment of the hairpin incorporated a trityl protected 5'-thiol modifier C6 while the 3' fragment incorporated an amino modifier C6 dT and either a 1μM biotin TEG CPG phosphoramidite or a 3' thiol modified CPG phosphoramidite. The 5' end of the biotinylated fragment was phosphorylated using T4 polynucleotide kinase (PNK).

Phosphorylation of 5' end of biotinylated DNA hairpin fragment. To 215 nM of biotinylated DNA in 480 μL of sterile ddH_2O was added 60 μL of 10x T4DNA Ligase Buffer, 50 μL of ddH_2O, and 100 units of T4 PNK. The reaction tube was briefly centrifuged and incubated at 37 °C for 3 h. The kinase reaction was purified by phenol:chloroform extraction and the DNA was ethanol precipitated. The thiol-containing oligonucleotide was labeled with TMR-maleimide while the phosphorylated, biotinylated, and amine containing oligonucleotide was labeled with Cy5-NHS ester. Free dye was removed by running a NAP 5 size-exclusion column followed by size-exclusion FPLC on a Superdex 75 column (Pharmacia). The labeled hairpin fragments were then HPLC purified as described above to separate unlabeled DNA from labeled DNA.

Ligation of the dye-labeled DNA hairpin fragments. 3.5 nM of the TMR labeled oligonucleotide, 4.3 nM of the Cy5 labeled oligonucelotide, and 4.5nM of the splint oligonucleotide were mixed in a centrifuge tube. The mixture was concentrated to dryness by vacuum centrifugation, followed by resuspension in 16 μL ddH_2O. To the resuspended mixture were added 2 μL 10x T4 DNA Ligase buffer and 10 units of T4 DNA Ligase. The ligation reaction was run at 16 °C overnight. The ligated hairpin was purified by size exclusion FPLC on a Superdex 75 column to separate the hairpin from the individual dye labeled oligonucleotides and the splint oligonucleotide. The ligated product was analyzed by using a 15% denaturing polyacrylamide gel.

dA40S9 HP Thiol and dA30S14 HP Thiol. These hairpins were purchased from Synthegen. Cy5 was incorporated into the DNA as the final phosphoramidite in the synthesis. Large control-pore glass resin was used to accommodate the length and multiple adenosine to adenosine couplings. The 3' thiol was protected by a disulfide bond to a thiol

modified thymidine. An 18-TEG phosphoramidite was used as a spacer between the DNA hairpin and the 3' thiol surface attachment.

Surface Preparations

The surface preparation methods are similar to those described previously in Chapter 3.

Biotin-Streptavidin Immobilization of DNA Hairpins to Glass Cover Slips. Gold Seal Clay Adams cover slips (No. 1, VWR Scientific) were cut in half and soaked in 5% HF acid for 2 min. The cover slips were washed twice with DI H_2O and were again soaked in 5% HF for 2 min. The cover slips were washed twice with DI H_2O, dried with N_2, and silanized by adding 10 μL of distilled 3-glycidoxypropyltrimethoxysilane (Aldrich) to the center of the cover slip and incubating in a HF-cleaned glass petri dish for 5 min. The silanized cover slip was washed with DI H_2O, dried with N_2, and reacted with 10 μL of a 0.1 mg/mL solution of streptavidin in 10 mM Na_2CO_3 buffer, pH 9 for 5 min. The cover slip was washed with DI H_2O, dried with N_2. The remaining epoxides were quenched with 10 μL of 2mM aspartic acid in a 0.5 M carbonate buffer, pH 9, followed by a DI H_2O washing/ N_2 drying step. Attachment of the hairpin to the coverslip was accomplished by reacting 10 μL of a 200nM biotinylated-DNA hairpin in a 50 mM PBS buffer, pH 7.0, with the coverslip for 5 to 15 min, followed by a final DI H_2O washing/ N_2 drying step. The slips were then stored in a N_2 glove box until used. Cover slips more than 10 hours old were discarded, and blank cover slips were examined to insure that there were no false fluorescent signals from surface contaminants.

Biotinylated-BSA and Streptavidin Surfaces. VWRBrand No. 1 glass cover slips were cleaned by a 20 min sonication followed by soaking in 1M KOH in a staining dish for a minimum of 3 h. Cover slips were then rinsed in DI H_2O and dried with N_2. Following the method of Gaub [73], 50 μL of a 29μM solution of biotinylated BSA (Pierce) was placed on the cover slip and incubated for 10 min. The cover slip was washed with DI H_2O and dried with N_2, and then 10 μL of a 0.1 mg/mL solution of streptavidin (Pierce) was incubated on the surface for 10 min. After incubation, the cover slip was once again washed and dried, and a 10 μL drop of 50nM biotinylated DNA was incubated on the surface for 30 min, followed by a final DI H_2O washing/ N_2 drying step. The slips were then stored in a N_2 glove box until used. Cover slips more than 10 hours old were discarded, and blank cover slips were examined to insure that there were no false fluorescent signals from surface contaminants.

Disulfide Bond Immobilization of DNA Hairpins to Glass Cover slips. The following procedure was adapted from Rogers *et al* [74] . VWRBrand No. 1 glass cover slips were cleaned by first sonicating for 30 min and then soaking in a 1 M KOH solution in a staining dish for a minimum of 3 hours to overnight. Cover slips were rinsed in bulk three times with a staining dish volume-full of DI H_2O. The slips were then incubated in a 1% 3-mercaptopropyl tri-ethoxysilane (MPTS) (Fluka) solution in a 0.1 M NaH_2PO_4 solution at pH 6 for 45 min to 1 h. The MPTS solution was shaken periodically to disperse the silane, which forms an emulsion in the phosphate buffer. The cover slips were then rinsed in bulk once with 0.1 M NaH_2PO_4, pH 6, followed by a single bulk rinse with DI H_2O. The slips were individually rinsed with DI H_2O and dried with a stream of N_2. The slips were placed in the covered staining dish and were cured for 30 min in a glassware-drying oven at 175 °C. After

curing, the cover slips were rinsed individually with a 0.05% solution of Tween 20, followed by a DI H_2O rinse and N_2 drying step. A 100 pM solution of DNA hairpin in a 0.5 M $NaHCO_3$, pH 9 buffer, was incubated on the surface for 10 minutes. The sample was rinsed with DI H_2O and dried with N_2. The slips were then stored in a N_2 glove box until used. Cover slips more than 10 hours old were discarded, and blank cover slips were examined to insure that there were no false fluorescent signals from surface contaminants.

Confocal Microscope Set-up

The apparatus used for these single-molecule detection experiments is the same as that described in detail previously in Chapter 2.

Single Molecule Data Collection and Analysis

Diffusion. For diffusion measurements, tens of picomolar concentrations of hairpin were dissolved in 50 mM sodium phosphate buffer, pH 7, 50 mM NaCl and 15 μl of this solution was placed between two clean cover slips, with a Parafilm gasket as a spacer between the cover slips. The 500 μW excitation beam was focused 10 μm into a sample cell using a 100X 1.4NA oil-immersion objective and a 100 μm pinhole was used to remove out-of-focus light, resulting in an effective femtoliter sample volume. Use of tens of picomolar concentrations reduced the probability of finding two molecules in the beam simultaneously to ~0.0005. Bursts of fluorescence photons were emitted as dye-labeled hairpin molecules diffused into and out of the excitation beam. These bursts were recorded over 5-10 min

intervals, with an integration time of 1ms, and the time traces of bursts were analyzed to collect statistics on the hairpin samples. A more detailed account of diffusion spFRET analysis can be found in [50, 75]. For the present work, the donor and acceptor channels were examined individually, rather than summed, and the threshold for events was set at 10 times the standard deviation of the background signal.

Use of Oxygen Scavengers for Diffusion Data Collection. Obtaining significant numbers of high FRET events in diffusion was initially very difficult due to the poor photophysics of the acceptor fluorophore Cy5 [76] and adequate diffusion data would have been difficult to obtain. Premature photobleaching of Cy5 also contributed significantly to the event peak at zero energy transfer efficiency, making it difficult to resolve any species with energy transfer efficiencies of 0.4 or lower. Hence, the photobleaching lifetime of Cy5 was dramatically increased by the inclusion of oxygen scavengers into the buffer. A glucose oxidase oxygen scavenging system similar to that of [77] provided some improvement in the Cy5 photostability, however it was not compatible with chemical or thermal denaturation experiments. We tested several small molecule scavengers such as imidazole, β-mercaptoethanol, Trolox (a water-soluble version of vitamin E), and propyl gallate [78]. Trolox (500 μM) and propyl gallate (500 μM) were found to be a very effective oxygen scavengers, and their use was found to dramatically decrease the photobleaching and oxidative damage of Cy5 (Figure 2). Further details of oxygen scavengers applied to fluorescence measurements on both hairpin DNA and with free dye will be presented in Chapter 6.

Images. Images of immobilized dually labeled hairpin in a 50 mM phosphate buffer, pH 7 solution were recorded. For surface-immobilized molecules, images of dye-labeled

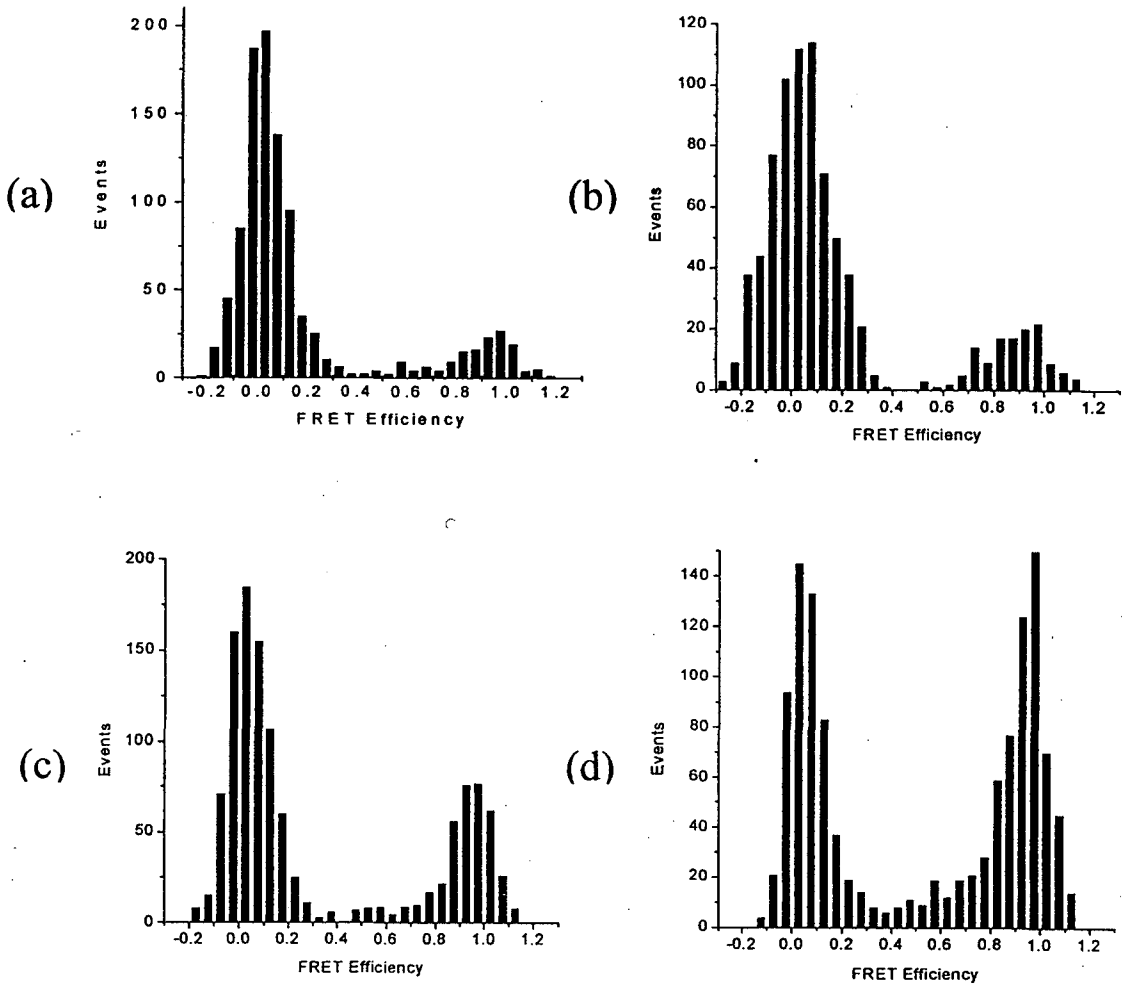

Figure 2: The use of oxygen scavengers greatly improves Cy5 fluorescence lifetimes for single hairpins in diffusion. Histograms of events versus FRET efficiency are plotted for the dA30s9 hairpin using (a) no scavenger (b) glucose oxidase, (b) trolox, and (c) propyl gallate.

hairpins were acquired by scanning the sample across the excitation beam. 128 x 128 pixel images were obtained by collecting data simultaneously per pixel on the donor and acceptor fluorescence channels with 5ms/pixel time resolution. The image of a single molecule at 78nm/pixel is on the order of 5 pixels in diameter, effectively imaging the diffraction-limited laser spot focused with the 1.4 NA objective. The images were then analyzed pixel

by pixel via an algorithm that first subtracted the backgrounds from both images, including any donor leakage onto the acceptor channel, and then calculated the pixelwise spFRET efficiencies. Calculating the spFRET efficiencies per pixel rather than over the entire point-spread functions allows the calculation to be done on a faster time scale and minimizes the effect of photobleaching on the mean value of the transfer efficiency, but results in a greater contribution of shot noise to the measurement. The thresholding used for image events was identical to that used for diffusion measurements. Evidence that we are observing single-pair FRET can be found in images (Figure 6c) in which the abrupt disappearance of the acceptor fluorescence (shown in red) upon acceptor photobleaching is accompanied by the emergence of the donor fluorescence (shown in green).

Time Traces. Time traces, or the fluorescence intensities over time, of immobilized single molecules were collected using a searching algorithm as previously described in [41]. These time traces were analyzed individually to determine the presence of opening and closing events of the DNA hairpins.

Polarization Anisotropy. The value obtained for FRET efficiency is dependent on the Förster radius (R_o), of the dye pair used, which is in turn dependent on the orientational factor, κ^2. R_o was calculated to be 53 Å for the tetramethylrhodamine (TMR) and cyanine-five (Cy5) pair used in these experiments. This value assumes an orientational factor of 2/3 for κ^2, a factor that must be justified by polarization anisotropy measurements of the rotational freedom of both fluorophores. We followed the method of Ha [37] and measured the s and p polarization components of single donor and acceptor fluorophore emissions for the various sample preparations used in our study. These measurements were then fit with

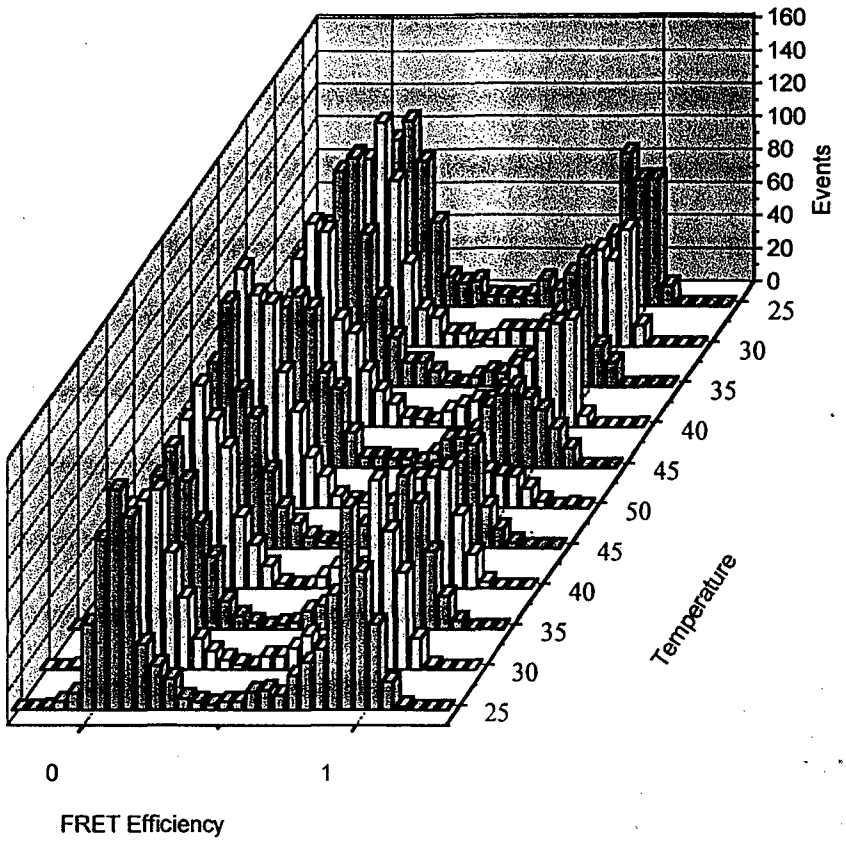

Figure 3. Temperature denaturation and renaturation of the dA40s9 hairpin in single-molecule diffusion. The FRET efficiency of fluorescence bursts from hairpins at 1 ms integration time was analyzed and plotted as a function of temperature for the same hairpin sample. Each histogram is normalized to include 1000 diffusion events. Temperature is given in degrees C.

an angle parameter that provided information on the freedom of rotation of the fluorophores during the data acquisition timescale.

Results and Discussion

Diffusion Data at the Single Molecule Level. Thermally and chemically denatured DNA hairpins were studied using single molecule diffusion experiments (Figure 3). All hairpins showed a peak at > 95% energy transfer whose relative area decreased with increasing temperature or denaturant concentration. An example of this effect for the

dA40s9 hairpin is shown in Figure 3. Data was acquired on hairpins heated from 25 °C to 50 °C and cooled back to 25 °C, in 5 °C intervals. As the temperature of the sample was increased from 25 to 50 °C, the high energy transfer peak decreased in area by 60.4% with a corresponding increase in the zero energy transfer peak area of 53.5%. This behavior was reversed upon cooling of the sample from 50 °C to 25 °C, indicating the denaturation and reannealing of the DNA hairpins. Relative quantum yields, spectral position, and polarization anisotropy varied less than 20% between 0 M and 8 M urea and 0 °C and 50 °C, contributing to changes in transfer efficiency of 20% at most. Hence, the changes in energy transfer measured in urea and temperature denaturation experiments are due primarily to hairpin denaturation. The reaction time for the opening and closing of the hairpin is slower than the rate of data acquisition (1ms/point), even at higher temperatures, because the peak at high transfer efficiency decreases in amplitude for the dA40s9 hairpin as the sample is heated or urea is added (data not shown) rather than shifting to lower efficiency values. If the conformational fluctuations were faster than the rate of diffusion the high FRET peak would gradually shift to lower FRET efficiency values as the sampled conformations are averaged over time. We corroborated this observation by performing fluorescence correlation spectroscopy (FCS) measurements on our hairpin species and found that any opening or closing time scales were slower than the diffusion time of the hairpin through the laser beam (~ 180 μs).

Specificity of Surface Immobilization Chemistries. We tested the biotin-streptavidin and the disulfide bond immobilization techniques to insure that the linkages to the glass were biospecific or chemospecific, respectively. Charge interactions were ruled out by imaging samples in 1 M NaCl solutions, and these samples showed negligible removal of

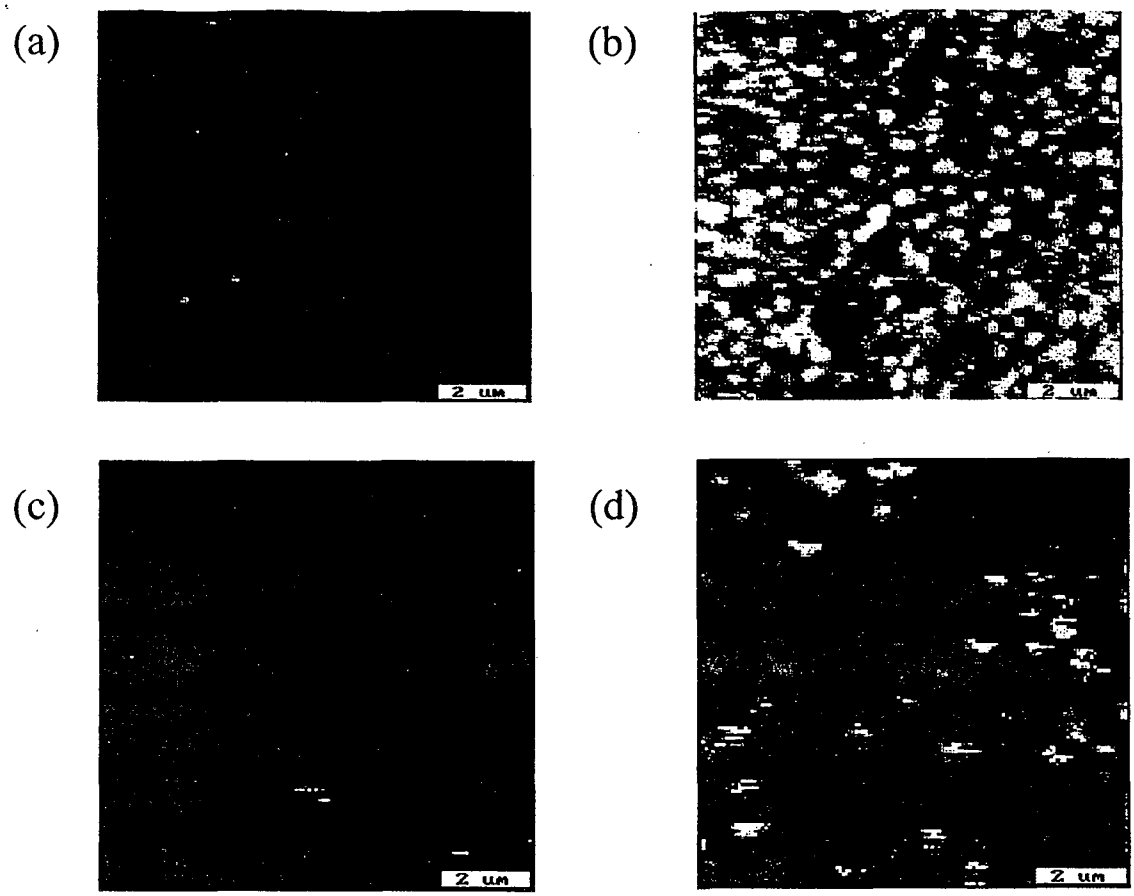

Figure 4. Surface preparation biospecificity and chemoselectivity. Non-biotinylated DNA does not bind (a), while biotinylated DNA binds streptavidin coated cover slips (b). DNA derivatized with a 3' carboxylic acid group does not react with mercaptopropyl silanized (MPS) glass cover slips (c), while disulfide protected DNA undergoes a disulfide exchange reaction with the thiol-derivatized surface (d).

DNA hairpins from the surface. Non-biotinylated DNA hairpins did not bind to the streptavidin-coated surface (Figure 4a), while the same concentration (200nM) of biotinylated hairpin was found to bind very well. This biospecific conjugation could be quantitated by image analysis. Images were converted to grayscale and examined using the histogram function in Adobe Photoshop™. The image in Figure 4a was found to have a mean of $0.39 \pm 1.77 \times 10^{-3}$ (arbitrary units) while the image in Figure 4b had a mean of 80.8 ± 0.39. Biotinylated-BSA sticks nonspecifically to the glass surface and tends to be washed off

under high liquid flow. Images 4a and 4b were performed with DNA concentrations higher than that used to achieve single molecule coverage in order to show conclusively that the surface preparation was biospecific. An oligonucleotide with a non-reactive carboxylic acid group at the 3' end did not react and bind to the thiol derivatized surface (Figure 4c). An image of 100 pM of these carboxyl-derivatized hairpins applied to the thiol surface is shown in Figure 4c. This image had a mean of 8.99 ± 0.039, while the accompanying image of the same concentration of sulfhydryl-functionalized hairpins shown in Figure 4d had a mean of 23.9 ± 0.10. This indicates that the hairpin with the thiol group attaches preferentially to the thiol-derivatized surface. In addition, hairpins bound to the surface via disulfide bonds could be competed from the surface with β-mercaptoethanol.

Polarization Anisotropy of Immobilized Hairpins. The DNA hairpins used in this study were designed to produce very large conformational changes that result in "on or off" energy transfer values; when the hairpin is closed, the energy transfer efficiency in all hairpins studied is high (~ 0.9) and when the hairpins were open, the energy transfer efficiency drops to zero. While the precise distance between the fluorophores used in our kinetics study was of secondary interest, determining the status of the rotational freedom of the fluorophores used was important in order to rule out any large changes in FRET due to rotational effects alone. In addition, the rotational properties of the dyes can provide information on the conformational freedom of the DNA hairpins themselves, e.g. if the dyes are immobilized, the hairpin is also likely to be kinetically trapped on the surface. It should be noted that what appears to be free rotation on the time scale of data acquisition does not necessarily translate to a value of 2/3 for κ^2, however, we can get some indication of the average rotational freedom of the dye. Time traces of freely rotating fluorophores

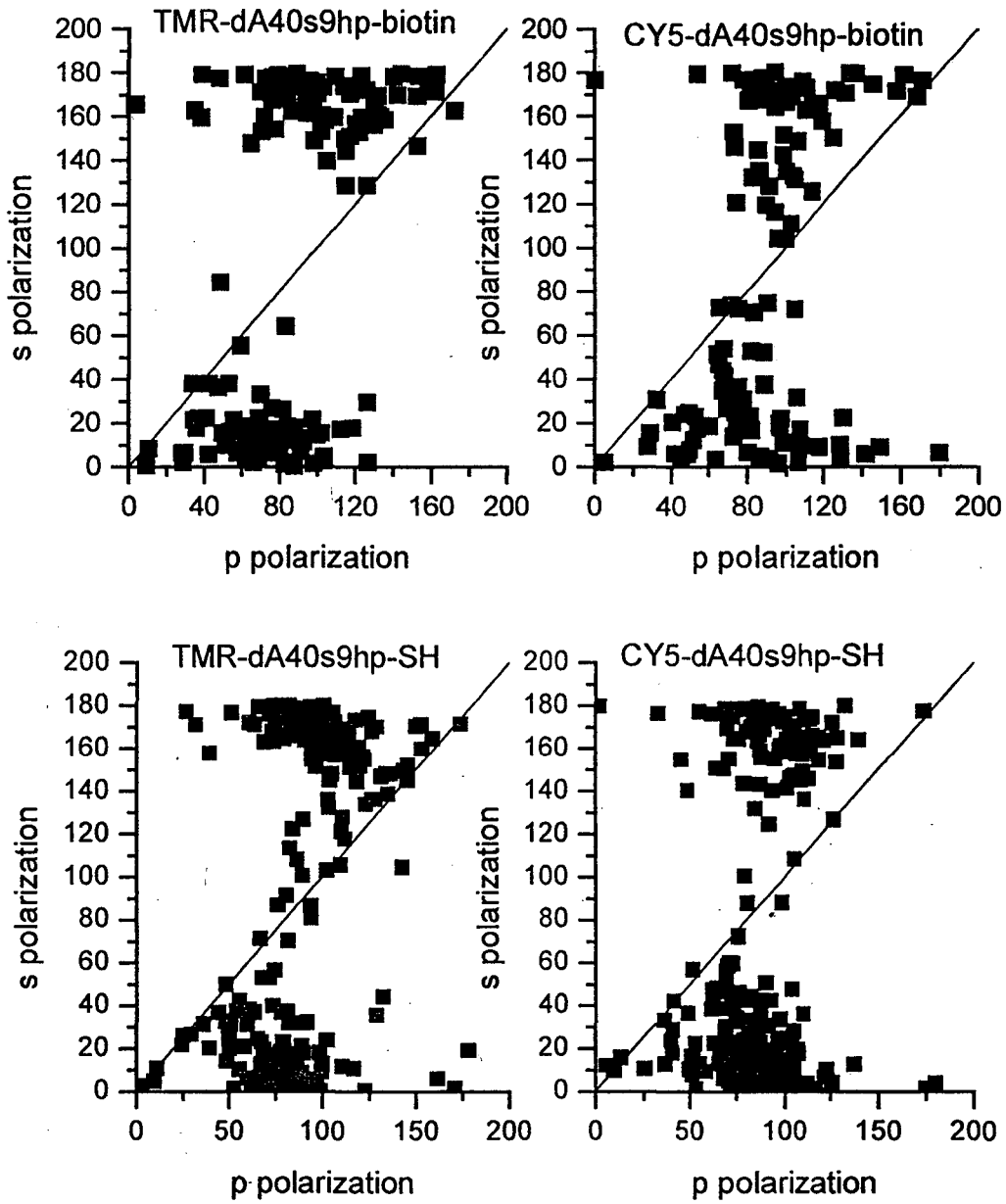

Figure 5. Polarization anisotropy data of dA40s9 hairpins bound via MPS or biotinylated-BSA-streptavidin surface preparations. Data clusters around 90 ° and 180 ° indicate freely rotating fluorophores, while points that lie along the line y=x indicate fixed fluorophores. Variation about 90 ° and 180 ° indicates limited fluorophore rotation. The majority of dye molecules are rotating for disulfide-linked hairpins (a) and biotin-streptavidin-linked hairpins (b).

show anti-correlated behavior on the p- and s-polarization channels, while fixed fluorophores show correlated behavior [37]. Data compiled over many single molecules is plotted as the angle parameter fitted p-angles versus the s-angles (Figure 5). Freely rotating fluorophores cluster around 90 ° and 180 ° (anticorrelated) while fixed fluorophores lie along the line y = x (correlated). Scatter around these two regimes indicates that rather than being fixed in place or having complete 2π freedom of rotation in the plane of measurement, there is some type of restricted rotational motion of the fluorophores. The biotin streptavidin surface preparation appears to offer slightly better fluorophore rotational freedom than the disulfide linkage. This may be attributable to an increase in surface interactions on the neutral mercapto-silanized glass surface than the negatively charged surface of the biotin-streptavidin surface preparation, which had additional quenching of the epoxy-silane derivitized surface by aspartic acid. In both cases, however, the majority of the fluorophores show significant degrees of rotational freedom, consistent with low interaction of the fluorophores with the glass surface.

Comparison of Diffusion and Immobilized Hairpins. Energy transfer efficiency histograms of DNA hairpins immobilized through a disulfide bond to the glass cover slips and freely diffusing in solution are compared in Figure 6. Diffusion data was acquired at 1 ms time resolution and the results indicated that fluctuations occurred on a slower time scale. The timescale of the hairpin fluctuations is also greater the 5ms/pixel image time resolution, consistent with our extrapolation from previous FCS data and data acquired in diffusion. Energy transfer efficiency histograms from image and diffusion acquired data were fit with Gaussian distributions. The width of the peak at zero energy transfer efficiency for the surface measurement is significantly broader than the peak in diffusion

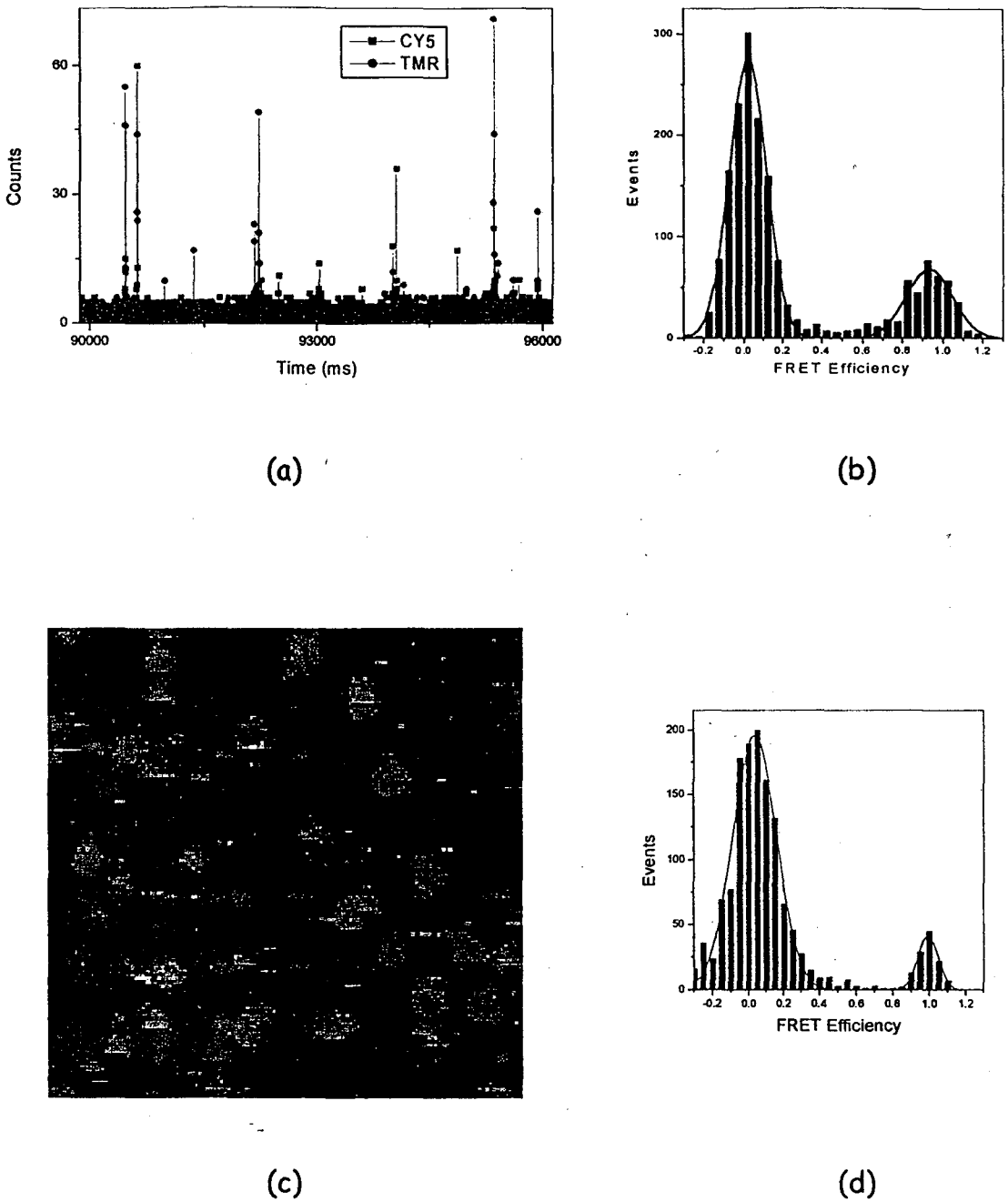

Figure 6. An example of diffusion (a) and image (c) data and analyses. Donor emission is shown in green and acceptor emission in red. The image is an overlay of simultaneously-acquired donor and acceptor images. Histograms are fit with Gaussian distributions. The high FRET peak position shows greater than 90% energy transfer efficiency for both immobilized (b) and diffusing hairpins (d). The width of the Gaussian fit is slightly larger for the image data than for the diffusion data, due to the higher background for surface immobilized hairpins. Image is formed scanning from left to right, top to bottom.

(0.25 versus 0.19) due the increased background that accompanies surface data. The comparable distributions of FRET events for image and diffusion data, along with the polarization data, indicate that while in some cases there is evidence of interaction between either the fluorophores or the DNA and the derivatized surface, the overall behavior of the immobilized DNA hairpins is similar to that of hairpins in diffusion.

The Effect of Stem Size on Opening and Closing Rates of DNA Hairpins. We monitored individual hairpins as a function of time to study the dynamics of the DNA fluctuations. Searches for molecules were accomplished by looking for emission from both donor and acceptor fluorophores. While the majority of molecules showed high degrees of energy transfer, no individual opening and closing events were observed out of over one thousand dA30s14 hairpin molecules sampled. We believe that the lack of measured opening and closing events for the 14-stem hairpin was due primarily to the limitations of the fluorescence technique used. Since the opening and closing rates for this hairpin were quite long, photobleaching of the fluorophores became a significant problem in the data acquisition. We were able to observe opening and closing events in 5 out of 200 (2.5%) of the smaller dA40s7 and 34 out of 1000 (3.4%) of the dA40s9 hairpins. Statistics on the conformational fluctuations were collected with these hairpins using the streptavidin-biotinylated-BSA surface. A longer ethylene glycol linker between the DNA and the surface-attaching group did not allow us to observe more folding events for the dA40s9-thiol hairpin.

The observed molecules typically showed constant FRET efficiency until photobleaching regardless of integration times that ranged from 0.2 to 25 ms. The photophysical behaviors of the fluorophores were taken into account when determining

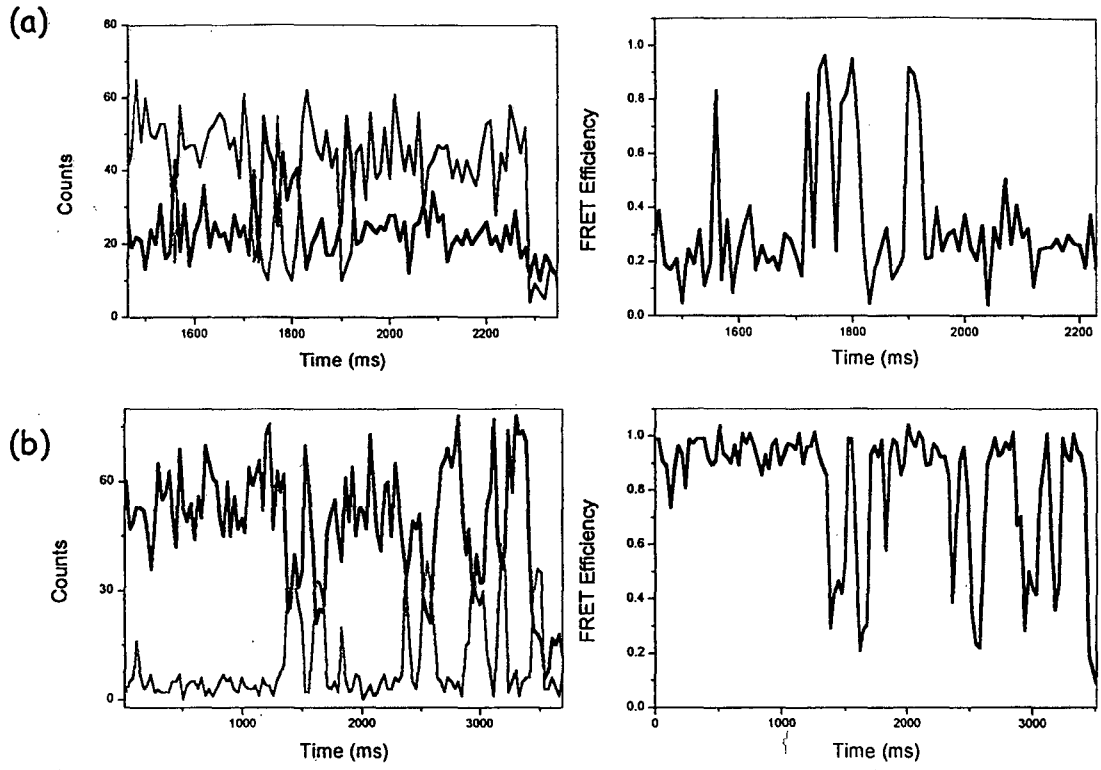

Figure 7. Examples of TMR and Cy5 fluctuations as a function of time for biotin-BSA-streptavidin immobilized hairpins (a) dA40s7 and (b) dA40s9. On the left, fluorescence signal shows anti-correlated behavior that is indicative of an energy transfer event. High Cy5 and low TMR signals indicate a folded hairpin, while low Cy5 and high TMR signals indicate a denatured hairpin. On the right are the calculated energy transfer efficiencies of the two traces. Acceptor is shown in black and donor in gray.

whether an observed time trace contained an opening or closing event. The addition of oxygen scavengers can have the undesirable effect of lengthening the triplet state lifetimes of fluorescent dyes, since molecular oxygen acts as a triplet state quencher. In addition, fluorescent dyes are known to have long dark states in which fluorescence is quenched. Both of these effects must be considered when deciding whether an anti-correlated change in donor and acceptor emission intensities is in fact an opening or closing event. Figure 7 shows time traces taken on dA40s7 and A40s9 hairpins. The advantage of using single pair FRET rather than the single fluorophore quenching of molecular beacons

for fluctuation measurements is evident in the time traces; it is easy to determine which fluctuations are due to conformations of the DNA and which are due to the photophysical behaviors of the dyes. For example, the open states of the hairpins shown in Figure 7 (a) and (b) differ from dark states of the acceptor because the acceptor fluorescence does not return to the background level but remains at E = 0.2, a value twice that expected from any leakage of the donor fluorescence onto the acceptor channel. The relatively long integration time used for time traces (5ms/point) effectively removes the complication of triplet states (typically ~μs) in the measurements. The time that the hairpin is open or closed was measured by the duration of an observed low or high energy transfer event, respectively. The duration of 39 high FRET events and 39 low FRET events were measured for the dA40s7 hairpin, and 98 high FRET and 94 low FRET events for the dA40s9 hairpin. For a simple reversible two-state process such as

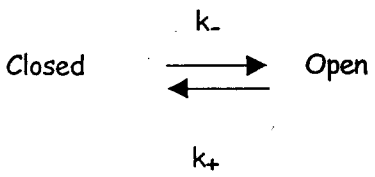

we expect exponential distributions for the closed and open state lifetimes, due to the Poissonian nature of the process [79]. Deviations from single exponentials in the state lifetimes would be indicative of a more complex kinetic process, such as kinetic trapping of the dyes or DNA by the surface. The measured open and closed state lifetimes were binned in histograms, and the distributions were fit with single exponential functions consistent with the two-state folding model of the DNA hairpin (Figure 8).

We observed exponential kinetics for the opening times of both the dA40S7 and dA40S9 hairpins that scaled consistently with their stem size. The dA40s7 hairpin was

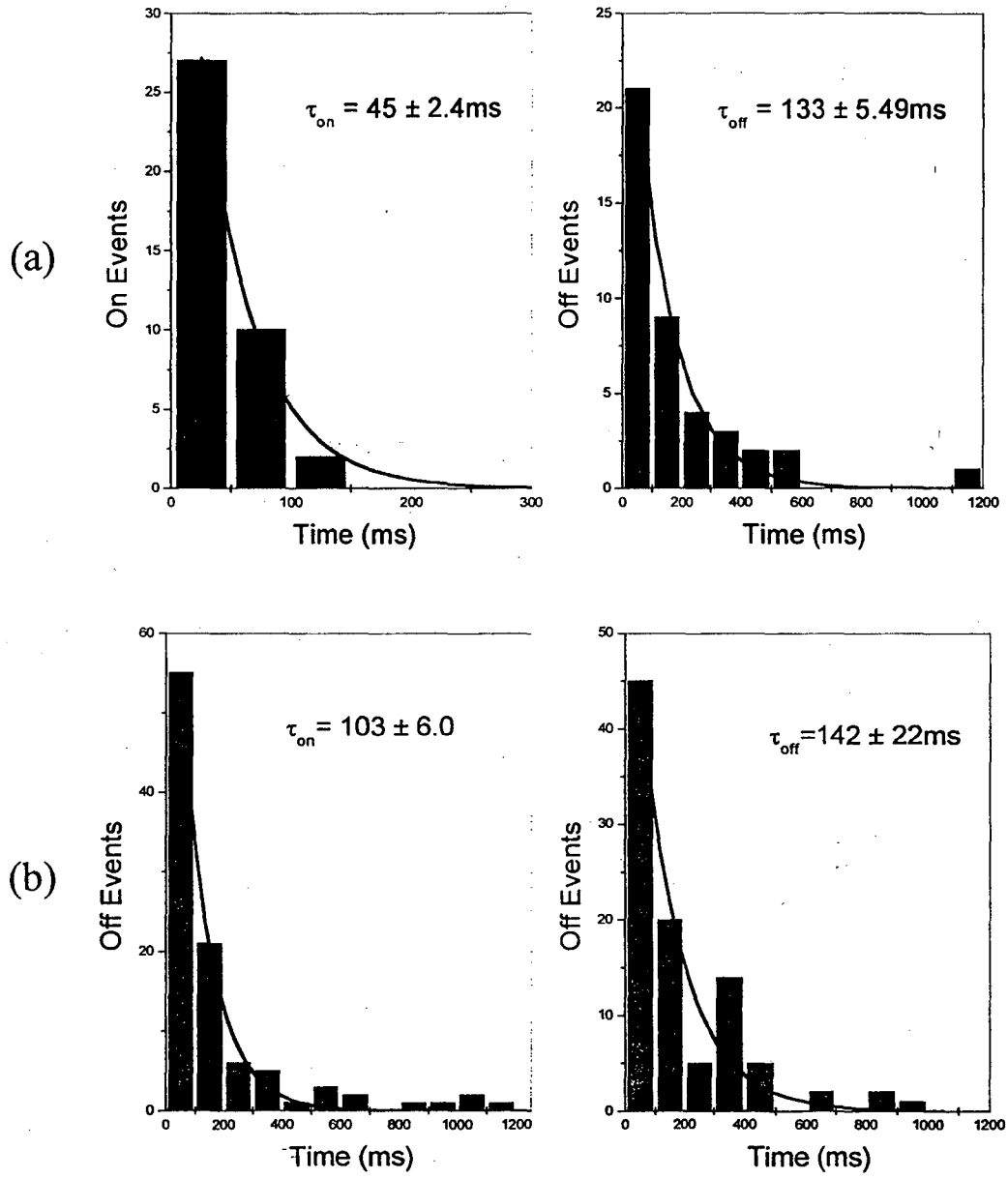

Figure 8. Exponential fits to on- and off-time (high and low FRET signals) for (a) dA40s9 and (b) dA40s7 hairpins. Fits assume two-state folding kinetics. On-time bin width for the dA40s7 hairpin is 50 ms, while off-time bin width is 100 ms. On-time bin width for the dA40s9 hairpin is 100 ms and off-time bin width is also 100 ms.

found to have an closed-time of 45 (± 2.4) ms while the dA40s9 hairpin had an closed-time of 103 (± 6.0) ms. The seven-stem hairpin had an open-time of 133 (± 5.5) ms and the nine-stem hairpin had an open-time of 142 (± 22) ms. These closed and open state lifetimes much

longer than the expected times of 0.5 to 2 ms that were extrapolated from the FCS work of Bonnet [72]. It is quite possible that tethering the hairpins to a glass surface has an effect on the overall kinetics of the hairpins. However, the hairpin opening and closing timescales measured by diffusion experiments were longer than expected, even at 50 °C, indicating that a simple extrapolation from the Bonnet data does not accurately describe the stability of these larger hairpins. It is important to note that while the timescales are increased in this case, the overall two-state kinetics of the system are preserved. The opening rates of the hairpins scale with stem size as expected, while the closing rates of the two types of hairpins agree within error, consistent with previous DNA hairpin results. The distribution of closed and open times in Figure 8 shows one of the advantages of single molecule measurements, since the timescale distributions would be hidden in an ensemble measurement.

Conclusions

spFRET was used to measure the denatured and folded-state lifetimes of DNA hairpins at single molecule resolution. While the overall kinetics of surface-immobilized hairpins qualitatively follows the kinetics expected from diffusion measurements, the timescales for the hairpins studied were found to be longer than those extrapolated from previous work by Bonnet *et al.* The longer time scales that we measure may be attributed to a surface effect that we were not able to detect. It is also possible that the scaling model derived from simulations does not accurately predict, for hairpins with a large number of adenines in their loops, the opening and closing timescales due to large excluded volume

effects [72, 80-82]. To conclusively rule out the possibility that the longer time scales that we observe for our hairpins are not due to surface effects, identical hairpins to those in Bonnet's study should be synthesized, surface immobilized, and studied either at the single molecule level or by surface-immobilized small-ensemble FCS.

We show that single molecule experiments allow direct measurement of the kinetic properties of biological systems, observations of rare events that are difficult if not impossible to detect at the ensemble level in the absence of synchronization, and examination of the distribution of properties within a population. The sensitive distance dependence of FRET measurements along with the surface immobilization and time trace analysis techniques described in this study may allow experimentation on more complicated hairpin kinetics. For example, single molecule FRET experiments may prove useful in studying the poorly understood kinetics of multiple alternate hairpin structures due to triplet base repeats (sliding hairpins) at sites of gene transcription and translation regulation that are thought to result in genetic diseases such as fragile X syndrome and myotonic dystrophia.

Chapter 5

Single Molecule Probes of the Local Environment

Introduction

The exquisite sensitivity of fluorophores to their immediate surroundings makes them ideal probes for the local environment. Fluorescent molecules can be found that are extremely sensitive to the surrounding solvent polarity, electric fields, ions such as Ca^{2+}, K^{+}, Mg^{2+}, or Na^{+}, and pH. This sensitivity can take the form of absorption and/or emission wavelength shifts and changes in quantum efficiency upon ion binding or solvent and potential changes. The natural fluorescence of the amino acid tryptophan has been used for years to study changes in protein structure upon denaturation or enzymatic activity, since tryptophan exhibits a large spectral shift to the red when its local environment is changed from a hydrophobic pocket to exterior solvent. In addition, tryptophan fluorescence can be quenched by nearby residues upon folding or externally supplied quenching agents upon denaturation [83]. The styryl dyes in the ANEPPS family are responsive to changes in local cell membrane potential, showing a large increase in fluorescence upon binding to the cell membrane and a linear response in fluorescence excitation ratio with changes in membrane potential [84]. Detection of Ca^{2+} levels is routinely performed in whole-cell microscopy

through the use of indicators such as aequorin, Fura-2, and Calcium Green [85]. By examining the individual dynamic behaviors of such fluorophores, information about the local environment surrounding a molecule may be obtained. In this chapter, the results from the study of such an environmental probe, the pH indicator seminaphthorhodafluor (SNARF) (C-1270 Molecular Probes) will be discussed.

Ratiometric Measurements

SNARF was studied using ratiometric diffusion and immobilization methods. Due to the low signal levels of single molecule measurements, shot noise, along with photophysical fluctuations (such as triplet states and long dark states) can cause severe fluctuations in the measured signal level of a fluorescent molecule. These fluctuations can lead to complications in the interpretation of the chemical or biological information obtained from the fluorescence measurement. By using ratiometric methods, some of these complications may be overcome. For example, by splitting the fluorescence onto two channels according to some parameter (eg wavelength or polarization), recording the intensities on two channels simultaneously, and then taking the ratio of the channels, photophysical events which affect both channels can be suppressed [75].

Protonation-deprotonation as a diffusion-limited reaction

As shown in Figure 1, upon protonation or deprotonation SNARF's ensemble absorption and emission properties shift to blue or red, respectively [86]. The protonated and deprotonated forms of the dye are shown in Figure 2. Because of the large shift in

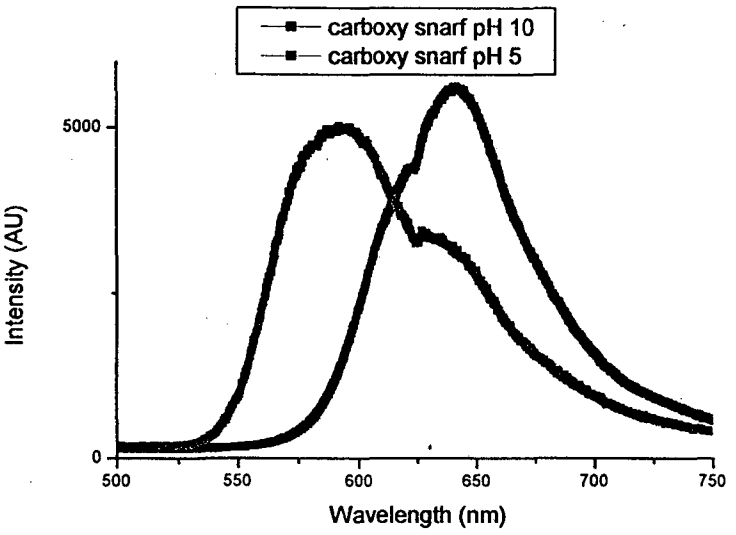

Figure 1: SNARF spectral shifts.

emission wavelength upon change in protonation state, it is possible to divide the emission of the acidic and basic forms into two detection channels by using a dichroic mirror centered at 610nm, the isosbestic point of the dye. The ratio of the emission on the two channels is then calculated as $I_{Long}/(I_{Long} + I_{Short})$. The pKa of SNARF has been measured to be 7.6 [87], making this dye an ideal pH indicator in the physiological pH range.

Because the protonation process itself is very fast, the speed of reaction of protonation and deprotonation of SNARF at the physiological pH's ranging from 6 to 8 used in this study are diffusion limited bimolecular reactions. This can be seen from a simple Fick's Law calculation. Following Daune [88], Fick's Law gives the flux of matter due to molecule A as

$$J_A = -D_A \frac{\partial C_A}{\partial r}$$

(assuming spherical symmetry). If molecule B is at rest and there exists a spherically symmetric reaction region of $r_0 = r_A + r_B$ around B that is devoid of A, we will have

$$C_A = 0 \qquad \text{for} \quad r < r_0$$

and $$C_A \rightarrow C_A^0 \qquad \text{for } r \rightarrow \infty$$

where C_A^0 is the mean concentration of A in molecules/volume. The flux of A flowing towards B through a sphere of radius r centered at B is given by

$$\frac{dn_A}{dt} = -4\pi r^2 D_A \frac{\partial C_A}{\partial r}$$

which is integrated to yield

$$\left(\frac{dn_A}{dt}\right)\int_{r_0}^{\infty}\frac{dr}{r^2} = 4\pi D_A \int_0^{C_A^0} dC_A$$

and we then have

$$\frac{dn_A}{dt} = 4\pi D_A r_0 C_A^0$$

Here, r_0 is in meters, D_A (the diffusion coefficient of molecule A) is in m^2s^{-1} and C_A in molecules per m^3, so that dn_A/dt is given in molecules s^{-1} and indicates the number of molecules of A colliding with B per second.

Taking into account the movement of B, D_A can be replaced with $D_A + D_B$, assuming the movements of A and B to be uncorrelated. The diffusion coefficient for a dye such as SNARF is ~ 10^{-6} cm^2/s, while the diffusion coefficient of the hydronium ion in water is ~ 10^{-5} cm^2/s. At pH 6, the concentration of hydronium ions is $1x10^{-6}M$, or $6x10^{14}$ molecules/cm^3. For a single

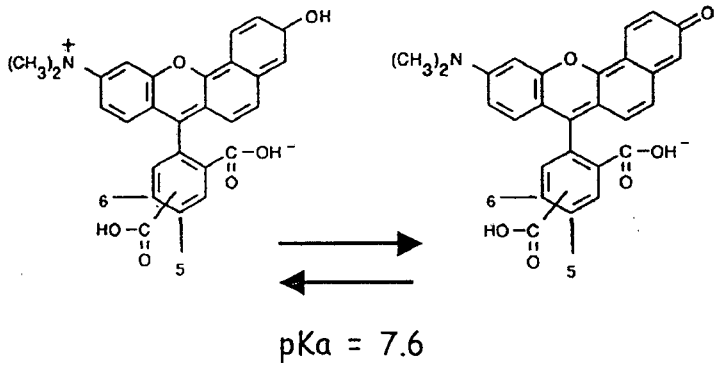

Figure 2: Protonated (a) and deprotonated (b) forms of SNARF.

dye molecule isolated within the femtoliter excitation volume of the laser, the rate of collision with a hydronium ion in pH 6 solution, assuming a rough reaction radius of 5Å, is then estimated to be $3.7x10^3 s^{-1}$. For diffusion measurements, an integration time of 0.2ms was used, which means that during a single time bin of the measurement at pH 7, there is approximately one diffusional collision event between the dye and a proton. Another way of looking at this is to note that in the femtoliter excitation volume at pH 6, there are 600 hydronium ions with which the SNARF molecule may interact. With each increase in the pH, the number of hydronium ions drops by a factor of ten, so that at pH 7 there are 60 and at pH 8 only 6. The likelihood of a protonation event is then very low at pH 8 and very likely at pH 6, and this is reflected in the observed SNARF population.

The assumption of only collisional interactions is overly simplistic, since there can be a charge interaction between the dye and hydronium or hydroxide ions depending on the charge state of the dye. It can be seen from Figure 2 that the deprotonated form of the dye is negatively charged, hence there will be a Coulomb attraction between the deprotonated form and nearby positively-charged hydronium ions. This attraction affects the estimated rate of protonation by introducing a multiplicative factor (5.7 in this case for an approximate reaction radius of 5Å). This extra attraction contribution manifests itself in the pKa of the dye, since $Ka = k_{dep}/k_{prot}$ and $pKa = -\log_{10}(Ka)$.

SNARF single molecule ratiometric measurements in diffusion

To demonstrate effectiveness of single molecule ratiometric techniques in resolving protonated and deprotonated dye population distributions, diffusion measurements of

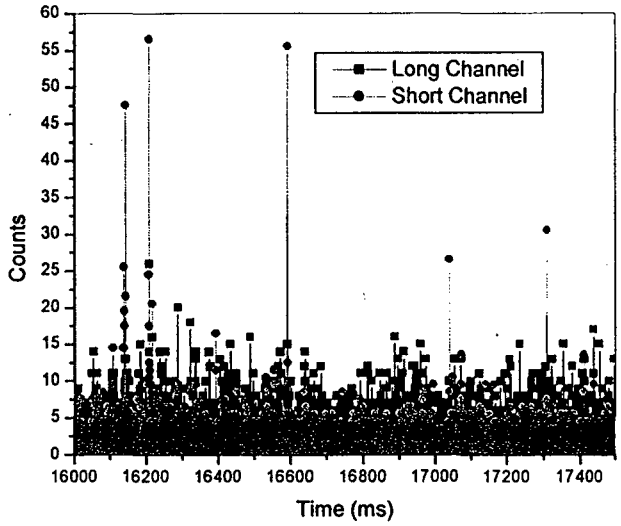

Figure 3: Example of diffusion time trace of fluorescent bursts in pH 6 buffer. The long channel (basic form) is shown in black and the short channel (acidic form) is shown in gray.

SNARF emission properties were performed. Single molecule diffusion measurements on SNARF consisted of the following: 55pM of carboxy-SNARF 1 was dissolved in sodium phosphate buffers ranging from pH 6 to pH 8 in increments of 0.2 pH units. Samples were made by sandwiching 15μL of solution between two hydrofluoric acid-cleaned coverslips, with a Parafilm gasket as a spacer between the coverslips. The samples were excited with circularly polarized light at 514nm, using the set-up described previously in Chapter 2. A 100μm pinhole was used to filter out out-of-focus background. 500μW of excitation was focused 10μm into the fluid from the lower coverslip and the fluorescent bursts were passed first through a dichroic centered at 530nm (530drlp Omega Optical) and then through a 550 long pass filter (Edmund Scientific). The long and short wavelength emission was then split at the 610nm dichroic onto two APDs. An example of such single molecule fluorescence bursts can be seen in Figure 3. Background was subtracted by measuring first buffer-only samples and then subtracting the average buffer-only emission from the

measurements of samples containing SNARF. Ten minutes of fluorescence bursts were analyzed and compiled into histograms for each pH. Only time bins that had signal levels greater than 10 times the standard deviation of the background were considered.

For each event above the cutoff threshold, the ratio of the emission on the long and short wavelength detectors was calculated according to $r = I_{Long}/(I_{Long} + I_{Short})$, where I_{Long} is the long wavelength (deprotonated) signal and I_{Short} is the short wavelength (protonated) signal. These r ratios were then compiled into a histogram for each pH run (Figure 4). For a pH of 6, with emission predominantly less than 610nm, we see a distribution closer to r = 0, while for the predominantly long wavelength emission of pH 8, the distribution is shifted towards r = 1. At pH 7, a bimodal distribution is clearly resolved, indicating separately the equilibrium protonated and deprotonated populations of the fluorophore. The two resolved states of the molecule suggest an equilibrium protonation/deprotonation conversion rate that is slower than the integration time (0.2ms). As can be seen in Figure 4, the pKa of ~ 7 measured in this manner differs from the ensemble value of 7.6. This is likely due to leakage of the tail of the protonated fluorescence spectrum onto the long wavelength detection channel and the higher quantum efficiency of the basic form of the dye.

An attempt was made to increase the reaction rate of the protonation-deprotonation process of SNARF free in diffusion by increasing the temperature of the sample. Since the quantum efficiency of SNARF is already quite low compared to most dyes (0.047 for the acidic form and 0.091 for the basic form) [87], the additional decrease in quantum efficiency produced by the increase in temperature made single molecule detection very difficult and this effort was abandoned.

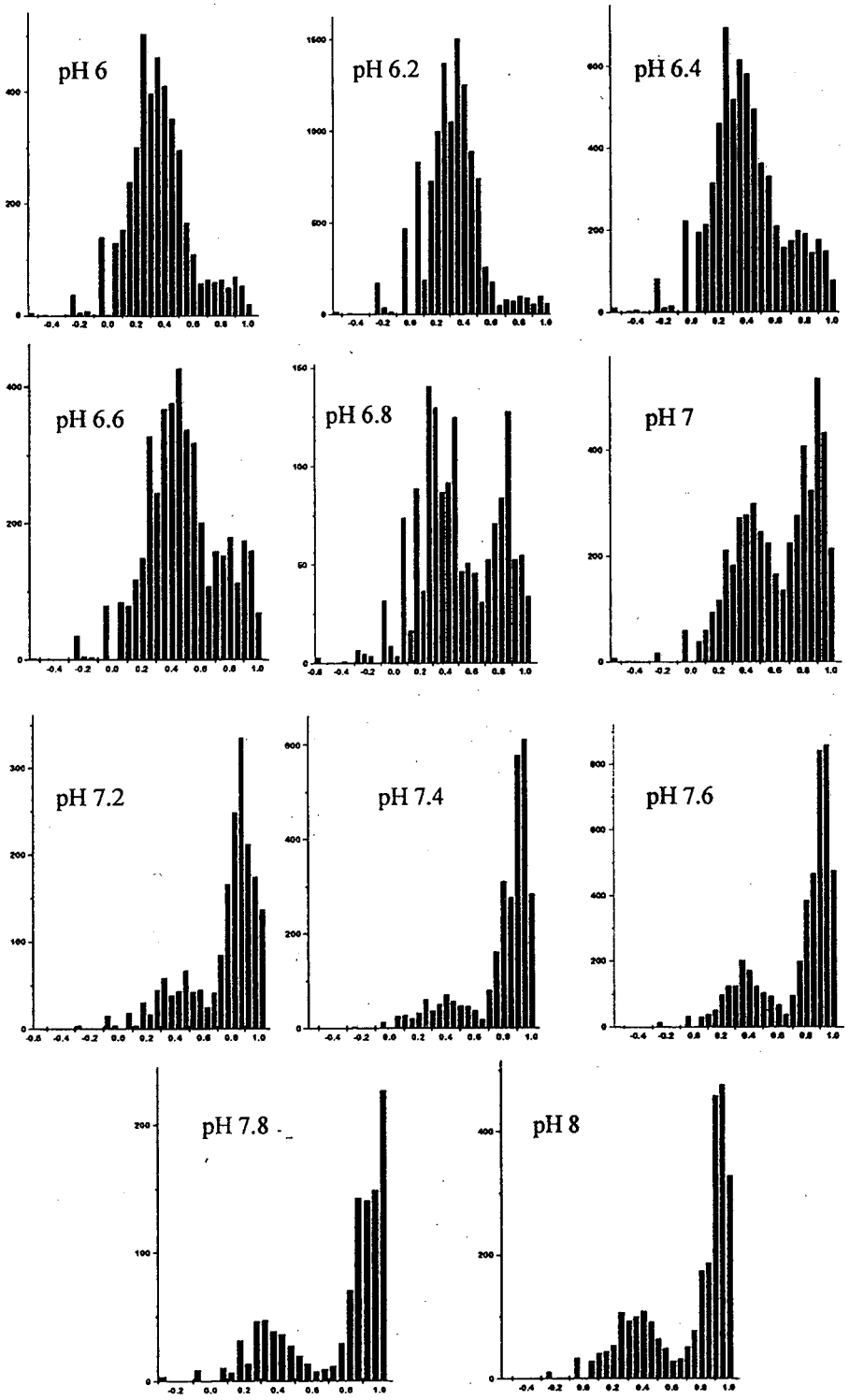

Figure 4: Distributions of protonated and deprotonated forms of SNARF. Here the number of events measured above the cutoff threshold is plotted versus the quantity $r = (1+I_{short}/I_{long})^{-1}$.

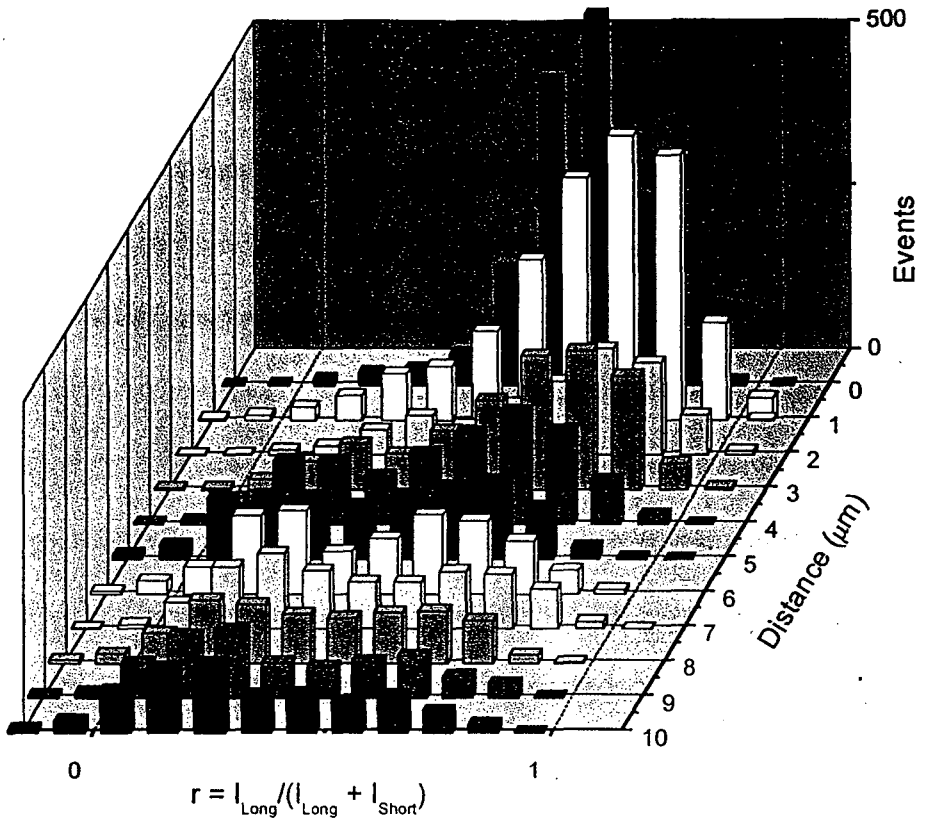

Figure 5: SNARF diffusion events for a pH 6 solution and an acetone-methanol-DI-cleaned coverslip. Diffusion traces are taken at 1μm increments starting at the coverslip and progressing into the sample. The number of events shown at the coverslip (0μm) has been reduced by a factor of five from the data to fit on the same scale as the other measurements.

Local Chemistry Reflected by Diffusing Single Molecules

The local chemistry of the glass surface was found to have a strong effect on the concentrations and distributions of the protonated and deprotonated forms of the free dye molecules in diffusion (Figures 5 and 6). For example, a glass surface cleaned with hydrofluoric acid resulted in a negligible concentration of fluorophores diffusing at or near the glass surface, while a glass surface cleaned with an acetone-methanol-deionized water

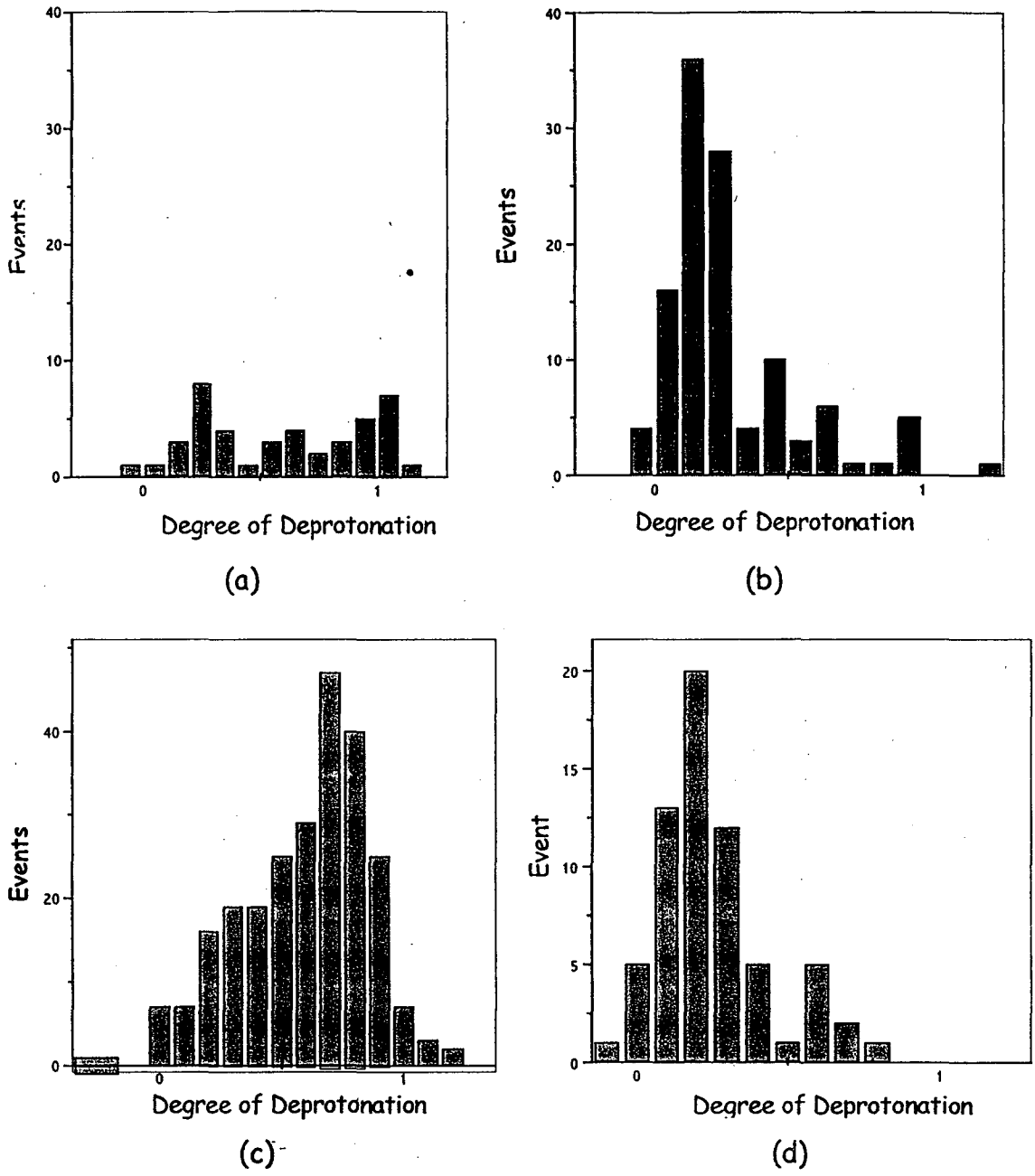

Figure 6: Distribution of SNARF diffusion events for a newly-HF-cleaned coverslip at the surface of the coverslip (a) and 10μm into the sample (b). Plotted is the number of diffusion burst events vs. $I_{long}/(I_{short} + I_{long})$. The large peak on the left side of (b) indicates a protonated, or acidic form of the SNARF indicator. The distribution of SNARF diffusion events (same concentration) for a coverslip cleaned in the same batch as that shown in (a) and (b) but after one week of storage is shown in the lower two plots. Diffusion events in (c) are at the surface of the coverslip while those shown in (d) occur at 10μm into the sample. It can be seen that the solution at the surface in (c) is primarily basic, while the bulk solution shown in (d) is primarily acidic. The pH of the buffer used in both cases was 6.4.

sequence resulted in a substantially higher concentration of fluorophores near the surface, with longer average residence times. Changes in the borosilicate glass surface chemistry could also be measured over time. A freshly HF-cleaned coverslip was shown to have a very low concentration of SNARF diffusing at or near the glass coverslip, while the population of the fluorophore deeper within the sample was higher and reflected the bulk pH of the sample. However, if these HF coverslips are examined a few days later, the fluorophore behavior reflects a completely different surface chemistry, with higher concentrations near the surface, and distinctly different pH's at the surface and within the bulk of the sample, even with the same bulk pH as before (Figure 6). A glass surface cleaned with hydrofluoric acid initially contains a large number of silanol groups, which are negatively charged at neutral pH. The measured change in surface pH over time is attributed to outgassing of alkaline species from the bulk of the borosilicate glass onto the surface [Corning, private communication]. This change in the local surface chemistry can have large unwelcome effects on experiments involving the immobilization of biological molecules at the glass surface, since the behavior of these molecules will also be modified by their environments.

Local Environment Effects of Surfaces

To examine the effects of the local environment of the glass surface on protonation-deprotonation rates of immobilized molecules, bulk spectra of surface-immobilized SNARF molecules were taken. In order to obtain surface spectra, surface chemistries were developed to attach SNARF molecules to glass coverslips. Initially,

SNARF-labeled dextrans (10,000MW dextrans with 0.5-2 dyes per dextrans) was purchased from Molecular Probes (D-3303), and residual amines left from the dye-labelling process were then used to couple the SNARF-dextrans to glass coverslips coated with activated 3-glycidoxypropyltrimethoxysilane (see Chapter 3). Due to the scarcity of residual amines in the SNARF dextrans, coverage was not optimal for the necessary ensemble measurements of spectra of the SNARF-dextrans at the surface, although the coverage was optimal for single molecule measurements, which will be discussed below. To increase the coverage for ensemble surface spectra, Carboxy-SNARF-1 was covalently bound to 3-aminopropyltriethoxysilane-coated glass via the sulfosuccinimidyl ester formed by activating the carboxylic acid dye in solution with 1-ethyl-3-(3-dimethylaminopropyl) carbodiimide (EDAC) and hydroxysulfosuccinimide (NHSS). Spectra taken of the ensemble dye at the glass surface showed that the rates of protonation and deprotonation were drastically different from that of the dye freely diffusing in solution (Figure 7). This result was borne up by single molecule time traces taken on individual surface-immobilized SNARF molecules, since even at pH 6 the average spectral weight of most fluorophores observed was to the red (data not shown). The difference between the ensemble and surface spectra is attributed to the

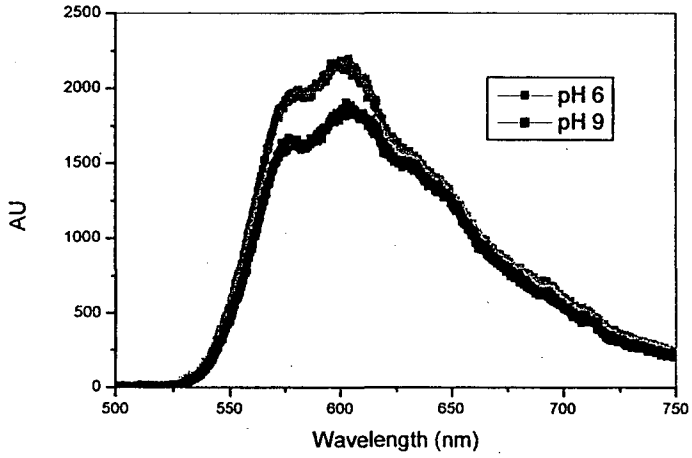

Figure 7: Spectrum of SNARF at coverslip surface.

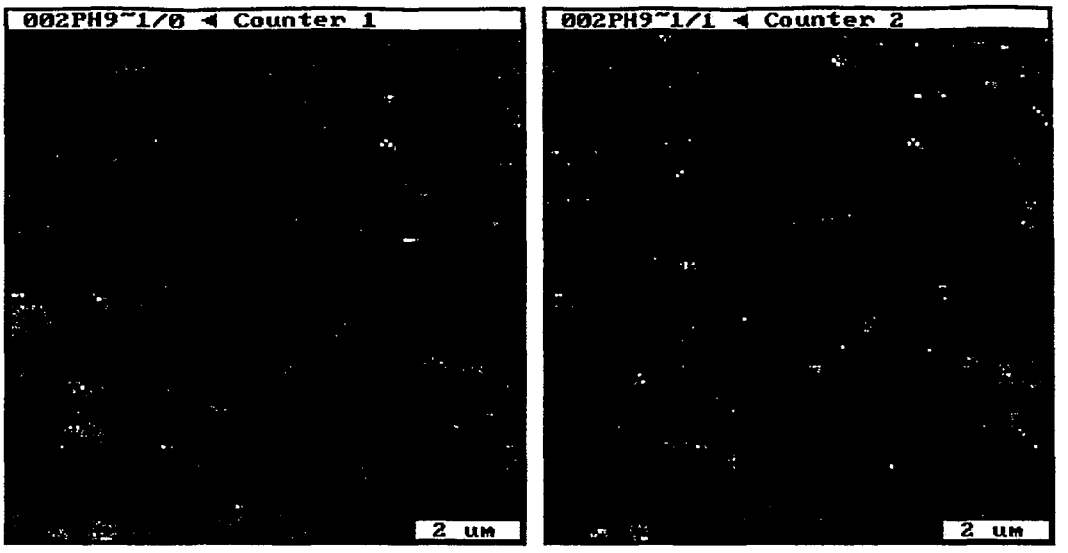

Long Wavelength Channel Short Wavelength Channel

Figure 8: Image of dextran-immobilized SNARF molecules on glass coverslip.

charge double layer that exists at the interface between the glass coverslip and buffer solution. This double layer is believed to be around 3nm thick at the pH's and ionic strengths used here [7].

Images and time traces of immobilized SNARF

The lower bound on the protonation/deprotonation conversion rate suggests that it should be possible to observe individual protonation/deprotonation events, provided that the fluorescence from a single SNARF molecule can be isolated and observed over longer periods of time than are allowed in diffusion. To accomplish this the dextrans surface-immobilization method was employed, resulting in a covalent attachment of the SNARF-dextrans to the glass and allowing single molecule measurements of SNARF (Figure 8). Analysis of 881 single molecule time trajectories in solution at pH 7 yielded 69 molecules

that showed spectral jumps after long dark states (see for example Chapter 1, Figure 2). The source of such long dark states has been speculated upon by many in the single molecule field. Interestingly, most of the spectral jumps observed in the population of SNARF molecules were jumps to shorter wavelength. While these changes in spectrum are related to the local environment and sudden chemical changes of the fluorophores, it is doubtful that they are actually protonation events. Similar jumps to the blue have been seen on other types of fluorophores [89], and the frequency of spectral jumps was far slower than expected for such a diffusion-limited reaction.

Snarf Immobilization in Gel

While molecules did show fluctuations in spectrum between blue and red on the millisecond time scale (Figure 9), the vast majority of time traces taken on surface-immobilized SNARF-dextrans molecules showed no spectral fluctuations indicative of protonation or deprotonation events. Since buffering the electric bilayer is not possible, various methods of extending the fluorophore distance from the glass surface or shrinking the double layer were tried, including protein-coating the surface, using aminosilanes with longer carbon linkers, and applying charge-quenching agents. These techniques did not improve the spectral response of the SNARF, so methods of single molecule detection in gel were pursued. Initially it was attempted to isolate single carboxy SNARF molecules in agarose gel, however, even with gel concentrations up to 10%, the pores were too big to trap the diffusing dye. Polyacrylamide 19:1 gels of concentrations from 4% to 30% were then tried, but the polyacrylamide was found to quench the fluorescence of the SNARF.

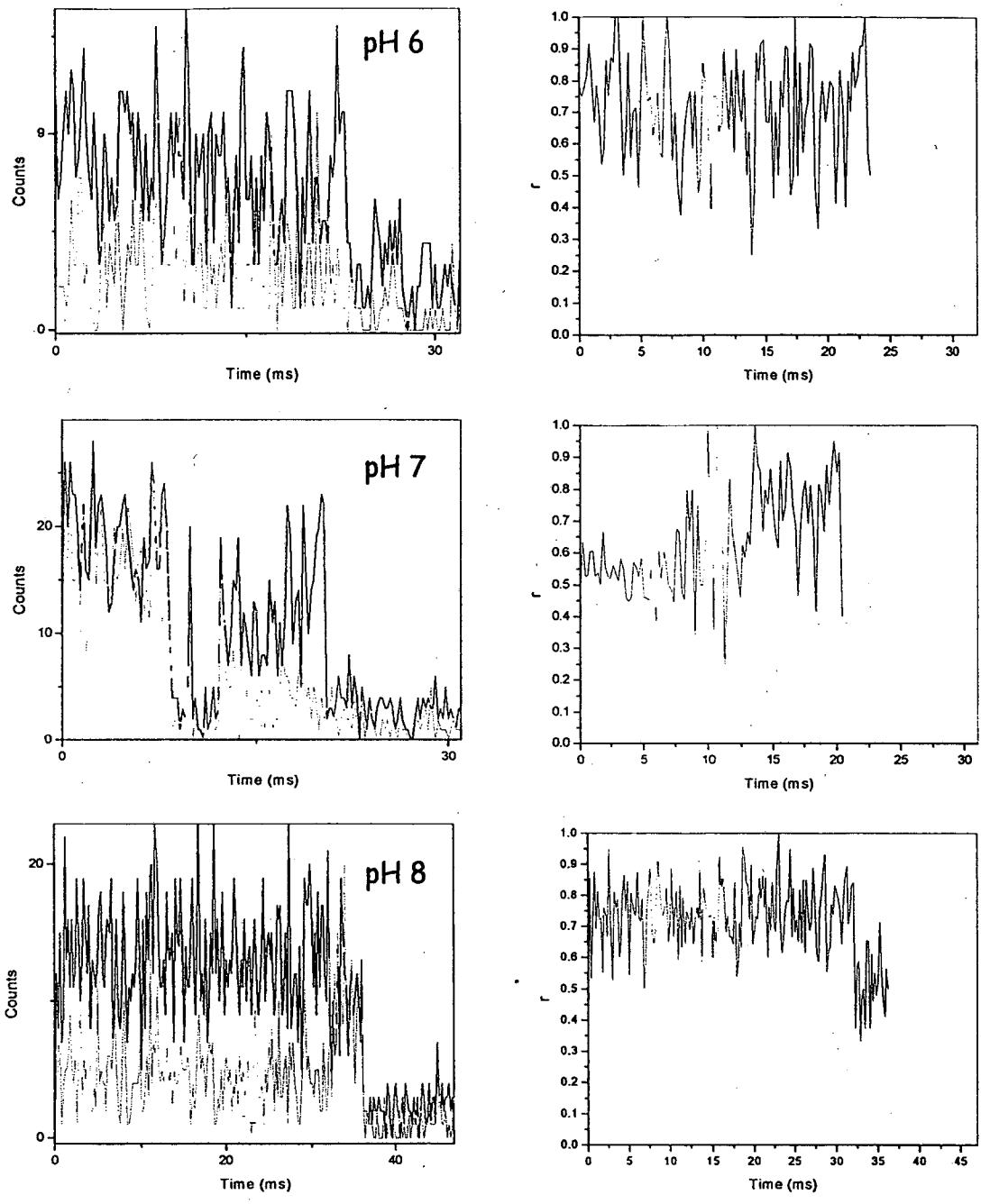

Figure 9: Spectral fluctuations of individual surface-immobilized SNARF-dextrans molecules: (a) time traces and (b) plotted r values as functions of time for the traces in (a). In (a), the long wavelength channel is shown in black and the short wavelength channel in gray. r values are shown up to the point of photobleaching.

Since the use of polyacrylamide was then ruled out, a new method of trapping the SNARF molecules in agarose was developed. The 60,000 MW protein streptavidin was labeled with SNARF (see Chapter 3), and the product was separated from the free dye in a 5000 MW desalting column. Gel samples were prepared in a manner similar to that of Xie et al [3]. HF-cleaned coverslips were spin-coated with 4% agarose gel, and the 1% gel containing the SNARF-labelled streptavidin was then sandwiched in between these coated slips. For pH's below the pI of the protein, there was a tendency of the protein to immobilize on the glass surface, rather than in the gel, due to glass-protein charge interactions. For pH's of 7 and higher there were far fewer fluorescent spots at the glass surface, with significantly more fluorescent spots within the gel itself. Time traces of these fluorescent spots were taken, however, the traces were found to be far noisier than on surface-immobilized molecules. Contribution to an increased background from the gel made data collection at millisecond time resolution difficult, even for a ratiometric measurement.

As the SNARF experiments discussed in this chapter were being performed, similar measurements of SNARF-dextrans immobilized in gel were made in Moerner's laboratory at Stanford by Sophie Brasselet [90]. The study of Brasselet was conducted at a rather long time resolution (20ms) for the observation of protonation/deprotonation events, and the distribution of spectral properties were taken over whole molecule time traces, yielding the average behavior of each fluorophore. This distribution showed large static inhomogeneities in the SNARF population at pH's near the pKa of the dye. The large distribution of emission properties was attributed to changes in the pKa's of the individual fluorophores, due to fluctuations in their local nanoenvironments. Such large distributions in behavior are intriguing, since they indicate that even in the relatively inert matrix of

agarose gel, macromolecules such as dextrans can sample a variety of environments. Communication with Brasselet indicated that their group also found difficulties in obtaining information from time traces taken at shorter time resolution, due to the poor quantum efficiency of this dye.

Conclusions

The pH indicator SNARF has proven to be very useful in demonstrating the advantages of single molecule ratiometric measurements. Observing the change in population of the two fluorescent states of the molecule for varying buffer conditions shows the power of single molecule measurements in examining the distribution of properties of a system. Specifically, directly viewing the protonated and deprotonated populations allows the direct determination of the pKa for this dye. The examination of the fluorescent behavior of individual SNARF molecules also provides an excellent example of another of the strengths of single molecule work, which is the ability to examine specific environmental changes over a very local scale. Such phenomena as the demonstrated change in pH over the few microns near a glass surface would be difficult, if not impossible, to resolve in ensemble measurements. The ability to resolve the protonation state of individual molecules leads directly to the idea of using a probe such as SNARF to study the nanonenvironments of individual macromolecules in much the same way that tryptophan residues are used to report local changes in protein structure via their sensitivity to solvent polarity. Biological macromolecules are highly sensitive to their local environments, and in the setting of a cell these environments can fluctuate greatly from molecule to molecule.

The use of individual fluorescent indicators in monitoring the nanoenvironments of proteins, nucleic acids, and other biological macromolecules could prove highly useful in understanding the distribution in nature of biological processes.

Chapter 6

Oxygen Scavenging

Introduction

Single molecule spectroscopy via laser-induced fluorescence has been plagued by the problem of photobleaching, the irreversible photochemical process in which a fluorescent molecule becomes non-fluorescent. Since single molecule fluorescence techniques involve detecting the emission from a single fluorophore, signal to noise is a critical issue and every photon counts. Photobleaching of the fluorophore ends the measurement, so in applications in which fluorescent molecules are used with biological systems, it sometimes becomes necessary to sample thousands of molecules in order to find a statistically significant number of molecules with fluorophores that survive long enough for the desired measurement to be completed. In order to compensate for the effects of photobleaching, one can reduce the power of the excitation light, but in order to collect enough photons for sufficient signal to noise data must be collected over long times, resulting in lower time resolution. In some cases photobleaching may serve a useful purpose. For instance, the presence of the abrupt, step-wise end of fluorescence emission is often used as an indication of the presence of a single fluorophore. In single pair fluorescence resonance energy transfer (spFRET) experiments, the photobleaching of the acceptor molecule and

the subsequent recovery of donor molecule emission is used as proof of the presence of a single FRET pair and also allows the pairwise calculation of the energy transfer efficiency. For the most part, however, photobleaching has presented a significant hurdle for researchers attempting to study systems using single fluorescent molecules. Photobleaching can skew statistics, make finding active molecules very difficult, and limit the ability to measure photophysical changes that occur over long time scales.

Role of Oxygen in Photobleaching

It is generally acknowledged that while other free radicals can attack fluorescent molecules, highly reactive singlet oxygen is a major culprit in the process of photobleaching [91,78]. Photobleaching can occur from either the singlet or triplet states of a fluorescent molecule. However, since the triplet state of the molecule is typically much longer lived than the singlet excited state (10^{-6} to 10^{-3} seconds for the triplet state versus 10^{-9} seconds for the singlet state) it is the triplet state of the molecule that is more susceptible to interaction with singlet oxygen. Triplet oxygen (the ground state of the oxygen molecule) serves the useful purpose of enhancing the intersystem crossing transition of a fluorophore from the excited triplet state to the singlet ground state by interacting with a fluorophore in the long-lived triplet state. This interaction can take the form of either physical or chemical quenching [92,93]. Triplet oxygen quenching of the singlet and triplet states of organic molecules is in general within an order of magnitude of the diffusional quenching constant [94], with S_1 quenching occuring at the diffusion rate and quenching of T_1 typically slower. Since the time the fluorophore resides in the triplet state is lessened, this triplet

quenching increases the excitation level at which the fluorophore emission saturates. It is often the quenching of the triplet state of the fluorophore by triplet oxygen that leads to the production of highly reactive singlet oxygen species:

$$S_o \xrightarrow{h\nu} S_1 \xrightarrow{ISC} T$$
$$T + {}^3O_2 \xrightarrow{ISC} S_o + {}^1O_2$$

Molecular oxygen is found typically at 250μM concentrations and the singlet form has a lifetime ~ 4μs in aqueous solution. Since the singlet oxygen is in close proximity to the dye molecule immediately after this conversion, it has a higher chance of reacting with the dye. This reaction can take many forms [95] and seems to be dye dependent [96], but the result of a dye-singlet oxygen reaction typically results in the destruction of the fluorophore. There is then a competition between the positive effect of triplet oxygen quenching and the negative effect of photodestruction due to singlet oxygen.

Oxygen Scavenging Systems

While ideally fluorescence measurements should be carried out in the absence of oxygen and in the presence of an effective triplet state quencher, most researchers have resorted at one time or another to oxygen scavenging systems, seeking to remove oxygen completely from their systems. The most popular of these currently is the glucose oxidase (GOD) enzymatic system. This system utilizes the catalysis of glucose into water and hydrogen peroxide. It is often necessary to provide the system with a second enzyme, catalase, in order to avoid unwanted build-up of hydrogen peroxide over time, since the breakdown of hydrogen peroxide by chlorine also produces singlet oxygen.

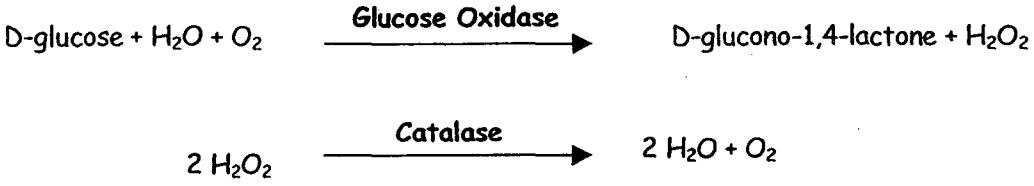

While the GOD system has been used with success in single molecule experiments [14,77], an enzyme-based oxygen scavenging system is often impractical. An example of this is protein denaturation-renaturation experiments, either by denaturants such as guanidine hydrochloride and urea or by temperature. In measurements such as these, the GOD system will obviously also be denatured. We describe here the investigation of the utilities of various small molecule oxygen scavengers for single molecule experiments. We present results of fluorescence correlation spectroscopy (FCS) measurements of the photophysical properties of fluorescein and rhodamine 6G with and without four different oxygen scavengers: GOD, a water-soluble vitamin E analogue known as Trolox™ ((R)-(+)-6-Hydroxy-2,5,7,8-tetramethylchroman-2-carboxylic acid), n-propyl gallate (PG), and 2-mercaptoethylamine (MEA or cysteamine). We then demonstrate the effectiveness of the different scavengers in single molecule diffusion measurements with DNA hairpins, using a tetramethylrhodamine (TMR) and cyanine five (Cy5) dye pair in single pair fluorescence resonant energy transfer (spFRET) experiments.

Fluorescence Correlation Spectroscopy

Measurements of the photobleaching rates and triplet lifetimes of both fluorescein and rhodamine 6G have been described previously in the presence of oxygen, with the

addition of potassium iodide (which is known to increase the intersystem crossing rate), and with the replacement of oxygen with argon in solution [97,98]. Following the method of Widengren et al, we performed FCS measurements on fluorescein and rhodamine 6G in the presence and absence of our four oxygen scavenging systems in order to measure the effects of the different oxygen scavengers on the photobleaching and triplet states of the fluorophores. For FCS measurements, the cross correlation of the intensity time traces was performed, and these cross correlations were fit by a function of the form

$$G(\tau) = \frac{\langle I(t)I(t+\tau)\rangle}{\langle I(t)^2\rangle} = \frac{1}{N(1-F_{triplet})}\frac{1}{1+\frac{\tau}{\tau_{diff}}}\left[F_{Triplet}e^{-\tau/\tau_{Triplet}} + (1-F_{Triplet})\right] + DC \quad (1)$$

in which N is the number of molecules in the excitation volume, $F_{triplet}$ is the fraction of molecules in the triplet state, τ_{diff} is the diffusion time of the molecule through the excitation volume, and $\tau_{triplet}$ is the triplet state lifetime. The cross-correlation of two detectors was performed instead of the autocorrelation of one detector in order to reduce effects due to the dead times of the detectors.

Single Molecule Measurements

To show the effect of oxygen scavengers on biological single molecule experiments, we examined the property distributions for single pair fluorescence resonance energy transfer in a DNA hairpin system. DNA hairpins serve as a simple model of a two state molecular system. A DNA hairpin is formed as a consequence of inverse repeats in a single

strand of DNA connected by a sequence of non-complimentary DNA. As part of our research, we have been studying the kinetic behavior of DNA hairpins freely diffusing in solution, using the method of single pair fluorescence resonance energy transfer (spFRET). In our case, the end of a DNA hairpin is labeled with an acceptor fluorophore while a base in the loop of the hairpin is labeled with a donor fluorophore. For the purposes of this chapter, our interest in the actual conformational behavior of our DNA hairpins is secondary. What is important is that the DNA hairpins can exist on one of two states, a "denatured" or open conformation, with a low degree of energy transfer efficiency, and a closed or "native" conformation, with a high degree of energy transfer efficiency. Further details of the kinetics of these hairpins can be found in Chapter 4. Our hairpins were designed so that in the closed state the distance between the donor and acceptor fluorophores produces close to 100% energy transfer (Chapter 4, Figure 1). In this case we expect to see only emission from the acceptor fluorophore. In the open state, the fluorophores should be far apart and the resulting energy transfer efficiency is predicted to be 0%, leaving only donor fluorophore emission. The use of the dye pair of TMR-CY5 is highly desirable for FRET measurements for a number of reasons: the donor is easily excited with the 514nm line of an argon laser while there is negligible excitation of the acceptor, there is a large spectral separation between the emission of the two dyes, and the Forster radius for these two dyes (53Å) is comparable to many relevant biological length scales. The drawback to this dye pair is the very poor photostability of the acceptor CY5. It has been shown previously [50] that if there is a large amount of preferential photobleaching of the acceptor fluorophore, the resulting distribution of energy transfer efficiencies may be skewed. This can give the appearance of either more low energy

transfer events within the population than is correct or incomplete double labeling of the sample.

Materials and Methods

Experimental apparatus: FCS and single molecule measurements were carried out using the Zeiss confocal microscope system described previously in Chapter 2. Laser light at either 488nm (fluorescein) or 514nm (rhodamine 6G or DNA hairpin) was first reflected off a dichroic beamsplitter (Omega Optical 495drlp or 530drlp) before illuminating the sample. A 63X 1.2 NA water immersion objective (Zeiss C-Apochromat) was used to focus the excitation light into a diffraction-limited spot. Polarizers and waveplates were used to maintain a circularly polarized excitation polarization. Fluorescence from the sample was collected by the objective and passed back through the dichroic. After passing through a holographic notch filter (Kaiser Optical HNPF 488 or 514) to further remove Rayleigh-scattered excitation light, the fluorescence was sent to two avalanche photodiodes. In the case of DNA hairpin spFRET measurements, the light from the donor and acceptor fluorophores was split at a second dichroic (Omega Optical 630drlp) and passed to separate avalanche photodiode detectors (APD's) (EG&G AQ141). To reduce cross-talk between the two channels in the DNA experiments, a band-pass filter (Chroma Technologies 585df60) was placed in front of the donor APD and a long-pass filter (Chroma E650LP) was placed in front of the acceptor APD. For single fluorophore measurements a simple bandpass (530 df60 for fluorescein) or long pass (550LP for rhodamine 6G) was used, and the fluorescence

was split using a non-polarizing beam splitter cube onto two separate APD's. The cross correlation of these two channels was then performed.

Blank samples containing only buffer and the oxygen scavengers were examined to make sure there were no false positive events due to contamination. The GOD system (Boehringer Mannheim) was prepared by first dissolving 500μM glucose in a NaP buffer, followed by the addition of 62.5nM of GOD and 62.5nM of catalase. For Trolox™ (Sigma), n-propyl gallate (Sigma), and cysteamine (Fluka), each was dissolved first in 50mM concentration in DMSO and 10μL of this solution was dissolved in a pH 7 NaP buffer (50mM NaP, 50mM NaCl) to yield a final concentration of 500μM of the oxygen scavengers. To each of these aliquots was added 50pM of DNA hairpin for single molecule measurements or 1nM of dye for FCS measurements. Use of tens of picomolar concentrations for single molecule measurements reduces the probability of finding two or more molecules in the beam simultaneously to a negligible value. A sample cell was formed by placing 15μl of either the DNA or dye sample solution between two hydrofluoric acid-cleaned coverslips, with a Parafilm gasket as a spacer between the coverslips. The excitation beam is focused 10μm into a sample cell and a 50μm pinhole is used to remove out-of-focus light, resulting in an effective femtoliter sample volume. Bursts of fluorescence photons are emitted as dyes or dye-labeled hairpin molecules diffuse into and out of the excitation beam. For the single molecule DNA hairpin samples, these bursts were recorded with a time resolution of 1ms over ten minute intervals and the time traces of bursts are analyzed via Matlab algorithms to collect statistics on the hairpin sample. A suitable threshold above background was chosen in order to reduce the likelihood of false positive events while retaining the maximum number of fluorescence bursts, and the number of events occurring above this

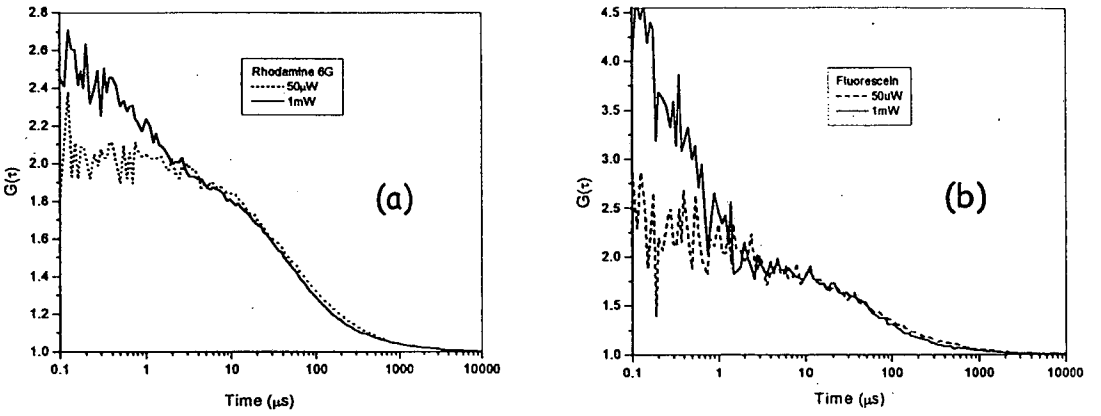

Figure 1: FCS cross correlation traces of (a) Rhodamine 6G and (b) Fluorescein in sodium phosphate buffer.

cutoff were recorded. Donor and acceptor channels were given independent thresholds of ten times the standard deviation of the background fluorescence.

FCS cross correlations were performed after data acquisition, rather than on the fly. Generally, ten-minute acquisitions were performed, however, for lower intensities the data acquisition time was lengthened in order to reduce noise on the cross correlation functions.

Results and Discussion

FCS: The normalized cross correlations of fluorescein and rhodamine 6G in NaP buffer (no scavengers) under intensities of 20kW/cm^2 and 400kW/cm^2 are shown in Figure 1. It can be seen that the increase in excitation intensity results in an increase in the number of molecules in the triplet state as well as a decrease in the time molecules are seen diffusing across the excitation volume. This decrease in the diffusion time is due to the increased photobleaching of the dyes under higher intensities. The same FCS

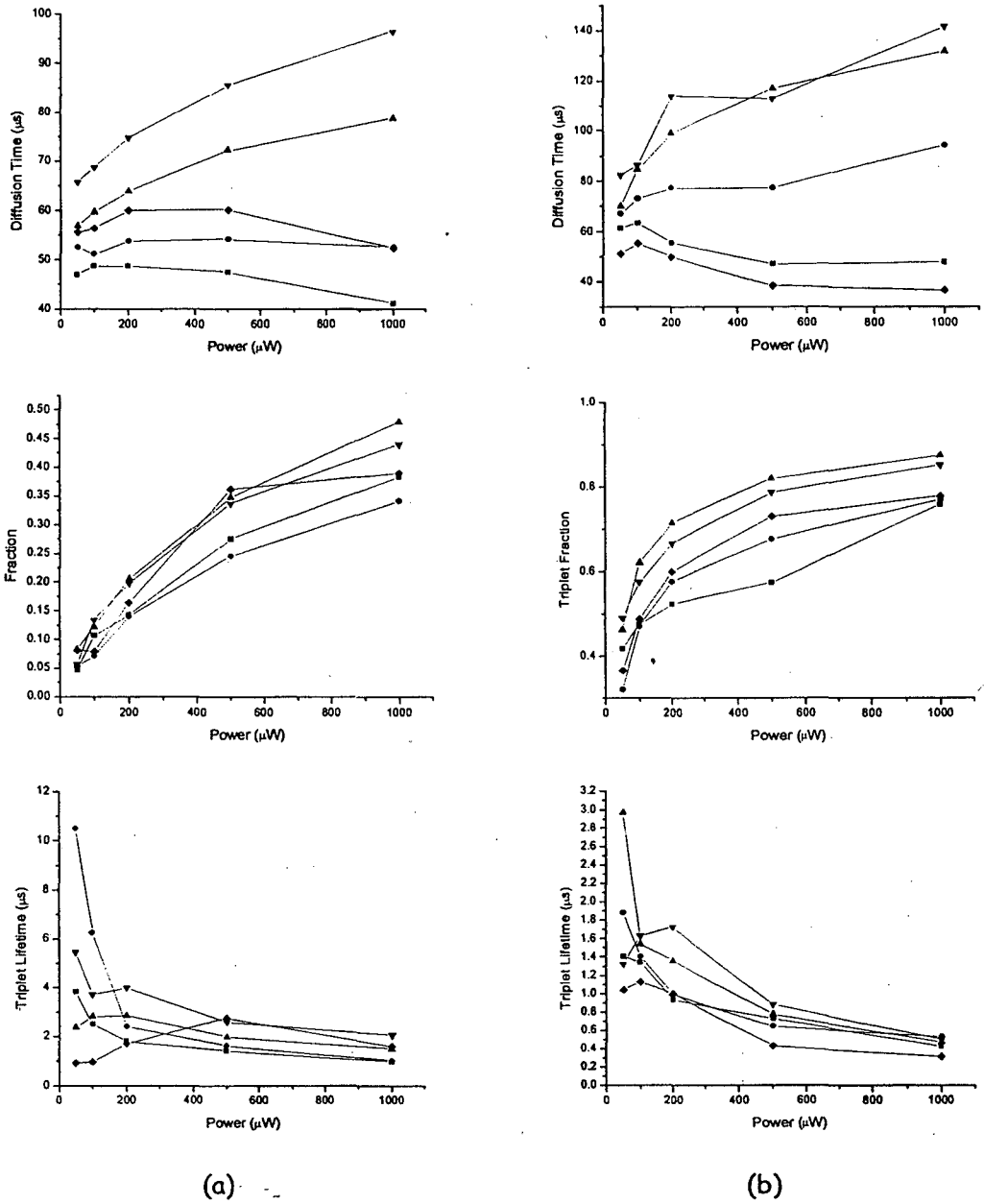

Figure 2: (a) Rhodamine 6G and (b) Fluorescein fluorescence parameters acquired from fits of Equation (1). Sodium Phosphate Buffer Only (■), Mercaptoethylamine (●), Glucose Oxidase (◆), Propyl Gallate (▲), and Trolox (▼).

measurements were then performed for the two dyes in the presence of each scavenger at varying excitation intensities. The cross correlation functions for all conditions were fit with Equation (1) to yield the diffusion time, fraction of molecules in the triplet state, and

the triplet state lifetime. These values are shown in Figure 2. From these fits it becomes clear that there are significant changes in the fluorescent properties of the dyes due to the addition of oxygen scavengers, but the scavengers differ in their effects. The addition of oxygen scavengers to the system is expected both to decrease the photobleaching rate of the dyes and to increase the triplet state lifetime. The contribution of both of these effects to the increase in the observed diffusion time has been documented previously in [97]. The increase due to reduced photobleaching is easily understood, since the fluorophores are able to sample more of the beam before photodestruction. The effect of the triplet state on the diffusion time is more complicated but can be understood in terms of a change in the population that contributes to the measured intensity fluctuations. What was previously an effective Gaussian cross-section of excited fluorophores becomes flattened, since those fluorophores in the center of the excitation beam are triplet-saturated and begin to contribute less to the overall signal than those on the wings. This results in an effective increase in the fitted diffusion time across the beam.

Small changes in the diffusion times as a function of power were observed with GOD and MEA, while quite large effects were seen for the Trolox™ and PG. The diffusion time increases in the cases of Trolox and PG for both fluorescein and R6G, and these two scavengers produce the highest fraction of molecules in the triplet state for both dyes. The spread of diffusion times seen between the different scavengers at the lowest power is simply due to differences in the alignment of each sample. Once a sample is aligned, no more changes to the alignment are made as power is increased. In the case of R6G, MEA appears to arrest the change in diffusion time while slightly decreasing the triplet fraction at higher powers compared to that found in the buffer-only sample. The effect of MEA on

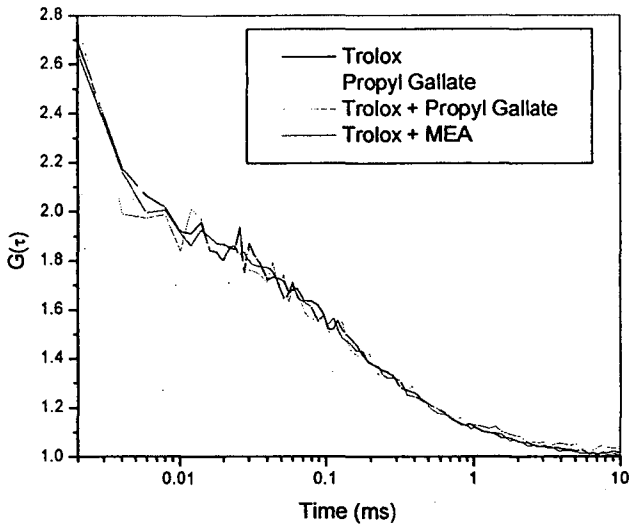

Figure 3: FCS cross correlations showing the mixing of oxygen scavengers. 1mW.

fluorescein is to increase the diffusion time while producing a faster saturation of the dye. The triplet fraction at the highest power used, however, is the same as in the buffer-only sample. These effects of MEA on fluorescein and R6G are consistent with those observed previously by Song, et al [99], who found that MEA's photobleaching protection occurs by interaction with the triplet state of the dye. It has been hypothesized that PG and MEA may act as both oxygen scavengers and triplet quenchers [97,99]. To determine if this was true we performed FCS measurements on two additional fluorescein and rhodamine 6G samples which contained both Trolox™ and either PG or MEA in the buffer. The reasoning in this was that Trolox™, a sacrificial oxygen scavenger, should remove the oxygen, which would result in an overall increase in the triplet state lifetimes of the dye molecules as seen before. Any reduction of these lifetimes from that seen in the Trolox™-only samples must then be due to the interaction of n-propyl gallate or MEA with the triplet states of the dye molecules. Results of these measurements are shown in Figure 3. From the plots shown, it does not appear that PG or MEA are acting as triplet quenchers.

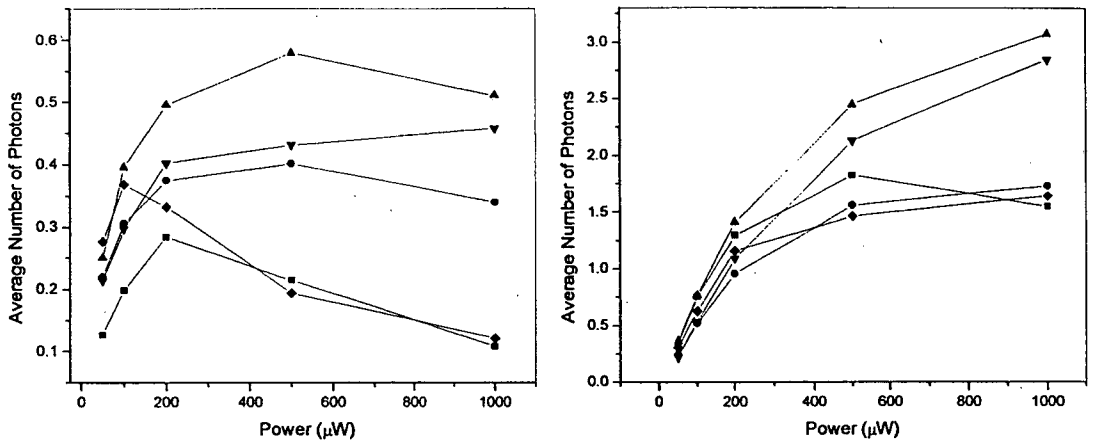

Figure 4: Calculated average number of photons emitted by (a) Fluorescein and (b) Rhodamine 6G in the following conditions: Sodium Phosphate Buffer Only (■), Mercaptoethylamine (●), Glucose Oxidase (◆), Propyl Gallate (▲), and Trolox (▼).

Figure of Merit

One figure of merit for a fluorescent molecule is the total number of photons it produces before photodestruction. To estimate this value for the various combinations of oxygen scavengers and dyes examined, we performed a simple calculation of the average intensity of our FCS traces divided by the fitted number of molecules to get the average rate of emission per molecule. This was then multiplied by fitted diffusion time of the molecules in the beam, to give the average number of photons emitted by a molecule as it traverses the excitation volume:

$$Num_{avg} = \frac{I_{avg}}{N_{fitted}} \tau_D$$

It should be noted that here the diffusion time is very short, due to the small focal volume employed, hence the low average number of photons per molecule.

The values for this figure of merit are shown in Figure 4 for both fluorescein and rhodamine 6G. By taking the ratio of the fitted diffusion time over the fitted number of molecules, the effects of saturation are reduced somewhat, since both depend on the same r^2 area factor (assuming a cylindrical FCS volume). There is still a contribution to the number of molecules from the height of the volume element, and it is not clear yet what effect saturation has in the z-direction. It can be seen, however, that for the buffer-only samples of both fluorophores, the number of photons decreases with increasing power, as is expected from photobleaching and triplet saturation. Glucose oxidase does not appear to greatly enhance the fluorescence emission of either dye, although the slope of the number versus power curve of GOD (and MEA) for R6G crosses that of the sodium phosphate buffer, perhaps indicating an improvement at higher powers than those measured here. MEA provides some improvement in the total emission of Fluorescein as well. Trolox and PG show clear enhancements of total photon output for both R6G and Fluorescein, indicating that in applications where the total number of photons is important, they are the preferred oxygen scavengers. The increase in the fraction of molecules in the triplet state due to the use of oxygen scavengers may prove to be a deleterious effect for many measurements, since this results in an overall decrease in the rate of emission from a molecule and thus a decrease in the signal-to-noise ratio of the experiment. The decision to use oxygen scavengers should then take into account which is more important for a given experiment, the rate of emission or the total number of photons emitted over time.

Hairpin DNA

For fluorophores with low intersystem crossing rates such as CY5 [76], the use of oxygen scavengers can provide marked improvements in single molecule measurements, since the effects of saturation are not as pronounced with such molecules. From the results of the single molecule diffusion measurements shown in Figure 5, it becomes clear that the small molecule oxygen scavengers are preferable to GOD in removing oxygen. There is a clear increase in the high energy transfer efficiency peak due to the addition of oxygen scavengers, with Trolox, PG, and MEA all showing a greater increase than that with the GOD system. It was found in previous attempts at performing temperature denaturation-reannealing measurements of hairpin DNA that at 50 °C the GOD began to contribute a large background to the measurement due to the protein's denaturation and aggregation (data not shown). The same experiment could be performed with the small oxygen scavengers, however, and an example of such a denaturation-reannealing measurement is shown in Chapter 4, Figure 3. In addition to the four oxygen scavengers discussed here, a number of other, less effective oxygen scavengers and antifading reagents were also tried. These included imidazole, beta-mercaptoethanol, Antifade ™ (Molecular Probes) and Prolong ™ (Molecular Probes). Bubbling solutions with nitrogen to physically replace oxygen was also tried. None of these methods proved to be as effective as the four scavengers shown here. Since propyl gallate, Trolox, and MEA are small molecules, easy to use, and not subject to denaturation by temperature or standard chemical denaturants, they should prove to be valuable additions to single molecule measurements in which photobleaching presents significant difficulties.

Conclusions

Because singlet oxygen plays such an important part in the photobleaching process, the removal of oxygen is the primary means employed in reducing photodegradation in single molecule experiments. Oxygen removal techniques such as bubbling with argon or nitrogen or employing enzymatic systems can be effective, however they are often inconvenient and cannot be applied universally. Since photobleaching often produces significant difficulties in single molecule experiments, any attempt to circumvent its effects is generally worthwhile, despite the increased difficulty in sample preparation that typically accompanies such an attempt. The use of small molecule oxygen scavengers can provide a simple and easy method of oxygen removal in many cases, and the use of such scavengers allows measurements such as denaturation-renaturation (either temperature or chemical) of macromolecules to be performed without the loss of oxygen scavenging ability under denaturing conditions that is found in enzymatic systems such as GOD. Two of the scavengers examined here (propyl gallate and Trolox™) have been shown to improve the overall number of photons emitted per molecule in FCS measurements, and of the four primary oxygen scavengers examined here (GOD, Trolox™, propyl gallate, and mercaptoethylamine), all showed some improvement in total number of detected events in single pair FRET measurements. Examples such as this show that by utilizing such oxygen scavenging systems, it is possible to improve the overall statistics of single molecule measurements.

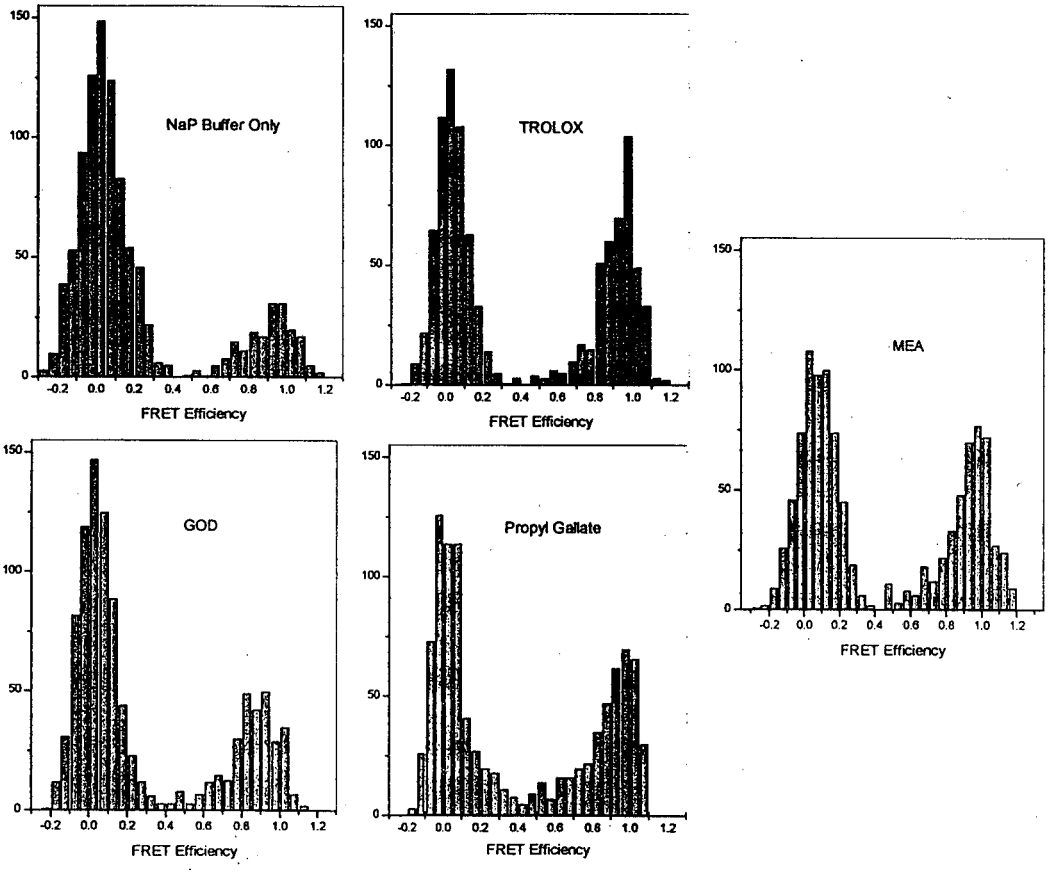

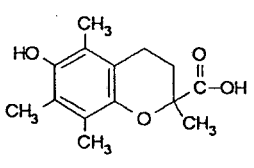

Trolox™

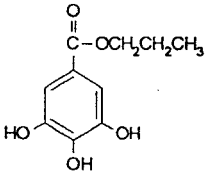

Propyl Gallate

Mercaptoethylamine

Figure 5: 14 stem DNA hairpin with oxygen scavengers. 1000 Events in each histogram.

Conclusions

The field of single molecule detection and spectroscopy is in its adolescence now, having passed through the years when the simple detection of a single fluorescent molecule was novel and could be documented in *Science* and *Nature* articles. The field is currently growing by leaps and bounds but has not yet reached maturity. Now that the initial thrill of finding such a potent new investigative method has worn off a bit, researchers are asking themselves, "How do I use these techniques to the greatest benefit? What are the questions I can answer using single molecule measurements? What are the advantages and what are the drawbacks? What place do these types of measurements have in biology, chemistry, and physics?"

The answers to some of these questions are clear. The ability of single molecule detection to resolve the distribution of behaviors within a population is an extremely valuable tool, and it is the strongest argument one can find in favor of attempting to measure the behavior of a system on a molecule by molecule basis. The ability to turn a magnifying glass on a single enzyme, a single strand of DNA, or a single fluorescent environmental probe, and then compare that molecule to the next and the next affords the opportunity for a more in-depth understanding of the inhomogeneous nature of complex

systems. Another advantage of using single fluorescent probes is the ability of such probes to report on their specific nanoenvironments. This exquisite sensitivity can be applied to material science, examining highly localized fields and charges, or to biology, investigating the inhomogeneous environment of a cell. In doing so, however, it is important to keep clearly in mind what one expects to learn from such measurements, since there is now a temptation in the scientific community to apply single molecule measurements to many systems simply because of the novelty of the measurements. The detection of single fluorescent molecules has become fairly routine over the past few years, but extracting meaningful information from such measurements has not gotten easier. Single molecule measurements must be clearly defined, the fluorescent labeling of the systems to be measured must be reliable and exact, and the basic photophysics of the fluorophores must be understood in order to gain useful information from such measurements, rather than simply introducing more complex questions.

That said, with proper usage single molecule measurements do have to potential to provide a wealth of new knowledge about many processes in physics, chemistry, and biology. The ability to measure single chemical reactions such as protonation and deprotonation and the direct observation of individual macromolecular conformational dynamics such as the opening and closing of DNA hairpins presented in this thesis have served as demonstrations of this powerful technique. Single molecule fluorescence detection is now in wide use, examining problems as diverse as ion channel gating, enzymatic turnover, nanocrystal photophysics, and small volume chemical reactions. The work presented in this thesis has introduced new methodologies for detection and immobilization, along with the development of better methods for understanding and controlling the photophysical properties of the

fluorescent probes. This type of work contributes to solidifying the foundation on which the field of single molecule detection and spectroscopy is growing. Without a firm understanding of the effects of the local environment on fluorescent molecules, without proper immobilization methods, and with the complications of poor photostability, single molecule measurements simply introduce more questions than they answer. With these issues addressed, single molecule fluorescence measurements can serve as a powerful tool applied to diverse problems in physics, chemistry, and biology.

References

[1] T. Ha et al, *Chem Phys Lett.* **271**: 1-5 (1997)
[2] W.P. Ambrose, W.E. Moerner, *Nature* **349**: 225-27 (1991)
[3] H.P. Lu and X.S. Xie, *Nature*, **385**: 143-6 (1997)
[4] T, Basche et al, *Phys. Rev. Lett.* **69**: 1516-19 (1992)
[5] D.T. Chiu et al, *Chem. Phys.* **247**: 133-9 (1999)
[6] A. Sonnleitner et al, *Biophysical Journal* **77**, 2638-42 (1999)
[7] X.N. Xu and E. Yeung, *Science* **281**, 1650-1653 (1998)
[8] T. Funatsu et al, *Nature* **374**, 555-9 (1995)
[9] Jia et al, *Chem. Phys. Lett.* **247** 69 (1999)
[10] R.D. Vale et al, *Nature* **380**: 451-453 (1996)
[11] I. Sase et al, *Proc. Nat. Acad. Sci* **94**: 5646-5650 (1997)
[12] D. M. Warshaw et al, *Proc. Nat. Acad. Sci.* **95**: 8034-8039 (1998)
[13] K. Kitamura et al, *Nature* **397**: 129-134 (1999)
[14] H. Noji et al, *Nature* **386**: 299-302 (1997)
[15] L. Kador, D.E. Horne, W.E. Moerner, *J. Phys. Chem.* **94**: 1237-48 (1990)
[16] M. Orrit, J. Bernard, *Phys. Rev. Lett.* **65**: 2716-19 (1990)
[17] S. Kasas et al, *Biochemistry* **36**: 461-468 (1997)
[18] E-L. Florin et al, *Science* **264**, 415-417 (1994)
[19] D.C. Nguyen et al, *Anal. Chem.* **59**: 2158-61 (1987)
[20] E. B. Shera et al, *Chem. Phys. Lett.* **174(b)**: 553-557 (1990)
[21] E. Betzig et al, *App. Optics*, **25**, 1890-1900 (1986)
[22] E. Betzig and J.K. Trautman, *Science* **257**: 189-195 (1992)
[23] E. Betzig and R.J. Chichester, *Science* **262**: 1422-1425 (1993)
[24] P. Ambrose et al, *Phys. Rev. Lett.* **72**: 225-227 (1994)
[25] T. Ha et al, *IEEE Sel. Topics in Quant. Elect.* **2**: 1115-1128 (1996)
[26] D. Chiu and R. Zare, *J. Am. Chem. Soc* **118**, 6512-13 (1996)
[27] S. Chu and S. Kron, *Int. Quantum Electron. Conf. Tech. Digest,* Optical Society of America: Washington, DC (1990) p. 202
[28] S. B. Smith et al, *Science* **258**: 1122-6 (1992)
[29] L. Tskhovrebova et al, *Nature* **387**, 308 (1997)
[30] T. R. Strick et al, *Science* **271**: 1835-7 (1996)
[31] J. Dapprich et al, *Exp. Tech. Phys.* **41**: 259-64 (1995)
[32] J.K. Trautman and J.J. Macklin, *Chem. Phys.* **205**: 221-9 (1996)
[33] J.J. Macklin et al, *Science* **272**: 255-8 (1996)
[34] T. Schmidt et al, *Proc. Nat. Acad. Sci.* **93**: 2926-9 (1996)
[35] E.J. Sanchez et al, *J. Phys. Chem. A* **101**: 7019-23 (1997)
[36] J. Mertz et al, Opt. Lett. 20: 2532-4 (1995)
[37] T.J. Ha et al, *Phys. Rev. Lett* **80**: 2093-6 (1998)
[38] H.P. Lu et al, *Science* **282**: 1877-82 (1998)

[39] W. Tan and E.S. Yeung, *Anal. Chem.* **69**: 4242-8 (1997)
[40] U. Haupts et al, *Proc. Nat. Acad. Sci.* **95**: 13573-8 (1998)
[41] T. Ha et al, *Applied Physical Letters* **70**: 782-784 (1997)
[42] D. Magde, E. Elson, and W. W. Webb, *Phys. Rev. Lett.* **29**: 705-708 (1972)
[43] R. Rigler et al, *Eur. Biophys. J.* **22**: 169-175 (1993)
[44] P. Schwille et al, *Biophys. J.* **72**: 1878-1886 (1997)
[45] B. Arkles, *Silane Coupling Agent Chemistry*, Silicon Compounds Register and Review, 5th edition, published by United Chemical Technologies.
[46] http://ntri.tamuk.edu/electrophoresis/pde.html "Polyacrylamide Disc Electrophoresis"
[47] http://www.bioproducts.com/technical/agarosephysicalchemistry.html "Agarose Physical Chemistry"
[48] T. Förster, *Modern Quantum Chemistry*, Academic Press: New York, NY (1966)
[49] L. Stryer and R. P. Haugland, *Proc. Natl. Acad. Sci. U.S.A.* **58**: 719-730 (1967)
[50] A. Deniz et al, *Proc. Natl. Acad. Sci. U.S.A.* **96**: 3670-3675 (1999)
[51] C. R. Cantor and P. R. Schimmel, *Biophysical Chemistry*, Freeman: San Francisco, CA (1980)
[52] B. Meer, *Resonance Energy Transfer: Theory & Data*, VCH: New York, NY (1994)
[53] T. Ha et al, *Proc. Natl. Acad. Sci. U.S.A.* 96: 893-898 (1999).
[54] S. Mariappan et al, *Nucleic Acids Res.* 24: 784-792 (1996).
[55] M. Rosenberg and D. Court, *Annu. Rev. Genet.* **13**: 319-353 (1979)
[56] A. Amir-Aslani et al, *Nucleic Acids Res.* **23**: 3850-3857 (1995)
[57] X. Chen et al, *Proc. Natl. Acad. Sci. U.S.A.* **92**: 5199-5203 (1995)
[58] S. Mariappan et al, *Nucleic Acids Res.* **24**: 775-783 (1996)
[59] E. Skripkin et al, *Proc. Natl. Acad. Sci. U.S.A.* **91**: 4945-4949 (1994)
[60] S. Tyagi and F. R. Kramer, *Nature Biotech.* **14**: 303-308 (1996)
[61] D. Muriaux et al, J. *Biochemistry* **35**: 5075-5082 (1996)
[62] S. Tyagi et al, *Nature Biotech.* **16**: 49-53 (1998)
[63] L. G. Kostrikis et al, *Nat. Med.* **4**: 350-353 (1998)
[64] L. G. Kostrikis et al, *Science* **279**: 1228-1229 (1998)
[65] A. Piatek et al, *Nature Biotech.* **16**: 359-363 (1998)
[66] X. Fang et al, *J. Am. Chem. Soc.* **121**: 2921-2922 (1999)
[67] D. A. Erie, et al, *Biochemistry* **32**: 436-454 (1993).
[68] V. P. Antao et al, *Nucleic Acids Res.* **19**: 5901-5905 (1991).
[69] G. Varani, *Annu. Rev. Biophys. Biomol. Struct.* **24**: 379-404 (1995)
[70] J. Gralla and D. M. J. Crothers, *Mol. Biol.* **73**: 497-511 (1971)
[71] C. W. Hilbers et al, *Biochimie* **67**: 685-695 (1985)
[72] G. Bonnet et al, *Proc. Natl. Acad. Sci. U.S.A.* **95**: 8602-8606 (1998)
[73] V. T. Moy et al, *Science* **266**: 257-259 (1994)
[74] Y.-H. Rogers et al, *Anal. Biochem.* **26**: 23-30 (1999)
[75] M. Dahan et al, *Chem. Phys.* **247**: 85-106 (1999)
[76] J. Widengren and P Schwille, *J. Phys. Chem. A* 104: 6416-6428 (2000)
[77] Y. Harada et al, *J. Mol. Biol.* 216: 49-68 (1990)
[78] R. Tsien, A. Waggoner, In *Handbook of Confocal Microscopy 2nd Edition*, J. Pawley Ed., New York, NY: Plenum, pp. 267-279 (1995)
[79] D. Colquhoun and A. G. Hawkes *Single-Channel Recording 2nd Edition*, New York, NY: Plenum (1995)

[80] A. Podtelezhnikov and A. Vologodskii, *Macromolecules* **30**: 6668-6673 (1997)
[81] G. Wilemsky and M. Fixman, *J. Chem. Phys.* **60**: 866-877 (1974)
[82] O. Berg, *Biopolymers* 23 (1984)
[83] J. R. Lakowicz, *Principles of Fluorescence Spectroscopy, 2nd edition,* Chapter 16 (New York, NY: Plenum) 1999.
[84] *Handbook of Fluorescent Probes and Research Chemicals, 6th ed,* by R. P. Haugland, Molecular Probes: 586 (1996)
[85] R. Haugland, *Fluorescent and Luminescent Probes for Biological Activity- A Practical Guide to Technology for Quantitative Real-time Analysis,* Chapter 3, W.T. Mason ed., Academic Press, London (1993)
[86] *Handbook of Fluorescent Probes and Research Chemicals, 6th ed,* by R. P. Haugland, Molecular Probes: 556 (1996)
[87] J. Whitaker et al, *Anal. Biochem.* **194**: 330-344 (1991)
[88] M. Daune, *Molecular Biophysics,* Oxford University Press, New York, NY (1999)
[89] T.J. Ha, *Ph.D. Dissertation,* University of California at Berkeley, Berkeley, CA (1996)
[90] S. Brasselet and W. E. Moerner, *Single Mol.* **1**: 17-23 (2000)
[91] L. Song et al, *Biophys. J.*, **68**: 2588-2600 (1995)
[92] L. Lindqvist, *Arkiv Kemi* **16**: 79-138 (1960)
[93] V. Kasche and L. Lindqvist, *J. Phys. Chem.* **68**: 817-823 (1964)
[94] N. Turro, *Modern Molecular Photochemistry* (Menlo Park, CA: Benjamin/Cummings) 1978.
[95] D. Kearns, *Chem. Rev.* **71**: 395-427 (1971)
[96] J. D. Spikes, *Photochem. Photobio.* **55**: 797-808 (1992))
[97] J. Widengren et al, *J. Phys. Chem.* **99**: 13368-13379 (1995)
[98] J. Widengren and R. Rigler, *Bioimaging* **4**: 149-157 (1996)
[99] L. Song et al, *Biophys. J.* **70**: 2959-2968 (1996)

Reviews:
S. Nie and R. N. Zare, *Ann. Rev. Biophys. Biomol. Struct.* **26**: 567-96 (1997).
"Frontiers in Chemistry: Single Molecules", special issue of *Science* **283**: 1667-1695 (1999).

Texts:

Handbook of Confocal Microscopy 2nd Edition, J. Pawley Ed. (New York, NY: Plenum) 1995
J. R. Lakowicz, *Principles of Fluorescence Spectroscopy, 2nd edition* (New York, NY: Plenum) 1999.
T. Basche, et al, *Single-molecule Optical Detection, Imaging and Spectroscopy* (Cambridge, VCH) 1997.

Ernest Orlando Lawrence Berkeley National Laboratory
One Cyclotron Road | Berkeley, California 94720

Prepared for the U.S. Department of Energy under Contract No. DE-AC03-76SF00098